Estimation of actual evapotranspiration and crop coefficient in the REMENDHUS area, Spain

Andres Saul Gonzales Amaya

February, 2010

Estimation of actual evapotranspiration and crop coefficient in the REMENDHUS area, Spain

by

Andres Saul Gonzales Amaya

Thesis submitted to the International Institute for Geo-information Science and Earth Observation in partial fulfillment of the requirements for the degree of Master of Science in Geo-information Science and Earth Observation, Specialization: Integrated Watershed Modeling and Management

Thesis Assessment Board

Dr. Ir. M.W. Lubczynski	Chairman (ITC Enschede)
Prof. Dr. W.G.M. Bastiaansen	External examiner
MSc. Ir. G.N. Parodi	First supervisor (ITC Enschede)
Dr. Ir. C. van der Tol	Second supervisor (ITC Enschede)

ITC

INTERNATIONAL INSTITUTE FOR GEO-INFORMATION SCIENCE AND EARTH OBSERVATION

ENSCHEDE, THE NETHERLANDS

Disclaimer

Abstract

The determination of the frequency and amount of irrigation water supply is necessary for sustainable development and water management. The estimation of the evapotranspiration (ET) is important for the water management in agricultural lands. The study area, REMENDHUS network in Spain, presents a high percent of agricultural land and its condition of semi arid Mediterranean region makes important the research and improvement of calculation the actual ET and crop coefficients (K_c) factors on this region.

The one dimensional model, Hydrus-1D, and field soil moisture (SM) measurements are used to determinate the daily actual ET over some specific crops typical for the area (wheat, sunflower, sugar beet and onion). Later a remote sensing (RS) model, SEBS, is used to determinate the daily actual ET and then compare with the outputs of Hydrus-1D to see the applicability of RS method to the area.

The water content predicted by Hydrus-1D matches very well in all 9 modelling runs during the years 2006 to 2009. The percentages of prediction vary between 72 and 92%. The actual ET predicted presents a realistic performance with values ranging between 0.02 and 4.18 mm/day after rain or irrigation. On the other hand SEBS4ILWIS is used in 8 MODIS images (1x1 km final resolution) producing considerable high values of actual ET (values between 1.11 and 8.71 mm/day) overestimating the daily actual ET. An analysis on these results is also suggested.

Due to the good trend and high percent of prediction by Hydrus-1D the actual ET of this model is assumed adequate to carry out the calculation of the crop coefficients (K_c). Once calculated the new K_c for some specific crop on a specific date it is compared with the literature of FAO 56 guidelines. The K_c values obtained in this research follow the trend dictated in the literature, as during the initial and final stages the K_c values are low, but during the middle season the K_c shows higher.

The crop coefficient for sunflower and wheat show an agreement with the values offered by FAO at least for the days with K_s equal to 1 or near to it (4 and 6 days respectively). On the other hand there is just 1 day available for onion and sugar beet so is more complex to come up with a general conclusion.

Acknowledgments

Thanks to god for illuminate my life with faith and hope…

I would like to thanks to my family for be there for me anytime that I need them. Thanks to my loved parents for encouraged me during all my life and for their support and love.

Thanks to ITC and all the staff, especially to my supervisor Gabriel Parodi for his support and excellent guidance during all this research stage. I highly appreciate his valuables advices and his excellent comments and criticism.

Thanks to my dear friends and classmates for their friendship, support and help during all these moments of pressure and stress.

Table of contents

List of figures

List of Tables

1. General introduction

1.1. Background

The climate of the Guareña basin is Mediterranean therefore hot and dry days are expected in summer season and a mild temperature in winter. Moreover the principal land use in this basin is agricultural; consequently accurate determination of irrigation water supply is necessary for sustainable development and water management (Rana and Katerji 2000).

The water consumption by crops normally refers to all the water evaporated from soil, transpiration from plants and water retained within plant tissues. However this retention in the plant tissues represents less than 1% of the water consumption (Jensen 1968). Therefore estimation of the evapotranspiration is important for the water management in agricultural lands.

Due the semi-arid condition in the Guareña catchment, the crops and agricultural fields are under water stress; therefore the losses of water by evapotranspiration indicate their consumption. The actual evapotranspiration can be estimated or measured (directly or indirectly). There are many methods to estimate and measure evapotranspiration, Rana and Katerji (2000) made the following classification.

Evapotranspiration measurement:

- Hydrological approaches
  - Soil water balance
  - Weighing lysimeters
- Micrometeorological approaches
  - Energy balance and Bowen ratio
  - Aerodynamic method
  - Eddy covariance
- Plant physiology approaches
  - Sap flow method
  - Chambers system

Evapotranspiration estimation:

- Analytical approach
  - Penman–Monteith model
- Empirical approach
  - Methods based on crop coefficient approach
  - Methods based on soil water movement and balance modelling.

The election of the method depends on the purpose of the study, the needed accuracy of the results, cost, space and time scales.

Hydrus-1D is a numerical model for analysis of water movement, heat and solute transport in variably saturated porous media. It is a finite element model that solves Richards' equation for flow. Information on soil texture and moisture, climatic factors and water uptake can be used to determine the actual evapotranspiration (Simunek, Van Genuchten et al. 2005).

This model estimates actual ET by using meteorological, physiographic, physiological and geographical data. The user obtains actual ET from the model output by the addition of the estimates of "actual root uptake" and "actual surface evaporation". It estimates infiltration, and surface runoff as the difference between precipitation and infiltration. Hydrus-1D is sensitive to time-step definition, and may require iterative runs to find an acceptable output (Hauser 2008).

Once Hydrus-1D is calibrated its estimates of actual ET will be used to weight against the actual ET from a Remote Sensing based Energy Balance algorithm like SEBS.

SEBS algorithm (Su, 2002) can estimate turbulent heat fluxes and evaporative fraction, based on three sets of input data (Kwast and Jong 2004):

- Data derived from remote sensing (albedo, emissivity, temperature, fractional vegetation cover, Leaf Area Index, height of vegetation or roughness height)
- Meteorological parameters at reference height (air pressure, temperature, relative humidity, wind speed)
- Radiation data (downward solar radiation, downward long wave radiation).
- Finally, instantaneous to daily values are plainly estimated assuming the conservation of evaporative fraction during the day, although this mechanism has divided the opinion of top researchers.

1.2. Problem Statement

Crop coefficients are functions of crop itself, stage of growth and cultural practices. Coefficients for semi to annual crops like row crops, or pastures vary widely through the season, with a small coefficient in the early stages of the crop when the crop is just seedling, to a large coefficient when the crop is at full cover and the soil is completely shaded (CIMIS 2008).

In order to improve the irrigation efficiency and scheduling of the study area it is a common practice to get a better description or understanding of the crop coefficients as applied for Guareña basin, in this case. As such, the actual evapotranspiration needs to be estimated for some irrigated areas allowing and improved crop coefficient estimation.

1.3. Research Objective

The general objective of this research is:

To estimate actual evapotranspiration on daily time steps and crop coefficient factor for a number of specific and typical crops usually found in Guareña basin, by using a model that simulates the balance in the saturated, unsaturated and root zone and compare with a RS approach to establish the adequacy and concerns of the RS approach, in view of the easiness of the later.

In order to achieve this objective a series of steps should be followed. These steps compose these specific objectives:

- To calibrate Hydus-1D model using soil moisture field measurements.
- To estimate actual evapotranspiration by SEBS for some specific days.
- To validate actual evapotranspiration between the two models.
- To estimate K_c (time) for some specific crops in the Guareña basin.

1.4. Research Questions

- What would be an adequate procedure to obtain an accurate value of actual evapotranspiration by using Hydrus-1D model considering the data available in REMENDHUS area?
- What is the applicability of SEBS in the area to evaluate Actual Evapotranspiration considering the limitations of data acquisition and RS resolution (MODIS 1Km) in relation to crop area and "pure" crop pixels (needed for crop dependent Kc)?
- Can SEBS explain the actual evapotranspiration at the local area of the modelling?
- Can crop coefficient be adjusted locally after the use of Hydrus-1D? And after SEBS at 1 Km resolution?
- Is the irrigation scheduling and quota adequate for the crops? Is in deficit or excess?

1.5. Methodology

The methodological steps for the fulfilling of the research objectives will be carried out in three stages: pre-fieldwork, fieldwork and post-fieldwork (Figure 1-2).

1.5.1. Data availability

The REMENDHUS network (Figure 1-1) has been working and collecting data in the area since June 1999 to the present. This network consists of a 23 soil moisture stations distributed over the basin, 150 soil samples points and precipitation is available from 7 stations near the area. Figure 1-1 shows the distribution of these locations.

1.5.2. Coordinate system

The maps and information in this research follow the next spatial coordinate system:
Projection: UTM. Zone: 30
Datum: European (ED 50)
Datum area: Portugal – Spain
Ellipsoid: International 1924
Ellipsoid parameters: a = 6378388, 1/f = 297

Figure 1-1 REMENDHUS area

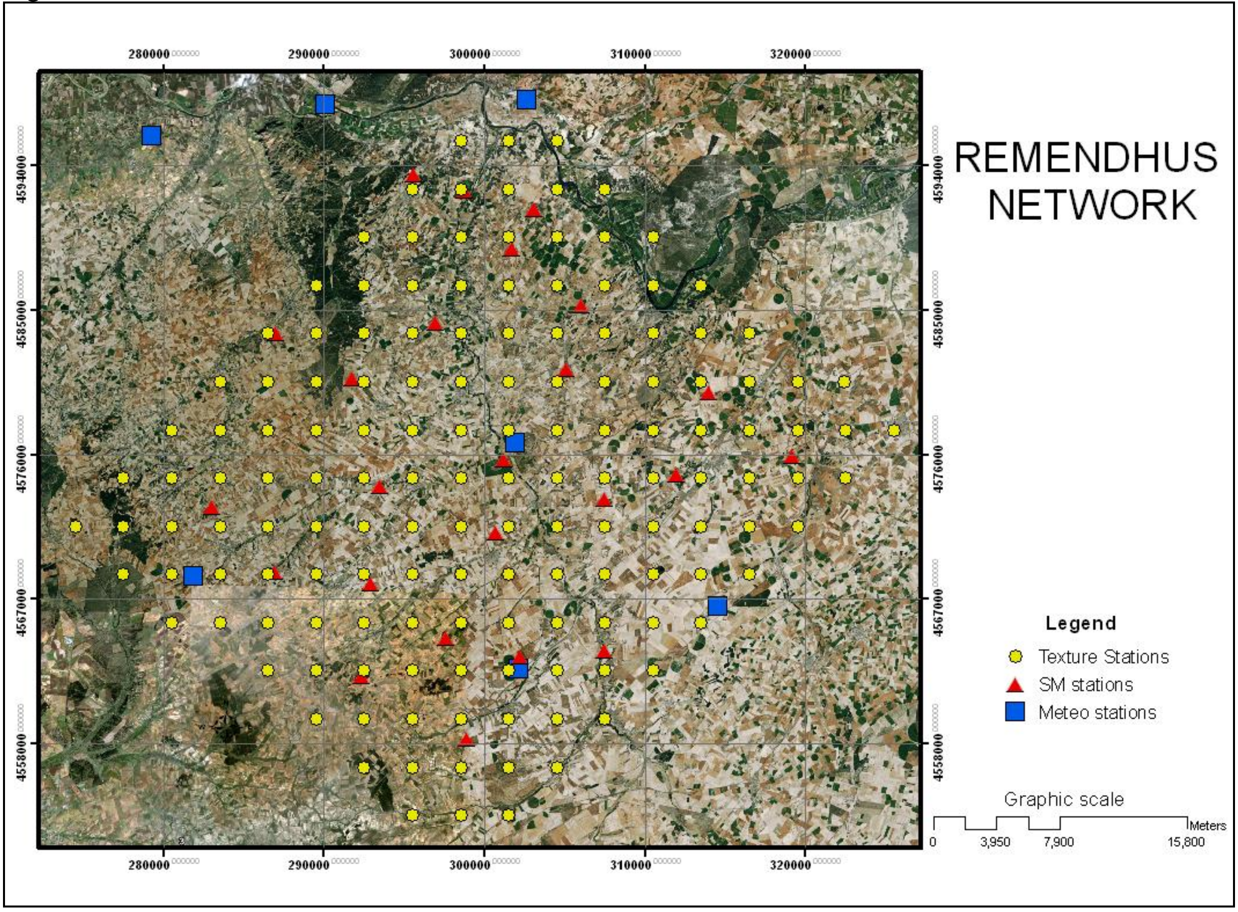

Figure 1-1 shows in yellow dots, the 150 soil texture samples, the red ones are the soil moisture samples and the blue ones are the meteorological stations. Therefore there are 3 main data sets available for this research: meteorological data, data on physical properties of soil and soil moisture data.

1.5.3. Pre Field Work

The pre-field work stage focused in the preparation of the activities which facilitate the field work. This stage includes the following activities.

- Literature review
- Visual interpretation of the study area
- Exploratory analysis of Hydrus-1D and determination of the input data requirement
- Field work program
- Localization of sites for modelling Hydrus-1D.

1.5.4. Field Work

The activities to be conducted in this stage will include:

- Area recognition.
- Collecting data: soil properties, meteorological, soil moisture, crop characteristics.
- On site verification of the experimental sites for modelling.

1.5.5. Post Field Work

The activities for this stage are:

- Calibration of Hydrus-1D model using the SM field measurements.
- Estimation of actual ET by Hydrus-1D
- Estimation of actual ET by SEBS.
- Validation of the actual ET.
- Determining the crop coefficient for the selected areas and crop stages.
- Elaboration of the final document for its submission.

1.5.6. Thesis Outline

This written report is organized in 5 chapters, as:

Chapter 1 describes the problem statement, objectives and main datasets of this research.

Chapter 2 summarizes the main aspects of theoretical background for this research: soil moisture, evapotranspiration from remote sensing, model of water moments, and others. The study area and the available data are also described.

Chapter 3 analyzes and explains the data process (pre-processing, processing and post-processing) for the model Hydrus-1D and SEBS algorithm.

Chapter 4 discuss and compares the results obtained by Hydrus-1D and SEBS.

Chapter 5 formulates the conclusions and recommendations of this research.

Figure 1-2 Stages of the research

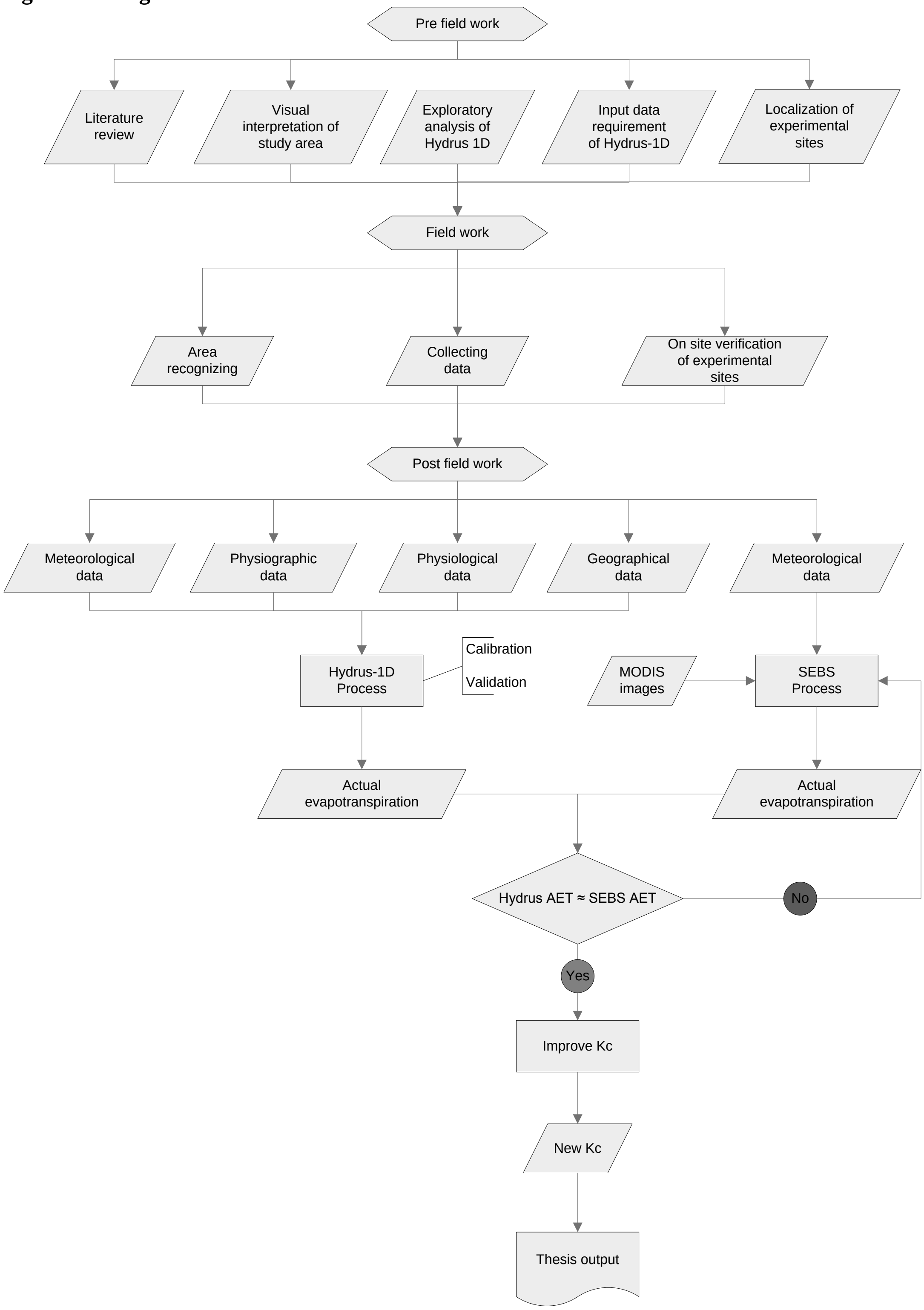

2. Theoretical background and description of the study area

2.1. Literature Review

The literature review is a continuing task during research study. The review focuses in estimation of evapotranspiration, crop coefficients and modelling for estimation of actual ET. For instance FAO Irrigation and Drainage Paper No. 56 (Allen, Pereira et al. 1998), Hydrus-1D (Simunek, Van Genuchten et al. 2005) and the Surface Energy Balance System (Su 2002), compose the basic information to build up the material required for the achievement of this topic.

2.1.1. Surface energy balance Models and RS

The surface energy balance describes the exchanges of energy and mass among the hydrosphere, atmosphere and biosphere. Available net radiation is used to do (energetic) work in the Earth system. The use of this net energy is in changing water into vapour (latent heat), changing the surface temperature (sensible heat), and subsurface (ground heat) (Su 2002; Ritter 2006). The energy balance equation read as:

$$R_n = G_O + H + \lambda E$$ **Equation 1**

Where 'R_n' is the net radiation, 'G_o' is the soil heat flux, 'H' is the turbulent sensible heat flux, and 'λE' is the turbulent latent heat flux ('λ' [$J.kg^{-1}$] is the latent heat of vaporization and 'E' is the actual evapotranspiration [$kg.s^{-1}.m^{-2}$]), all units in ($W.m^{-2}$) except otherwise. The equation is instantaneous, so valid for instants and then it can be integrated in time to evaluate accumulation of fluxes in terms of energy. Soil moisture controls the partition of latent and sensible heat, and then, the evaluation of the moisture is the key to estimate AET.

Evapotranspiration links the water balance to the surface energy balance (van der Kwast, Timmermans et al. 2009); therefore its quantification is important. As it is mentioned in section 1.1 there are different methods to estimate the evapotranspiration. Remote sensing (RS) is a valuable tool which can be used for the surface energy balance. Therefore models were developed to incorporate RS; one of these models is SEBS.

SEBS and other energy balance models, were developed to estimate atmospheric turbulent fluxes and surface evaporative fraction at the time of the image using satellite earth observation data in the visible, near infrared, and thermal infrared frequency range, in combination with meteorological data (Su 2002). Extrapolation to daily values relies in energy ratios that remain relatively constant in time.

2.1.2. Evapotranspiration

The combination of water lost from the soil surface by evaporation and from the crop by transpiration is referred to as evapotranspiration (Allen, Pereira et al. 1998).

The reference crop evapotranspiration or reference evapotranspiration (ET_o) is the ET rate from a reference surface not short of water. The reference surface is a hypothetical grass reference crop with specific characteristics (crop height of 0.12 m, a fixed surface resistance of 70 $s.m^{-1}$ and an albedo of 0.23, closely resembling the evapotranspiration from an extensive surface of green grass of uniform height, actively growing, well-watered, and completely shading the ground) (Irmak and Haman Z. 2003). As water is fully replenished, the only factors affecting ET_o are climatic parameters. Consequently, ET_o is a climatic parameter and can be computed from weather data.

The ET_o can be estimated using the equation number 6 propose in FAO56 (Allen, Pereira et al. 1998):

$$ET_o = \frac{0.408\Delta\left(Rn - G\right) + \gamma \frac{900}{T + 273} u_2 \left(e_s - e_a\right)}{\Delta + \gamma\left(1 + 0.34 u_2\right)}$$ **Equation 2**

Where 'ET_o' reference evapotranspiration ($mm.day^{-1}$), 'R_n' net radiation at the crop surface ($MJ.m^{-2}.day^{-1}$), 'G' soil heat flux density ($MJ.m^{-2}.day^{-1}$), 'T' air temperature at 2 m height (°C), 'u_2' wind speed at 2 m height ($m.s^{-1}$), 'e_s' is the saturation vapour pressure (kPa), 'e_a' actual vapour pressure (kPa), 'e_s-e_a' saturation vapour pressure deficit (kPa), 'Δ' slope vapour pressure curve ($kPa.°C^{-1}$), 'γ ' psychrometric constant ($kPa.°C^{-1}$).

Allen, Pereira et al.(1998) defines the crop evapotranspiration under standard conditions (ET_c) as the ET free from disease, well fertilized crops, grown in large fields, under optimum soil water conditions, and achieving full production under the given climatic conditions.

$$ET_c = K_c ET_o$$ **Equation 3**

Where 'ET_c' crop evapotranspiration ($mm.day^{-1}$), 'K_c' crop coefficient (dimensionless), 'ET_o' reference crop evapotranspiration ($mm.day^{-1}$).

The crop evapotranspiration under non-standard conditions (ET_{cadj}) is the ET from crops grown under management and environmental conditions that differ from the standard due to non-optimal conditions such as the presence of pests and diseases, soil salinity, low soil fertility, water shortage or water logging. The following equation is proposed when evaporation from the soil is not a large component (Allen, Pereira et al. 1998).

$$ET_{cadj} = K_s K_c ET_o$$ **Equation 4**

Where 'K_s' describes the effect of water stress on crop transpiration (for soil water limiting conditions, $0 < Ks \leq 1$ and where there is no soil water stress, Ks = 1). The effect of water stress can be expressed as follow:

$$K_s = \frac{TAW - D_r}{\left(1 - p\right)TAW}$$ **Equation 5**

Where 'TAW' is the total available soil water in the root zone (mm), 'D_r' is the root zone depletion (mm) and 'p' is the fraction of TAW that a crop can extract from the root zone without suffering stress (dimensionless), values for 'p' are listed in table 22 of FAO 56 paper (Allen, Pereira et al. 1998).

Figure 2-1 Water stress coefficient, Ks

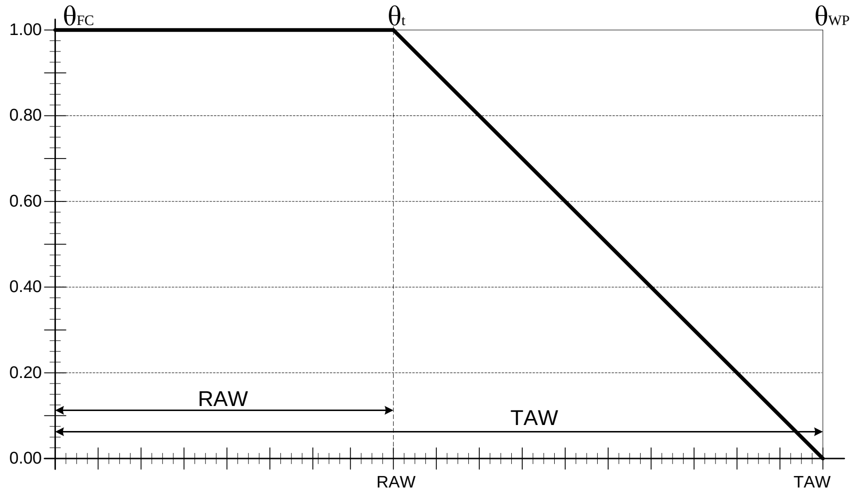

Source: FAO 56 paper, page 167.

When soil water is extracted by evapotranspiration, the depletion increases and stress will be induced when D_r becomes equal to RAW. After the root zone depletion exceeds RAW (the water content drops below the threshold (θ_t), the root zone depletion is high enough to limit evapotranspiration to less than potential values and the crop evapotranspiration begins to decrease in proportion to the amount of water remaining in the root zone (Figure 2-1).

The total available soil water in the root zone (TAW) can be expressed as:

$$TAW = 1000(\theta_{FC} - \theta_{WP})Z_r$$ **Equation 6**

Where 'θ_{FC}' is the water content at field capacity ($m^3.m^{-3}$), 'θ_{WP}' is the water content at wilting point ($m^3.m^{-3}$) and 'Z_r' is the root depth (m).

Finally the root zone depletion at the end of one day (D_r) is expressed as:

$$D_{r,i} = D_{r,i-1} - (P - R)_i - I_i - CR_i + ET_{c,i} + DP_i$$ **Equation 7**

Where subindex 'i' stands for the end of day 'i'and 'i-1' the end of the previous.
'D_r' is the root zone depletion, 'P' is the precipitation, 'R'is the runoff from the soil surface, 'CR' is the capillary rise from the groundwater table, 'ET_c'' is the crop evapotranspiration and 'DP' is the water loss out of the root zone by deep percolation, all units in [mm].

2.1.3. Soil characteristics

2.1.3.1. Soil moisture

Soil Moisture (SM) is the content of a mass of water in a mass of soil and depends on the physical and chemical characteristics of a soil to hold water (soil water content). SM is essential for vegetation grow, soil aeration, microbial activity, the movement of nutrients to in the soil to the roots, etc.

Two distinctive moisture points, in the SM curve, are the wilting point and the field capacity. The wilting point is the minimal of soil moisture at −1500 KPa of suction pressure that is considered the minimum soil holding pressure before no water can be extracted by the soil for the crop. The field capacity is the soil moisture held in the soil after excess of water drains; the field capacity is defined as the water content at -33 KPa of suction pressure.

2.1.3.2. Soil texture

The soil texture is defined by the distribution and size of the particles in the soil. Therefore a classification is made according their sizes in a textural triangle where the axes are: Sand, Silt and Clay in percentages.

There are different methods for the realization of the texture classification; however the USDA (United States Department of Agriculture) is widely used and moreover the FAO-UNESCO recommends its use.

2.1.3.3. Hydraulic conductivity

Hydraulic conductivity, describes the ease which water can move through a porous medium such as a soil profile. It depends on the intrinsic permeability of the material and on the degree of saturation. Saturated hydraulic conductivity, describes water movement through saturated media with no cracks (preferential flow).

The Pedotransfer function (PTF) is a predictive function of certain soil properties from other more available, easily, routinely, or cheaply measured properties. With these PTF is possible to find out the hydraulic conductivity or build up an estimate of the water retention curve (pF).

There are several models (even expressed in software) able to use these PTF to determine some of the hydraulic properties of the soil. For instance the Hydrus-1D uses de Rosetta module (that includes many models) to get the soil characteristics.

2.1.3.4. Van Genuchten-Mualem model

The van Genuchten Mualem model has been widely used to describe soil hydraulic behaviour resulting from the non-linear interactions of soil water pressure, saturation level, and hydraulic conductivity (Seaman, Singer et al. 2009).

$$\theta = \frac{\left(\theta_{sat} - \theta_{res}\right)}{\left(1 + \left|\alpha\Psi\right|^{n}\right)^{m}} + \theta_{res}$$

Equation 8

$$K(\Psi) = K_{sat} \frac{\left| 1 - (\alpha|\Psi|)^{nm} \left(1 + (\alpha|\Psi|)^{n}\right)^{-m} \right|^{2}}{\left(1 + (\alpha|\Psi|)^{n}\right)^{ml}}$$ **Equation 9**

Where ‘K(ψ)’ is the unsaturated hydraulic conductivity (m), ‘θ’, ‘θ_{sat}’, and ‘θ_{res}’ represent the actual, saturated, and residual water contents ($m^3.m^{-3}$), respectively, ‘α’ is the soil retention function (m^{-1}), ‘l’ is the pore connectivity and tortuosity factor, ‘ψ’ is the pressure head (m), ‘K_{sat}’ is the saturated hydraulic conductivity ($m.s^{-1}$), and ‘m’ (-) and ‘n’ (-) are water retention curve parameters (Seaman, Singer et al. 2009). The pore connectivity parameter ‘l’ in the hydraulic conductivity function is usually assumed to be 0.5 as an average for many soils. Finally ‘m’ can be obtained as function of ‘n’ ($m = 1 - n^{-1}$) (Simunek, Kodesova et al. 1999).

2.1.4. Water movement models

The water movement in the soil starts with the infiltration, under the force of gravity. After the water achieves some depth it begins to percolate and ultimately reach the ground water zone.

This water movement among the soil is governed by several factors, such as the water content in the soil, the head pressure, characteristics of the soil (texture, bulk density, hydraulic conductivity, etc), presence of roots, etc. The movement can occur both vertical and horizontal.

Some models have been developed to understand and explain this process. The model Hydrus-1D uses the Richard’s equation. This equation (explained in section 3.1) represents the movement of the water in one dimension.

2.2. Description of the study area

2.2.1. Location

The study area is situated in the Guareña basin which is located in the western part of Spain between 5º23’W to 5º44’W and 40º53”N to 41º32’N (Figure 2-2), the estimated area of this basin is 1080 km^2. The area of REMEDHUS network mostly falls in the Guareña river basin.

Figure 2-2 Localization of the study area in Spain

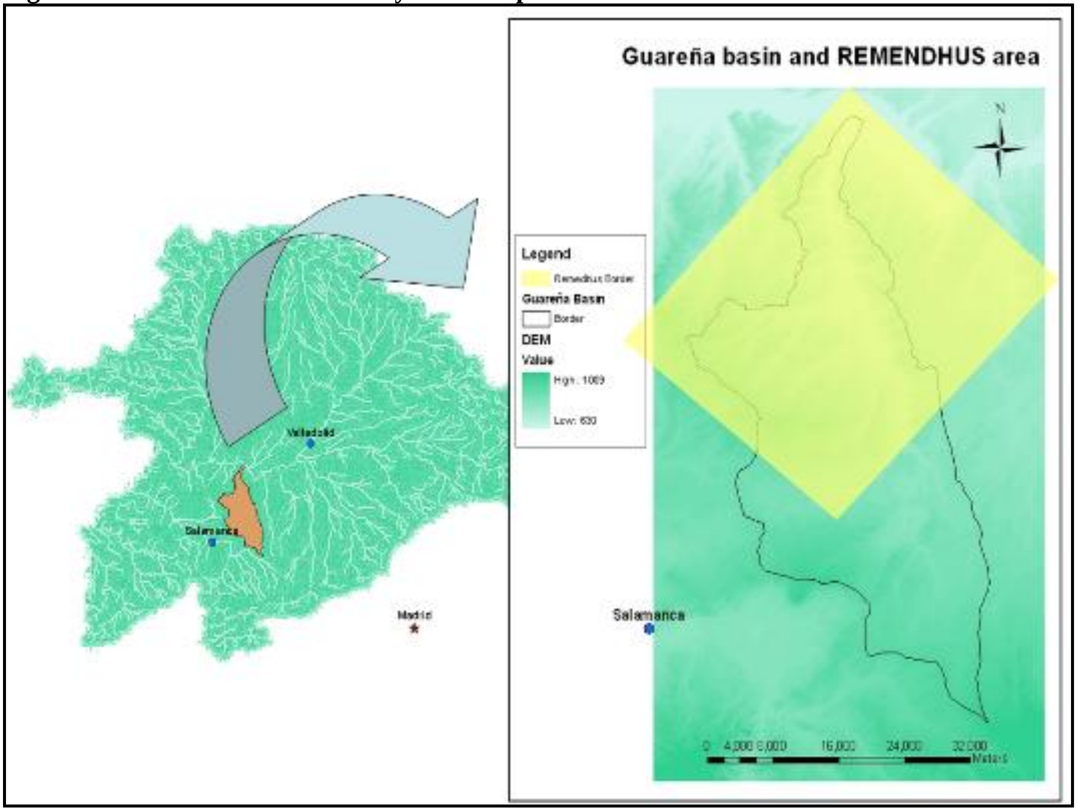

2.2.2. Climate

2.2.2.1. Precipitation

The Guareña catchment has a semi-arid Mediterranean environment characterized by low annual precipitation and hot dry summers. The six year average precipitation from three weather stations is about 430 mm per year. With rainfall records of 8.4 mm and 77.3 mm, July and October are the driest and wettest months respectively.

2.2.2.2. Temperature

The temperature of the basin varies considerably between summer and winter. The average temperature is about 12 °C. July and August are the hottest months while December and January are the coldest. Temperatures records as high as 37 °C and as low as -10 °C were recorded during the period 2002 to 2007.

2.2.3. Land cover and land use

The percentage of agricultural land occupation fluctuates around 74%. The seasonal agricultural activities are:

Table 1 Crop calendar

Condition	Crop	Planting	Maximum	Harvesting
Irrigated	Potatoes	April	June	September
	Maize	April	August	November
	Sugar beat	March	July	October
	Alfalfa	April	June	More than 1
	Sunflower	April	July	October
Not irrigated	wheat	February	May	June
	Oat	February	May	June
	Barley	February	May	June
	Lentil	March	June	July
Variable	Vineyard	--	June	September

The land use in the area is mainly rain feed agriculture, with small but significant proportion of supplementary irrigation schemes (Carabias-Martínez, Rodríguez-Gonzalo et al. 2003).

2.2.4. Soils

The soil in Guareña basin and in REMENDHUS area is mainly sandy (mean sand content 71%). Sand is present as first horizon, and occasionally there are clayey horizons at the bottom of the profiles. The organic matter content is very low (mean, 0.9%) (Martínez-Fernández and Ceballos 2005).

In Figure 2-3 shows the 150 soil samples collected from the REMENDHUS network database, these soil samples shows that the presence of sand is very high in all the area. In appendix A is summarized these 150 soil samples.

Figure 2-3 Soil texture in REMENDHUS area

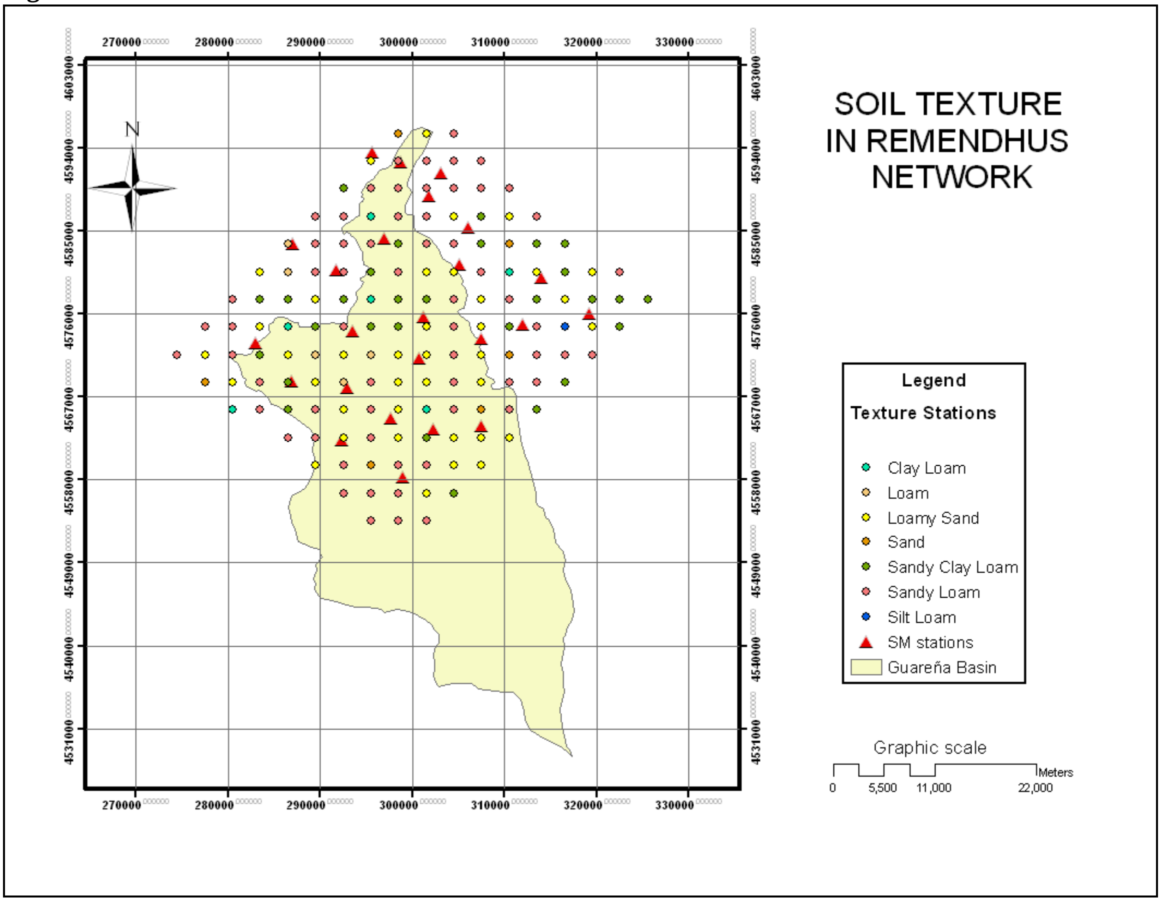

3. Data analysis

3.1. Hydrus-1D

3.1.1. Introduction

Hydrus-1D is a numerical model for analysis of water movement, heat and solute transport in variably saturated porous media. It is a finite element model that solves Richards' equation for flow. Information on soil texture and moisture, climatic factors and water uptake can be used to determine the actual evapotranspiration (Simunek, Van Genuchten et al. 2005).

This model estimates actual ET (AET) by using meteorological, physiographic, physiological and geographical data. The user obtains AET, from the model output, by the addition of the estimates for "actual root uptake" and "actual surface evaporation". It estimates infiltration, and surface runoff as the difference between precipitation and infiltration. Hydrus-1D is sensitive to time-step definition, and may require iterative runs to find an acceptable output (Hauser 2008).

Hydrus-1D requires a calibration to obtain adequate results. The parameter optimization module in Hydrus-1D uses the Marquardt-Levenberg optimization algorithm, it re-runs the model as many times as it needs while adjusting its parameters until discrepancies between selected model outputs and field measurements is reduced to a minimum in the weighted least-squares sense (Simunek, Van Genuchten et al. 2005). This thesis uses this algorithm for optimization.

For this project the soil hydraulic properties measured in the field by ITC and USAL in several campaigns are set, and the initial estimates of water content is iteratively improved during the minimization process until a desired degree of precision is obtained with the soil moisture field measurements (observed values).

3.1.2. Basic theory of the model

Hydrus-1D works essentially with the Richards' equation for flow:

$$\frac{\partial \theta}{\partial t} = \frac{\partial}{\partial x}\left[K\left(\frac{\partial h}{\partial x} + \cos\alpha\right)\right] - S$$

Equation 10

Where 'h' is the water pressure head (cm), 'θ' is the volumetric water content ($cm^3.cm^{-3}$), 't' is time (day), 'x' is the spatial coordinate (cm) (positive upward), 'S' is the sink term ($cm^3.cm^{-3}.day^{-1}$], 'α' is the angle between the flow direction and the vertical axis and 'K' is the unsaturated hydraulic conductivity function [$cm^3.day^{-1}$].

The model requires introducing an initial water pressure head, which in the process of the model will be adjusted. The angle between the flow direction and the vertical axis is assumed

0. The unsaturated hydraulic conductivity is obtained from the intern model Rosetta of Hydrus-1D, which solves the pedotransfer function.

The sink term, S, is defined as the volume of water removed from a unit volume of soil per unit time due to plant water uptake. Simunek et al. (2005) defined S as:

$$s(h) = \alpha(h) S_p \qquad \textbf{Equation 11}$$

Where the root-water uptake water stress response function ‘α(h)’ is a prescribed dimensionless function of the soil water pressure head ($0 \leq \alpha \leq 1$), and ‘S_p’ the potential water uptake rate (day^{-1}). Hydrus-1D offers 2 root water uptake models: Feddes and S-Shape. For this research the Feddes model is used because it is possible to use a database where all the parameters for different crops are described. The database is adequate for the crops in Guareña.

After all the initial conditions are defined, it is necessary to build up a scheme of the soil profile column. In this scheme it is specified the depth of the profile, the variation of the root water uptake, the water pressure head, the material (soil texture) and water content. It is also possible to declare points of control at different depths, where output will be explicit.

Finally the model runs and the iterative process continues until a satisfactory degree of convergence is obtained, i.e., until at all nodes in the saturated or unsaturated region the absolute change in pressure head or water content between two successive iterations becomes less than some small value determined by the imposed absolute pressure head or water content tolerance (Simunek, Van Genuchten et al. 2005).

3.1.3. Selection of the time period

Data in soil moisture and meteorology is available since 2006 to 2009. It is possible to differentiate two periods in the REMEDHUS area (Figure 1-1, notice that the numbering in the evapotranspiration axis is inverted for displaying purposes) among a year.

Figure 3-1 Annual distribution of precipitation and potential evapotranspiration.

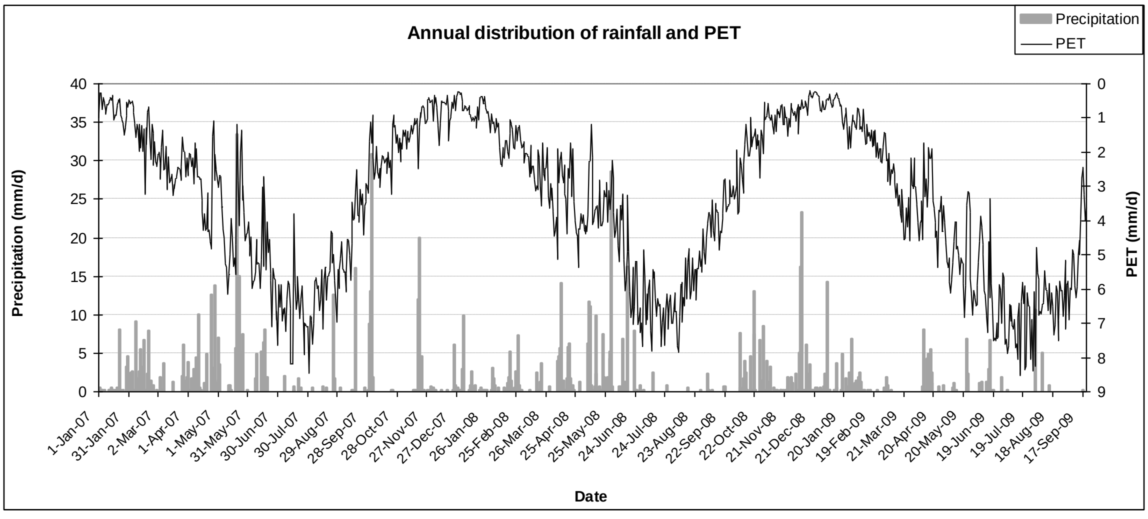

During the months of summer (June, July and August) the precipitation is low and potential evapotranspiration presents higher values that the rest of the months, on the other hand during the months of winter (November, December and January) the potential evapotranspiration shows lower values.

The selection of sites for this research was based on the availability of the data, yielding 6 possible sites to make the modelling (E10, L03, H09, Q08, K10 and J14). However from these 5 stations only 3 fulfil the conditions to be selected for the modelling, i.e., have a crop in the area and SM series without errors or many blanks. These stations are K10 (wheat), Q08 (wheat, onion and sugar beet) and J14 (sunflower).

Figure 3-2 Vegetative cycle of wheat and maize in the study area

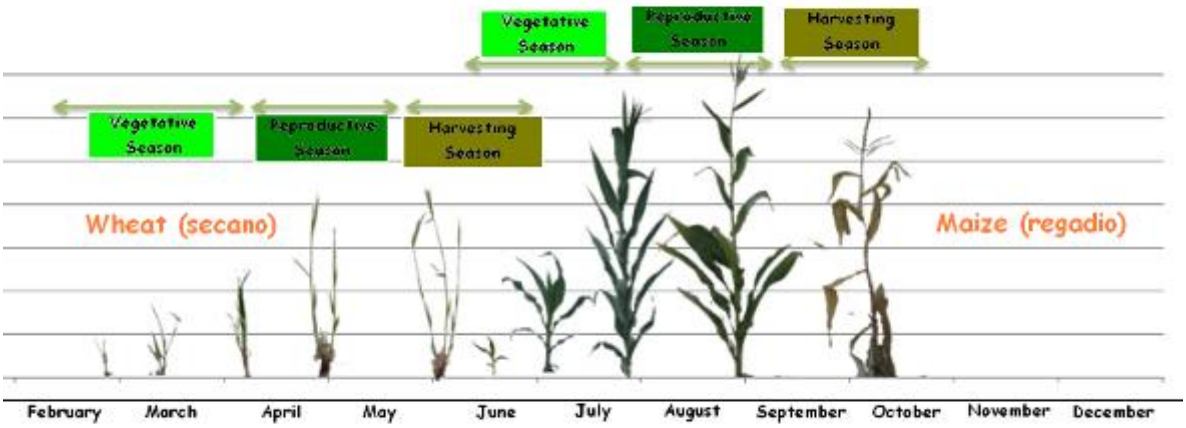

From Sanchez Martin (2009)

In two sites the crop is wheat and irrigation does not take place in the cycle of this crop, and in the other cases the crops are under irrigation.

The vegetative cycle (Figure 3-2) for the wheat starts in February and the harvesting is during the months June and July. Consequently the time period selected for this research is from January to July of the years 2006 to 2009. In the case of the other crops (sunflower, sugar beet and onion) the period selected is from April to October (see Table 1).

3.1.4. Input data

3.1.4.1. Meteorological

The meteorological data includes precipitation (mm.d^{-1}), solar radiation (MJ.m^{-2}), minimum and maximum daily temperatures (°C), relative humidity (%), wind speed (m.s^{-1}) and hours of solar sunshine (hr). These data is collected from the nearest meteorological stations and the time step is every 10 minutes in 3 stations (Villamor, Ema Granja and Ema Canizal stations) and daily in the rest of the stations. Therefore for location Q08 meteorological data is used from station VA_02, for location K10 meteorological data is used from station Ema Granja and for J14 data from Ema Cañizal is used (Figure 1-1).

3.1.4.2. Soil moisture

The observed values of soil moisture have been collected from the University of Salamanca (USAL). This data set consists in voltages of the hydra probe at the depth of 5 centimeters. The voltages were converted into soil moisture measurements using the calibration equation of the measuring equipment (done at USAL). Some of these values showed unusual behaviours and filters were used to smooth the pattern. For the parameter optimization the model requires the position, type and description of each observed value. See in appendix B.

3.1.4.3. Soil hydraulic properties

Hydrus-1D needs the characterization of the hydraulic properties of the soil, and the user can specify among six types of models to get these properties. For this research Rosetta (Neural Network Prediction) is used to predict the van Genuchten-Mualem soil hydraulic properties. In this case soil texture, bulk density and two retention points are used as predictors. This corresponds to the ideal number of predictors, increasing considerably the degree of accuracy of the predictions (Schaap, Leij et al. 2001).

The available soil data at the selected positions are:

Table 2 Available soil data

Station	Depth	Sand (%)	Silt (%)	Clay (%)	ρ (g/cm^3)	θ_{33} (cm^3/cm^3)	θ_{1500} (cm^3/cm^3)
K10	5 cm	91.16	5.71	3.31	1.36	0.041	0.022
Q08	5 cm	86.07	5.68	8.25	1.46	0.075	0.036
J14	5 cm	66.81	80.98	12.21	1.50	0.141	0.041

Where 'ρ' is the bulk density of the soil, 'θ_{33}' is the water content at 33 kPa suction (field capacity) and 'θ_{1500}' is the water content at 1500 kPa suction (wilting point). With these soil data the neural network prediction of Hydrus-1D is used to obtain the soil hydraulic properties.

With these soil parameters, Rosetta is used for the determination of the necessary parameters (initial values) for the van Genuchten-Mualen model. Then in Hydrus-1D is specified that this initial parameters are going to be iterated until the SM predicted is close enough to the SM measured in field. The optimization produces the final values of these parameters at the end of the process (Table 3). In addition to these initial values it is also necessary to define the boundary values (lower and upper limit). The process was carried out interactively and the outputs of this process are summarized in Table 3.

Table 3 Predicted soil hydraulic properties

Variable	Initial value	Final value	Lower limit	Upper limit
K10 Station				
Residual Water content ($cm^3.cm^{-3}$)	0.031	0.0065	0.001	0.01
Saturated water content ($cm^3.cm^{-3}$)	0.416	0.448	0.0925	0.803
Alpha (cm^{-1})	0.053	0.013	0.00394	0.0221
n (-)	2.57	1.82	1.48	2.16
Hydraulic conductivity ($cm.day^{-1}$)	100.19	90.4	10	325
l (-)	0.5	0.5	0.5	0.5
Q08 Station				
Variable	**Initial value**	**Final value**	**Lower limit**	**Upper limit**
Residual Water content ($cm^3.cm^{-3}$)	0.03	0.0346	0.01	0.154
Saturated water content ($cm^3.cm^{-3}$)	0.4	0.458	0.282	0.634
Alpha (cm^{-1})	0.062	0.066	0.0192	0.151
n (-)	1.78	1.32	1.1	1.53
Hydraulic conductivity ($cm.day^{-1}$)	56.17	27.9	10	1320
l (-)	0.5	0.5	0.5	0.5
J14 station				
Variable	**Initial value**	**Final value**	**Lower limit**	**Upper limit**
Residual Water content ($cm^3.cm^{-3}$)	0.02	0.004	0.001	0.03
Saturated water content ($cm^3.cm^{-3}$)	0.36	0.31	0.24	0.38
Alpha (cm^{-1})	0.35	0.03	0.01	0.06
n (-)	1.37	1.45	1.19	1.71
Hydraulic conductivity ($cm.day^{-1}$)	79.68	120	22.72	216.86
l (-)	0.5	0.12	0.5	1.19

Where 'θ_r' and 'θ_s' are the residual and saturated water content respectively, 'α' and 'n' are parameters in the soil water retention function, 'K_s' is the saturated hydraulic conductivity and 'l' is the tortuosity parameter in the conductivity function. In Table 3 are the adjusted final values after optimization.

Using the Equation 8 and Equation 9, and the values of the parameters from the last table is possible to build up the modelled water retention curves. Figure 3-3 explains these typical physic properties of the soil: to high head pressure the water content in the soil is low (until it is achieved the wilting point at 1500 KPa) and to low pressures the water content is higher. On the other hand the hydraulic conductivity is higher when the water content is higher in the soil and is lower when this water content is near to the wilting point.

Figure 3-3Water retentions curves for stations K10, Q08 and J14

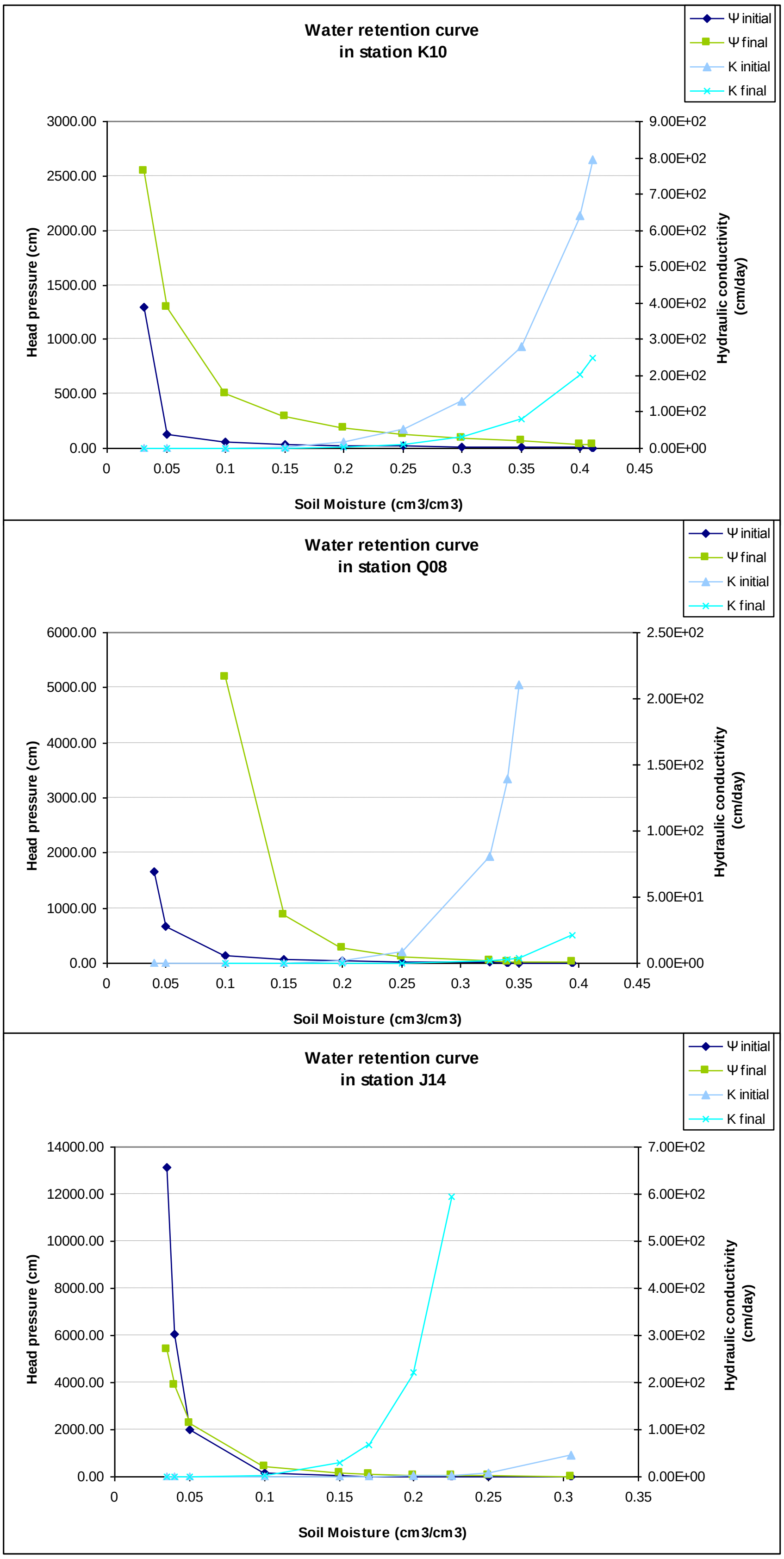

3.1.4.4. Physiological and geographical data

The physiological and the geographical data has been measured in the field and supported with the literature review. There are stations situated over wheat, one over sunflower and finally a station over onion and sugar beet. Sanchez Martin (2009) proposes a variable root depth according to the station. The altitude and coordinates were taken in the field work using a GPS. These properties are summarized in the next table.

Table 4 Geographical and physiological properties

Station	X	Y	Altitude (m)	Crop	Max. Root depth (m)	Max. Crop height (m)
K10	300702	4571119	723	Wheat	0.90	0.70
Q08	319187	4575901	800	Wheat	0.90	0.70
Q08	319187	4575901	800	Sugar beet	1.06	0.30
Q08	319187	4575901	800	Onion	0.30	0.40
J14	298915	4558267	752	Sunflower	1.00	1.6

3.1.5. Modelling

Since modelling is a process which helps to understand or simplify the reality of the world, its needs a thorough job to obtain the nearest results to the reality. Modelling requires calibration and validation.

3.1.5.1. Calibration

Because Hydrus-1D allows using the Marquardt-Levenberg optimization algorithm, the results are quite near to the observed values. For this research the water content was optimized as data was available from sensors. After the prediction of the soil hydraulic properties, minimum and maximum values are assigned to each parameter, these new values are necessary to realize the iteration only in this range. Then a comparison is done among the water content predicted and the measured in field (observed values), therefore is necessary to specify the day of measurement as well as the depth of this measurement. The depth of the measurements is 5 cm below the surface in all the SM stations, appendix B summarizes these soil moisture observed. The final result of this optimization ended up by adjusting the initial soil parameters to the final values that were already presented in Table 3.

The first calibration attempt showed a reasonable fit to the observed values during the second stage of drying-up as the slope of the soil moisture in time was reproduced. This is positive in the sense that the model was reproducing the rate of the moisture extraction, obviously related to evaporation. However this model does not represent very well the wetting moments and the steepness of the initial drying up. Figure 3-4 and Figure 3-5 shows these first attempts of calibration.

Figure 3-4 Calibration of the model in K10 station (first attempt)

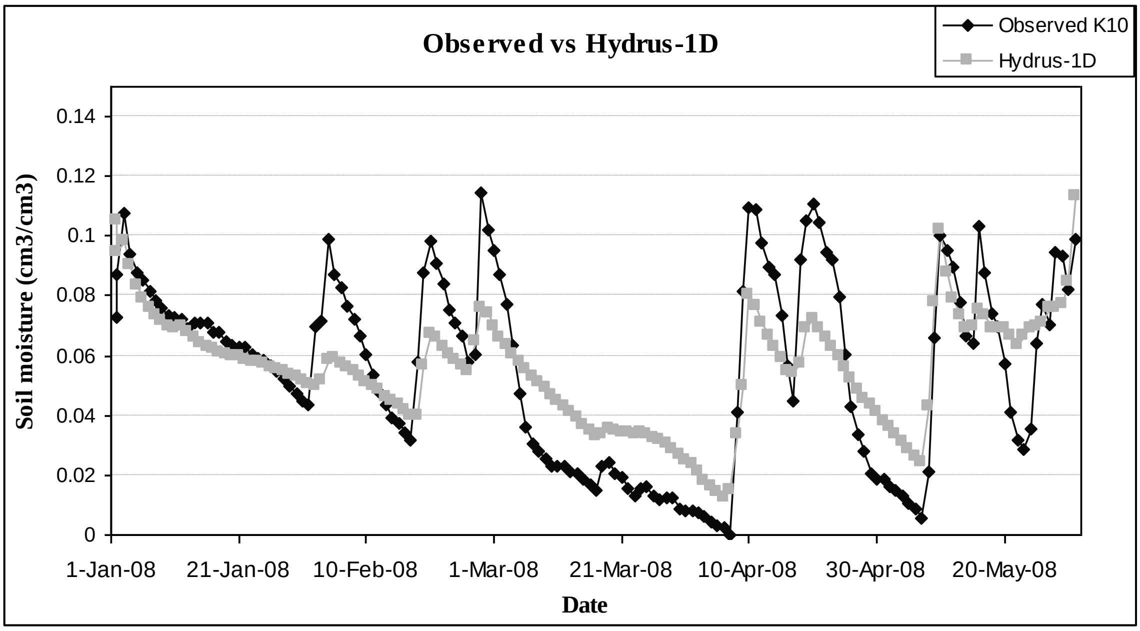

Figure 3-5 Calibration of the model in Q08 station (first attempt)

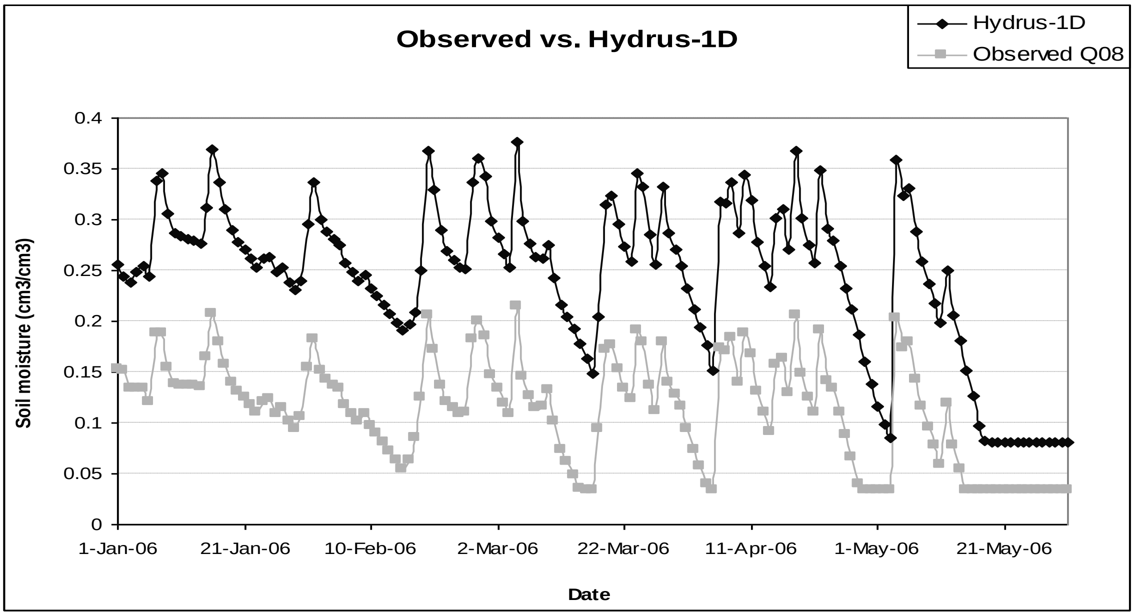

Several attempts were made to calibrate the model modifying and calibrating all the possible parameters. In Figure 3-5 the trend was observed but there was a consistent bias that could only be explained by a bias in the initial conditions of the run and the input meteorological variables, specifically in the rainfall. There are few stations measuring rainfall in the area. For station K10 the distance to the nearest meteorological station is 6 kilometers, for station Q08 the distance is 10 kilometers and for station J14 the distance is 5.4 kilometers.

Researchers from USAL and ITC established in the area, have revealed and reported severe deficiencies in the distribution of the rainfall stations, as rainfall varies in space and time more than expected (Guido Baroncini Turricchia, personal communication). Contrarily, the second research area (SARDON), which is close to the area of this research, shows a quiet uniform rainfall distribution as landforms does not play a major role. Researchers are considering increasing the number of stations considerably, as costs permit, to be better situated to close the Water Balance.

Figure 3-6 Soil moisture in station K10 and input precipitation for the model

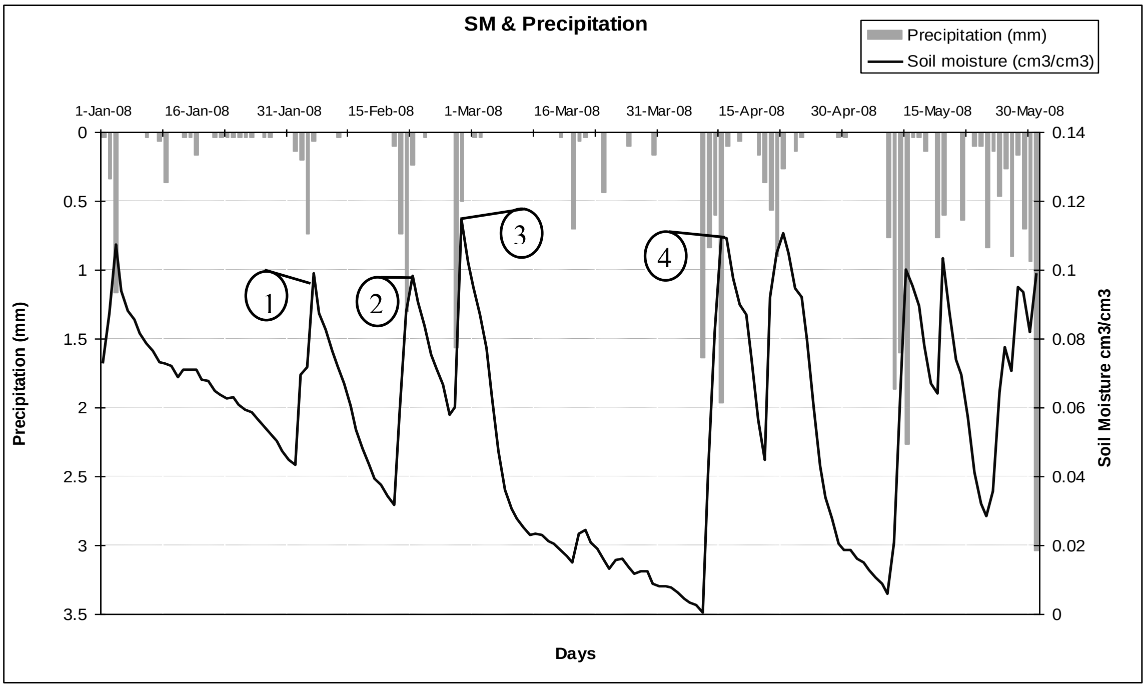

This information explains why in this experiment the rainfall bias is constantly negative. This is a clear indication that the input rainfall measured in the stations does not match to the site without a correction. Figure 3-6 shows these discrepancies, and for instance, in the soil moisture curve peak 1 is similar to peak 2 however for this last peak a heavier rainfall has occurred therefore this peak should be higher; same behaviour is for peaks 3 and 4 where a heavier rainfall occurred in peak 4 however the soil moisture is lower than peak 3 where a slight rainfall occurred.

Figure 3-7 Double mass curve for station K10

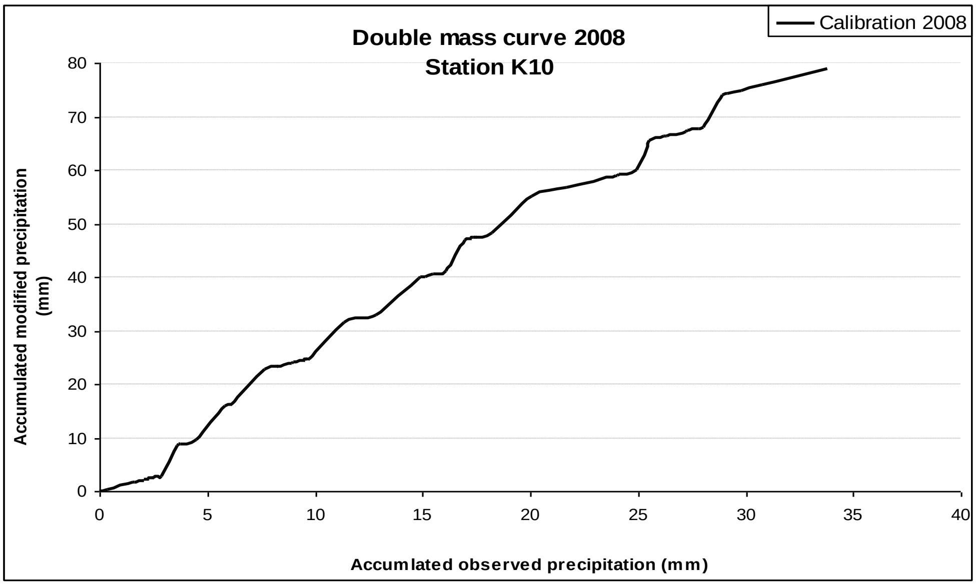

Figure 3-8 Double mass curve for stations Va_02 and Villa Amor

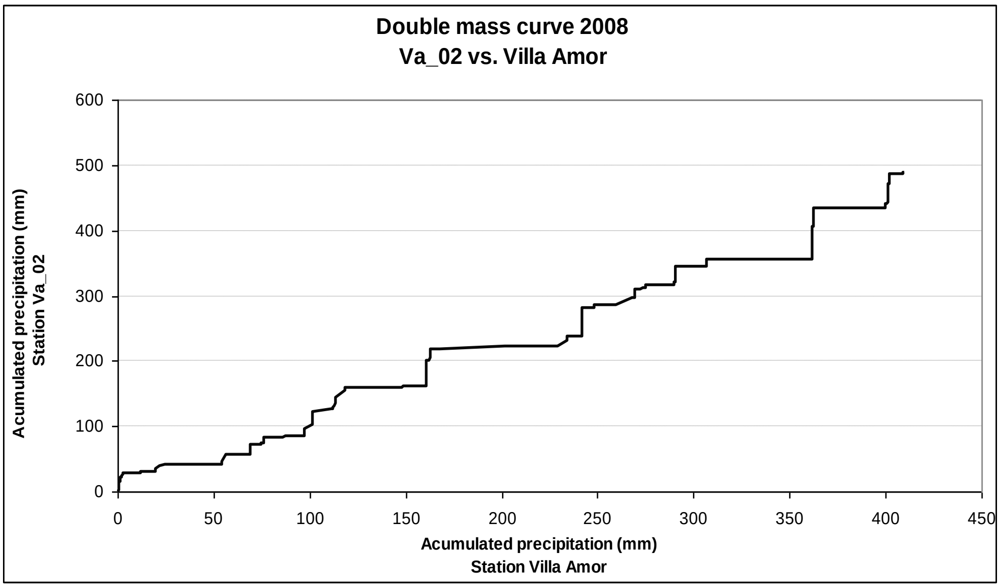

Hence there is no possibility of establishing a good modelling on a daily time step without the correction of the bias in the input rainfall. Therefore the bias increment was implemented to the peak of precipitation events and consequently the fitness of both curves improved considerably. The double mass curve in Figure 3-7 shows that the rainfall modified and the observed have some discrepancies, therefore the slope in these curve changes several times supporting the idea that the initial input precipitation does not correspond or relate to the soil moisture station. Similar behaviour occurred in both soil moisture stations. From Figure 3-8 also is possible to conclude that the precipitation is not well represented just with this station.

Figure 3-9 Final calibration of the model in K10 station

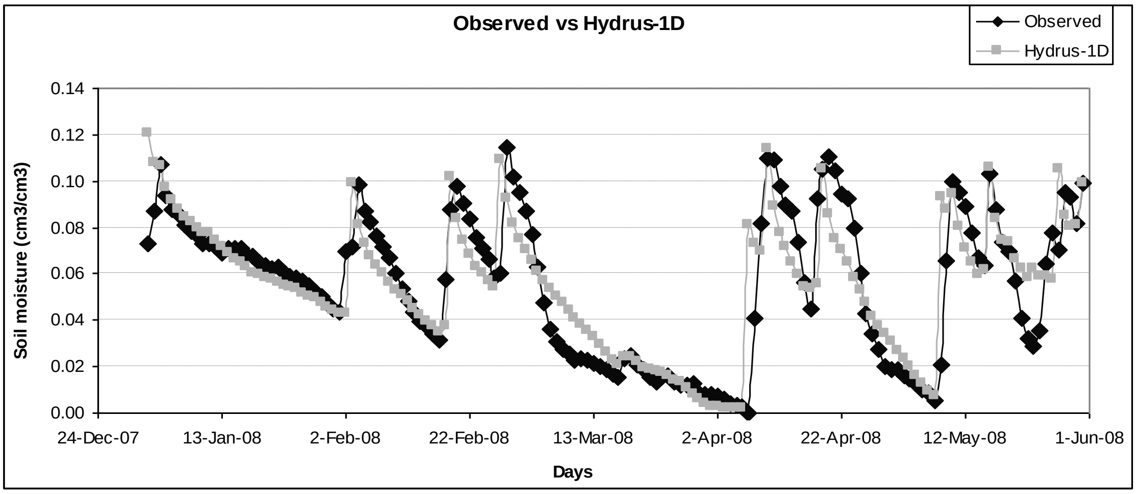

Figure 3-9 and Figure 3-10 shows the final adopted calibration of Hydrus-1D for stations K10 and Q08. The R-squared value for station K10 is 0.72 and for station Q08 is 0.81.

Calibration for station Q08 followed the same procedure, therefore some inconsistencies occurred due the precipitation, in Figure 3-10 the zones 1 and 2 shows a lower values in the observed soil moisture than the modelled by Hydrus-1D. This is because the rainfall has been modified only by increasing some peaks of the precipitation, and in this case it is necessary to obviate some rainfall because they might not occur in the experimental area.

Figure 3-10 Final calibration of the model in Q08 station

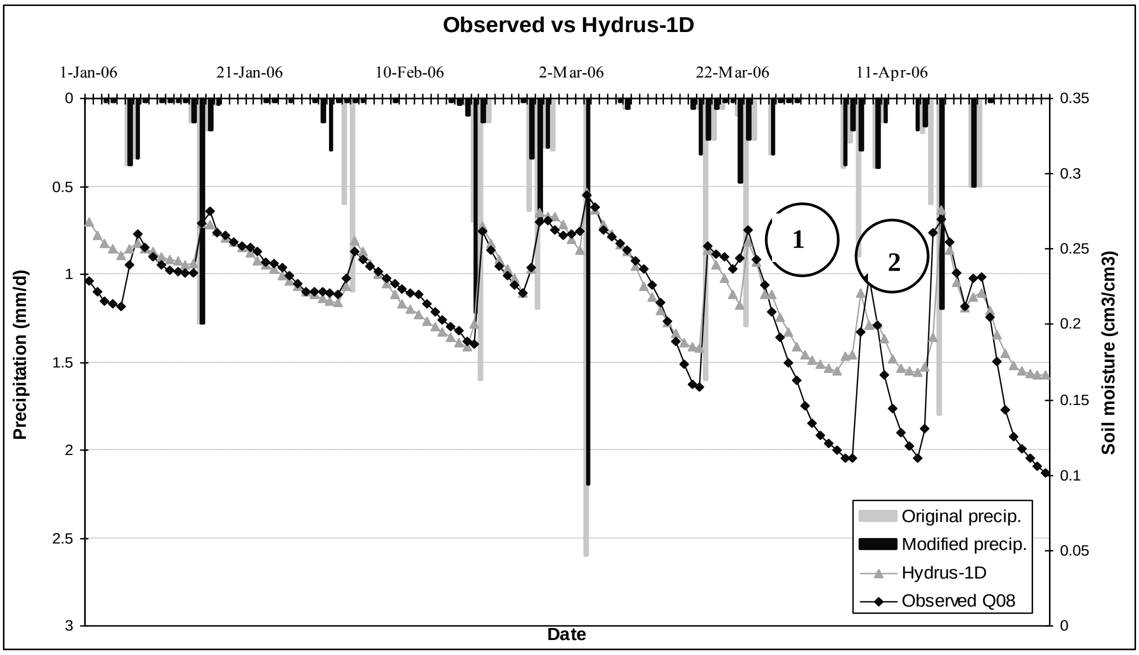

As it is displayed in the last figure, the modification in precipitation yields a quite good representation of the SM, however in some days this representation does not match very well due the process followed for this modification was only increasing or decreasing the amount of rainfall, and no the omission or addition of rainfall events. The database of SM measurements is quite trustful because of the validation done by work and research (USAL and ITC researches) which has proved good results. The data is also validated every two weeks with independents measurements with other instrumentation.

3.1.5.2. Model Validation

The model validation process is done in order to verify that the model adjust well to other period independent from the period that was used for calibration. If the model can not reproduce the observations, then it must be reviewed or rejected. Therefore for station K10 the year 2008 was used for calibration and years 2006, 2007 and 2009 for validation. For the station Q08 year 2006 is used for calibration and years 2008 and 2009 validation.

The following graphs show the comparison between field measurements of soil moisture and water content from the model Hydrus-1D.

Figure 3-11 validation in K10 for year 2006

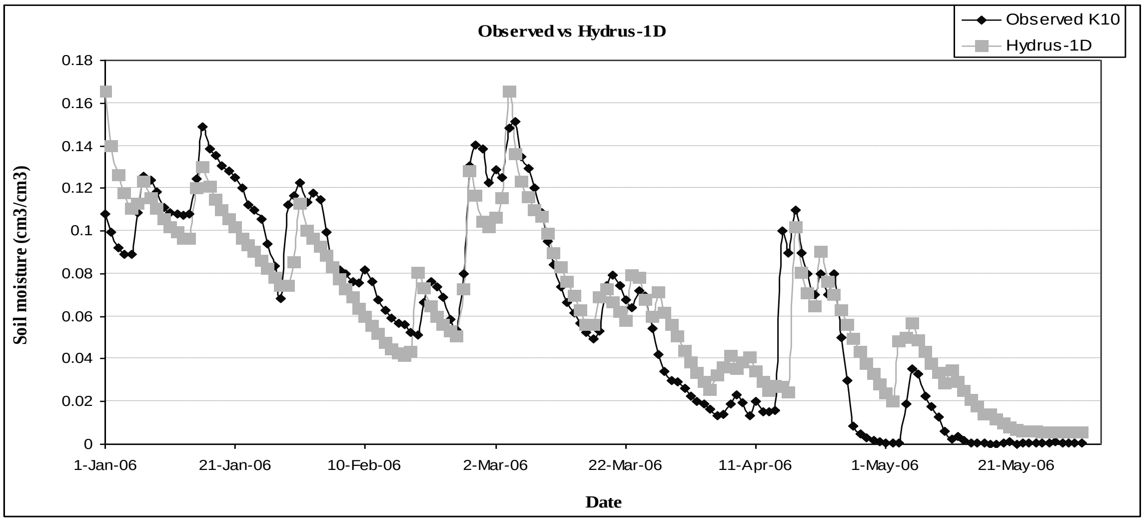

Figure 3-12 Validation in K10 station for year 2007

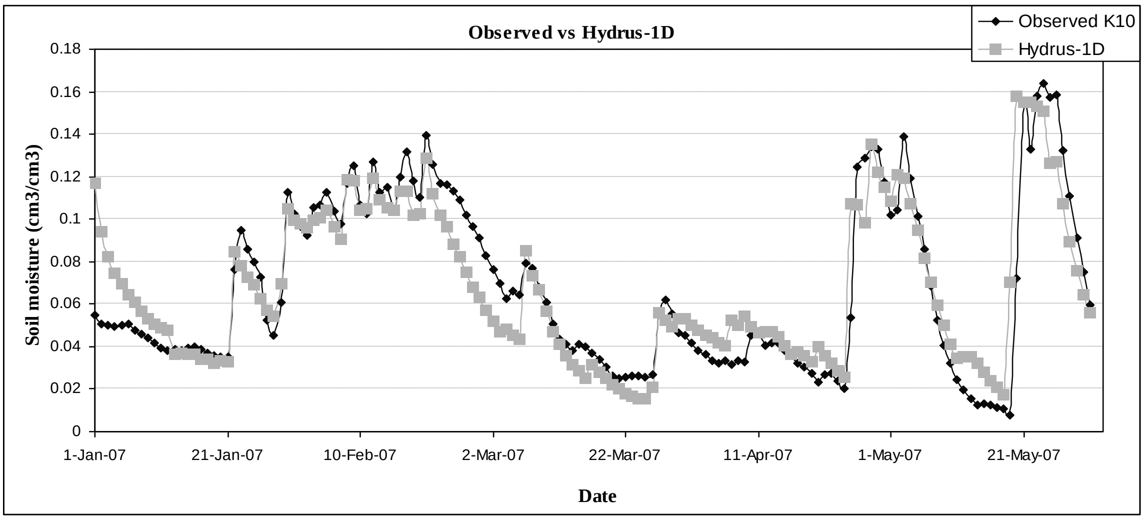

Figure 3-13 Validation in K10 station for year 2009

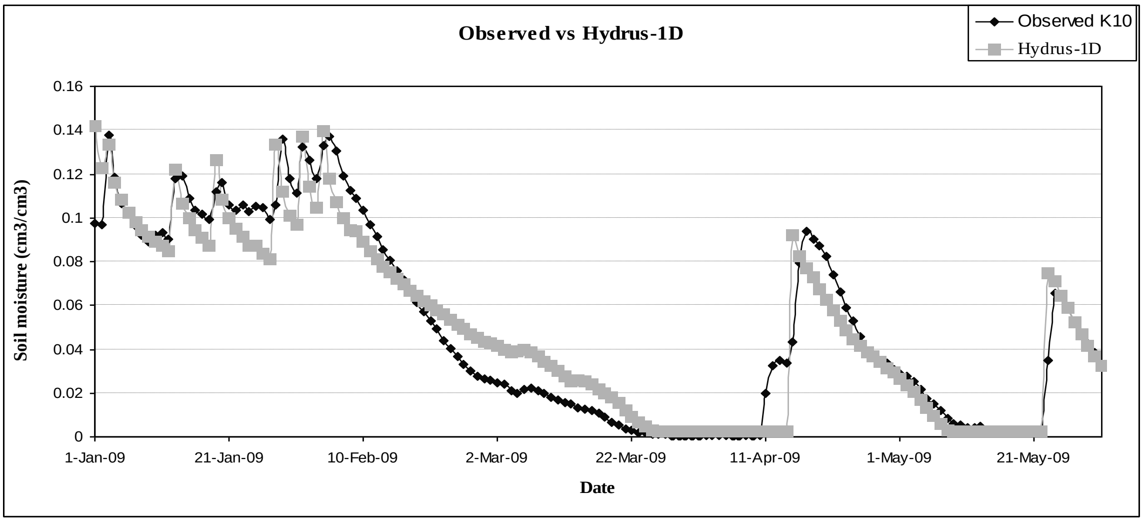

Table 5 R-squared values from the linear regression for station K10

Year	R-squared
2006	0.828
2007	0.813
2008	0.724
2009	0.912

The linear regression showed a high prediction by Hydrus-1D, demonstrating that for the year 2009 the prediction of the model is very high (0.91). The trend of the soil moisture curve by Hydrus-1D is quite similar to the observed values, therefore is possible confirm the good performance of the model.

Figure 3-14 and Figure 3-15 are the comparison between the soil moisture from Hydrus-1D and field measurements for the station Q08 (for sugar beet and onion crops).

Figure 3-14 Validation in Q08 station for year 2008

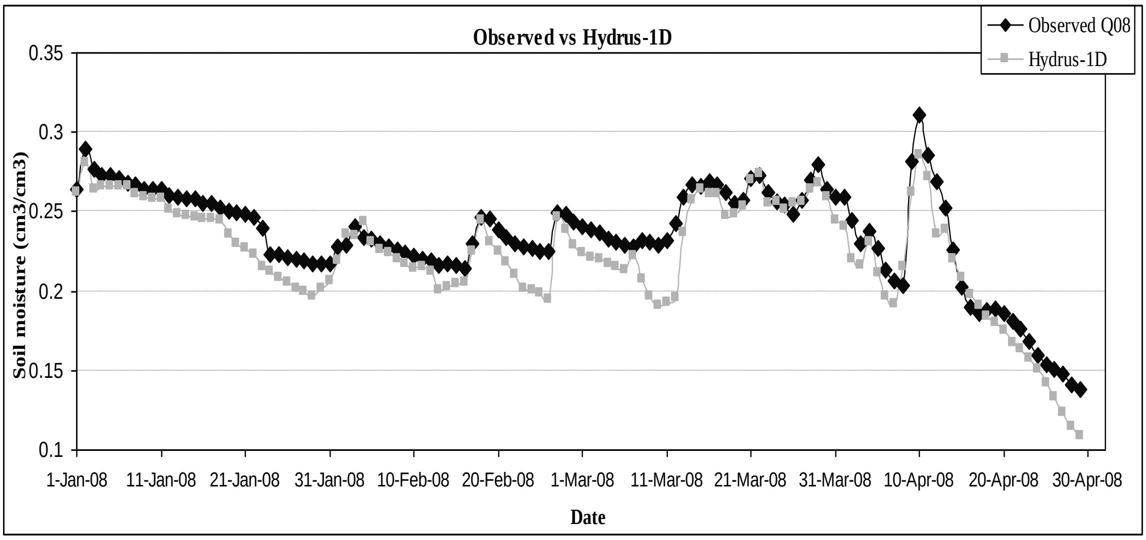

Last figure shows a good trend, however in some parts (January, February and the beginning of March) the modelled curve decreases faster that the observed SM, this probably happened as the up-taking water from the soil by the crop was set to a constant routing depth during all the modelling, while in the real conditions is not, because the crop planting starts by the end of March and from this date the trend curve is practically perfect (same criteria for Figure 3-15). A constant root depth is assumed in all the modelling cases because the lack of information about growth stage and its root depth.

Figure 3-15 Validation in Q08 for year 2009

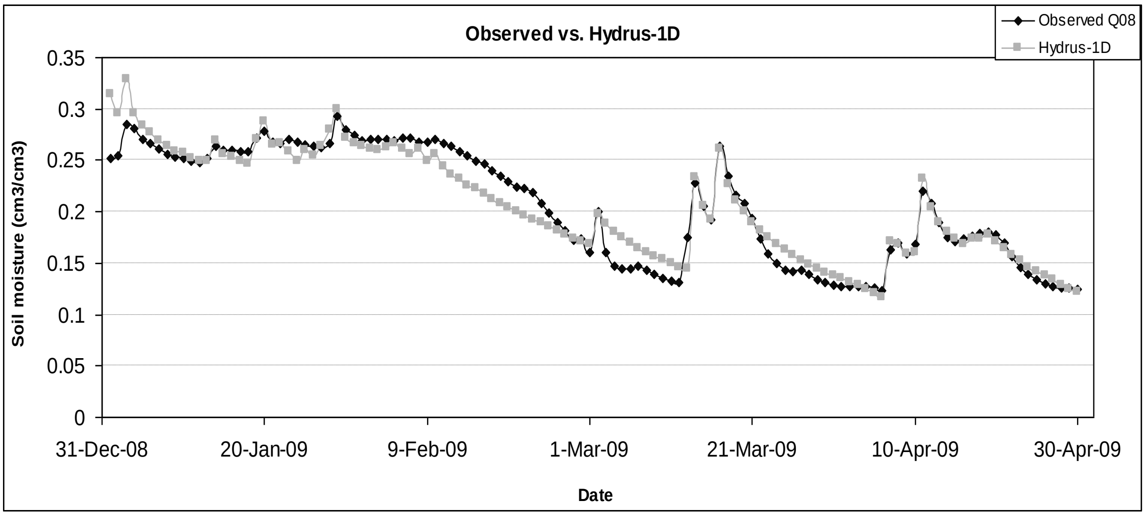

Table 6 R-squared values from the linear regression for stations Q08

Station	Year			
	2006	2007	2008	2009
Q08	0.81	NA	0.92	0.92

In the same way the process of validation and calibration shows the good trend between the curves of soil moisture by Hydrus-1D and field measurements for the station Q08. In addition to this, the prediction of the model is adequate; all the r-squared values are over 0.8 being the year 2008 and 2009 the most accurate years for prediction.

The station J14 is over sunflower crop, for this station the year 2007 is used for calibration and year 2009 for validation (year 2008 presents too many errors in the SM measured in field).

Figure 3-16 Final calibration for station J14 year 2007

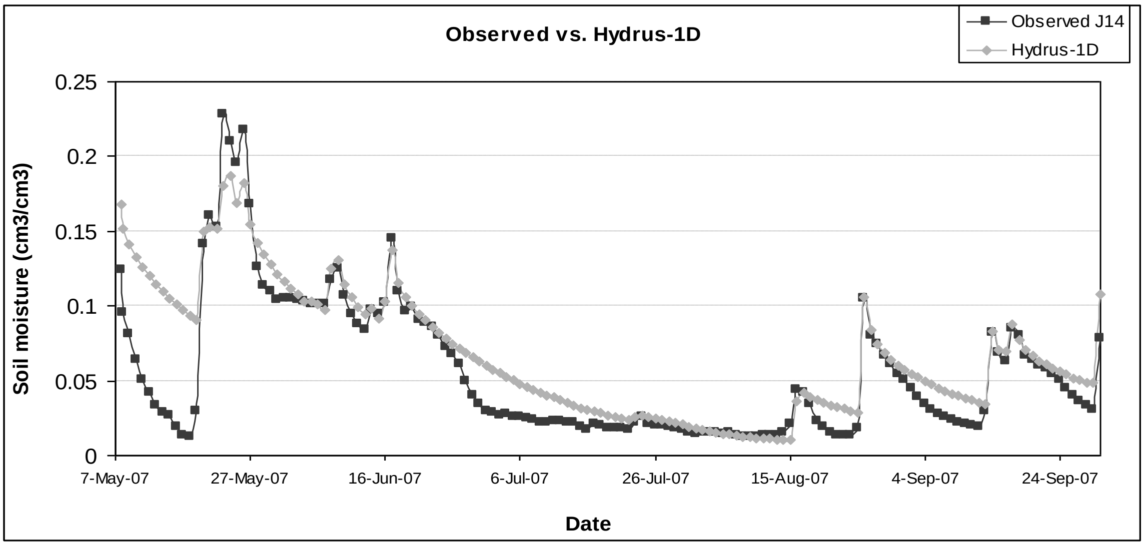

Figure 3-17 Validation for station J14 year 2009

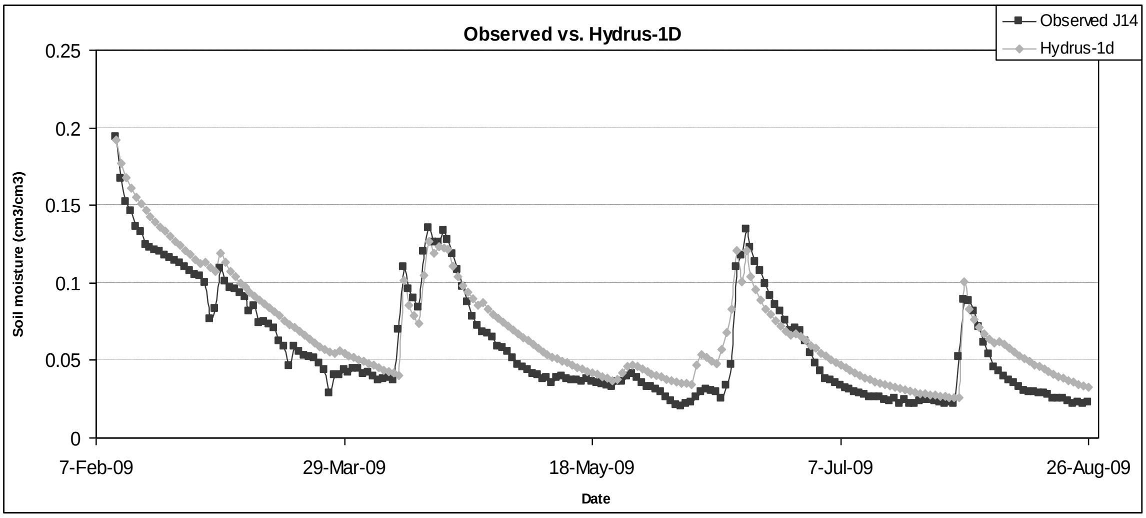

The trends in both years are quite good and the r-squared (predicted) values are also high:

Table 7 R-squared values from the linear regression for stations J14

Station	Year			
	2006	2007	2008	2009
Q08	NA	0.92	NA	0.92

As final remark, it is noticeable that the parameterization of the soil properties participating in the model were not modified after the calibration period, what makes this procedure very attractive as it does not require constant professional attention in terms of calibration.

3.1.6. Actual evapotranspiration by Hydrus-1D

Hydrus-1D evaluates the amount of the water content on a soil profile, and in the process obtains the (potential ET) PET and (actual ET) AET. The setup made for this modelling was in a daily time-step.

The Figure 3-18 shows the PET and AET obtained by Hydrus-1D for the station K10 (wheat) for the years 2006 to 2009. The PET follows the trend in increasing its value according it is near to the middle of the year (summer season) and the AET is governed by moisture availability and obviously affected by the meteorological conditions (precipitation).

The sunflower crop (station J14 and Figure 3-19) shows quite high values of PET and low values of AET (Figure 3-19), because the modelling was done during the middle of year where the PET is maximum and the AET only achieves high values after precipitation. During the first months the AET is high because in those months the sunflower is under irrigation.

Figure 3-18AET and PET obtained by Hydrus-1D for station K10 for years 2006 to 2009

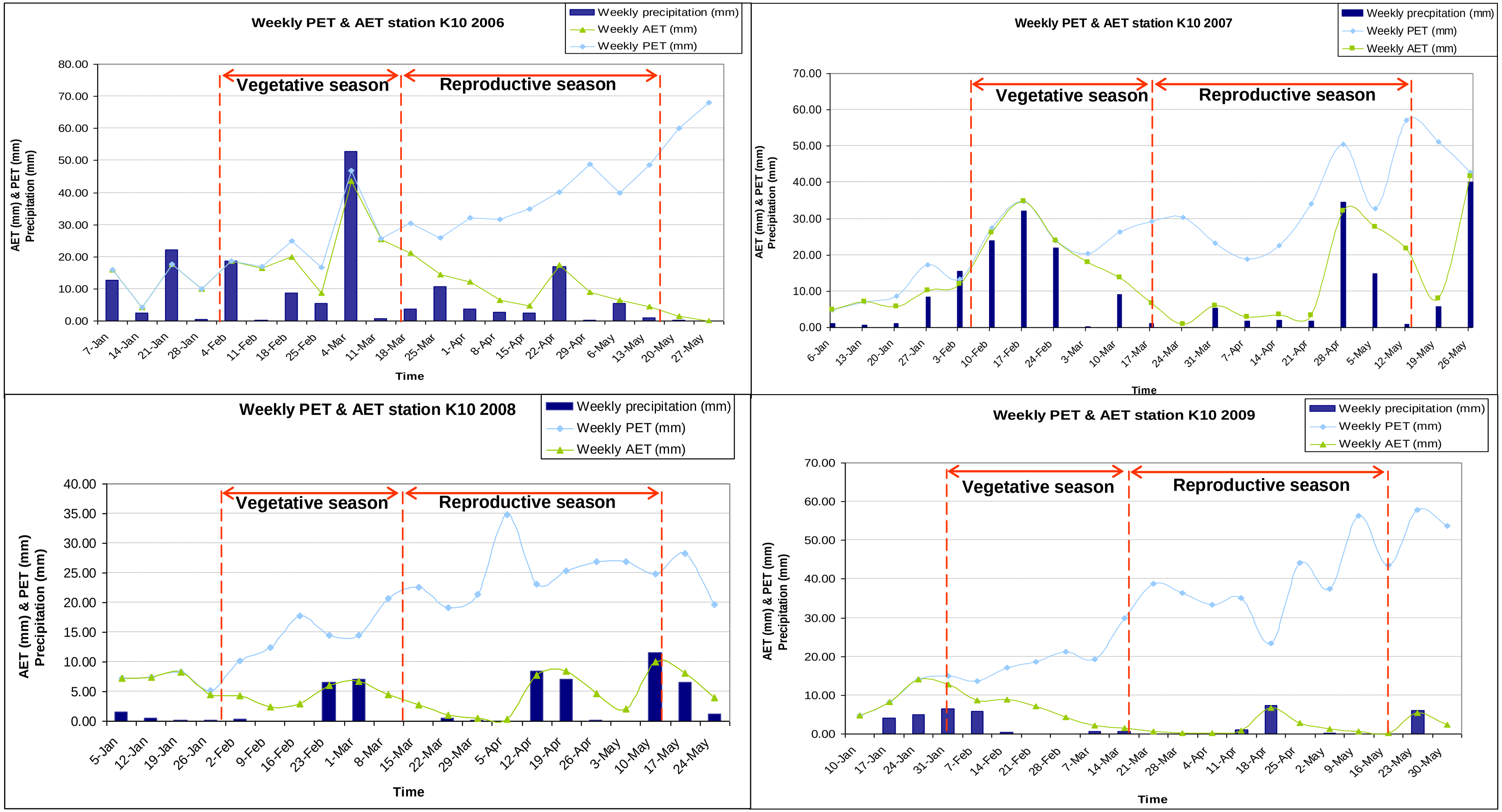

Figure 3-19 AET and PET obtained by Hydrus-1D for station J14 for years 2007 to 2009

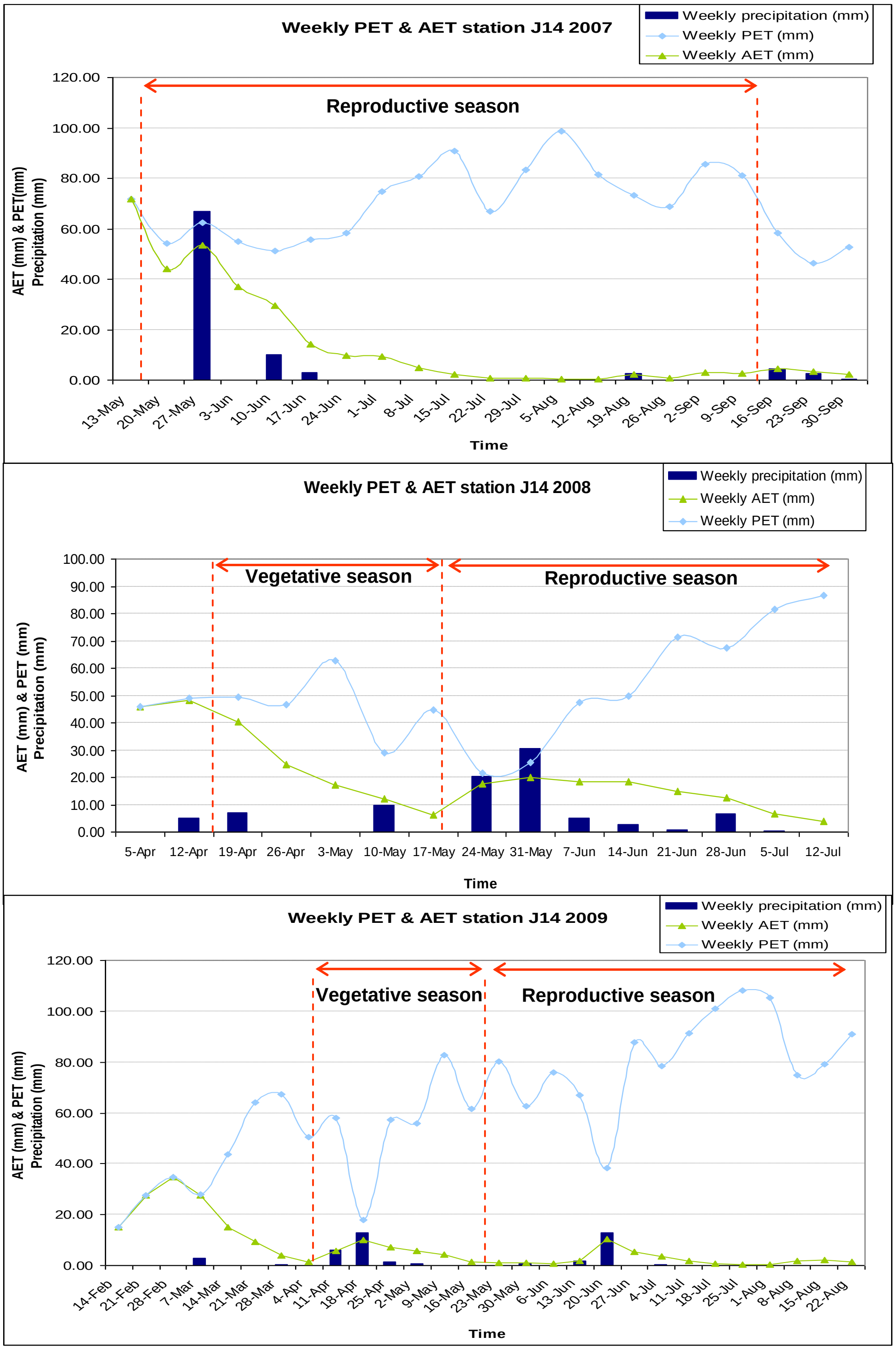

In (Figure 3-20) for sugar beet (station Q08 during 2008) is again seen the trend of high values of AET after events of precipitation, and the tendency of increasing PET while it is near of the middle of the year.

Figure 3-20 AET and PET obtained by Hudrus-1D for station Q08 during 2008

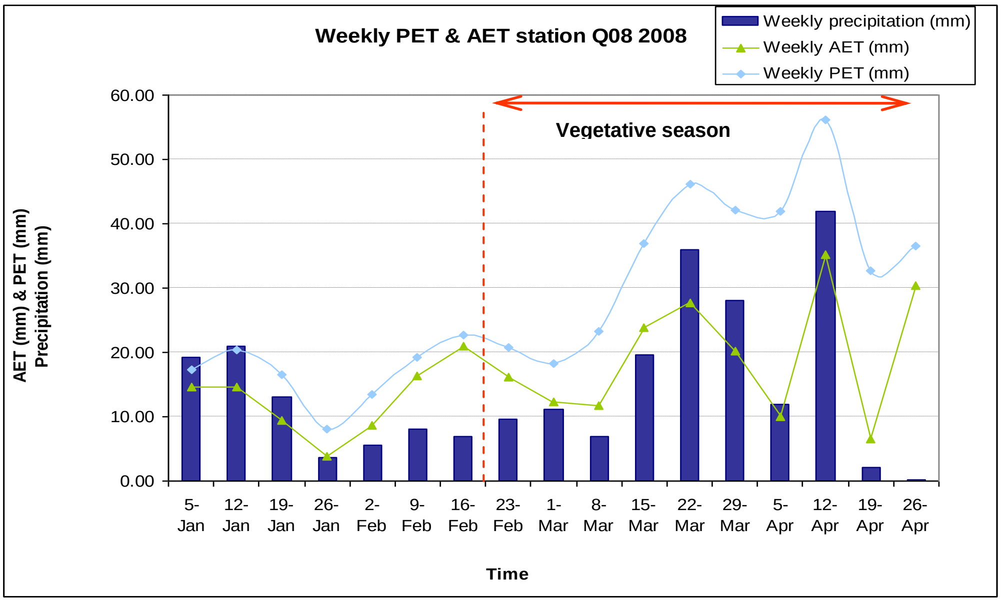

The onion (station Q08 during 2009) presents highs values of AET during the months of February and March, when onion is planted, but approaching summer these values diminish (Figure 3-21).

Figure 3-21 AET and PET obtained by Hudrus-1D for station Q08 during 2009

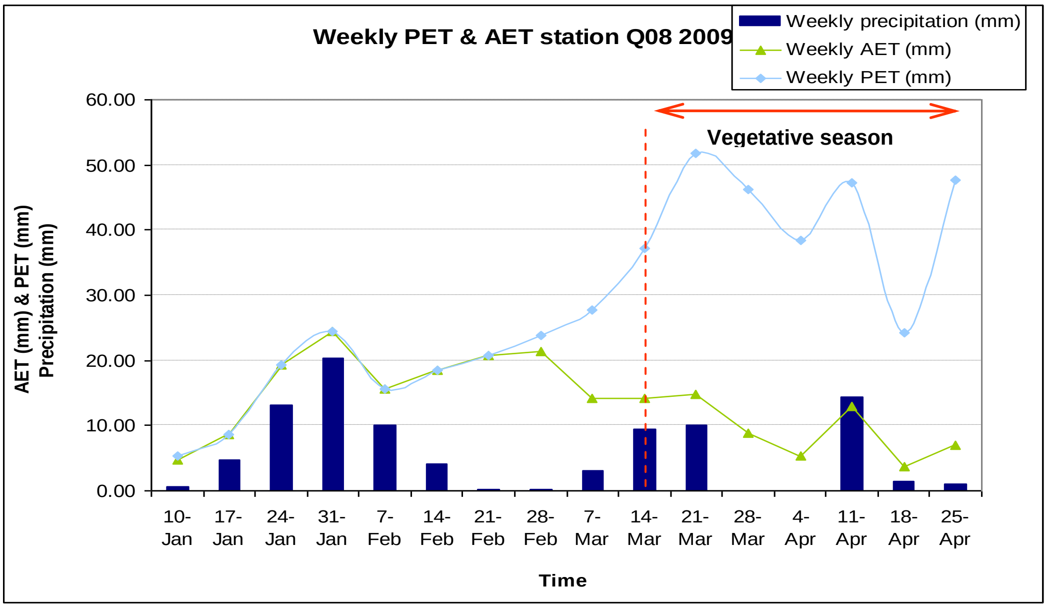

The following tables summarizes the values of AET by Hydrus-1D over the soil moisture stations and the potential ET calculated using FAO Penman-Monteith during the months of April and May for the years 2006 to 2009.

Table 8 Daily AET and PET by Hydrus-1D and FAO Penman-Monteith respectively on April for the years 2006 to 2009

Model	Station	Date			
		19-04-06	22-04-07	17-04-08	22-04-09
AET by Hydrus-1D (mm/day)	Q08	1.42	--	1.02	1.02
	J14	--	1.65	0.62	1.2
	K10	1.36	4.18	0.8	0.54
PET by FAO 56 (mm/day)	--	3.94	7.09	2.93	4.95

The values of AET obtained by Hydrus-1D are below the PET calculated by using FAO Penman-Monteith, but not necessarily under stress.

Table 9 Daily AET and PET by Hydrus-1D and FAO Penman-Monteith respectively on May for the years 2006 to 2009

Model	Station	Date			
		31-05-06	10-05-07	20-05-08	19-05-09
AET by Hydrus-1D	Q08	--	--	--	--
	J14	--	--	1.25	0.15
	K10	0.72	0.4	1.04	0.02
PET by FAO 56 (mm/day)	--	6.76	4.84	4.53	5.8

The input data and process of the calculation of the PET by FAO Penman-Monteith is in the appendix C.

3.2. SEBS model

3.2.1. Introduction

The Surface Energy Balance System (SEBS) was developed to estimate atmospheric turbulent fluxes and surface evaporative fraction using satellite data in the visible, near infrared and thermal infrared spectrums range in combination with meteorological data.

This model requires three mainly sets of information. The first set are the land surface properties derived from RS and some additional ground data (albedo, emissivity, temperature, fractional vegetation, LAI and the height of the vegetation NDVI). The second set is related to meteorological data or maps of air pressure, air temperature, humidity, and wind speed at a reference height (PBL or ASL). The third data set deals with incoming SW and LW radiation either from direct measurements, model output or parameterization.

The process of SEBS is summarized in the next flowchart where MODIS was indicated as sensor source (For this research as SEBS is an algorithm sensor independent). Mostly this section makes reference to (Su 2002) due to the extensive documentation and the limited space of this thesis.

Figure 3-22: SEBS process

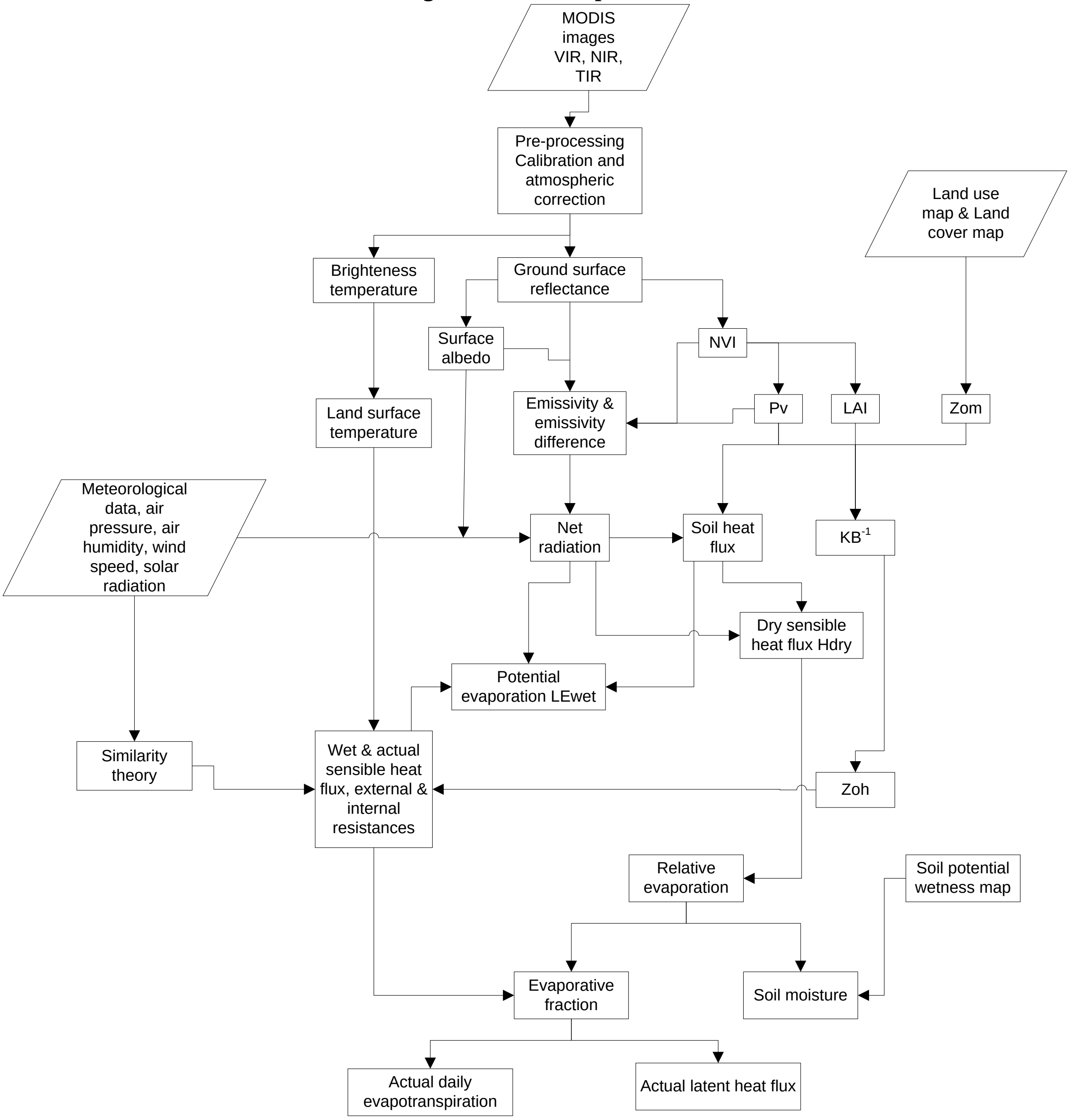

3.2.2. SEBS process

3.2.2.1. Input information

The input data used in this thesis for SEBS (as a module of ILWIS) are MODIS or ASTER images in the VIS, NIR and TIR bands. However most of the time these images are not atmospherically corrected therefore the SMAC method (Rahman and Dedieu 1994) was used.

It requires input data of aerosol optical thickness (550 µm), average in the air pressure (hPa) and water vapour content ($g.cm^{-3}$). From the web page of Aeronet (http://aeronet.gsfc.nasa.gov) the aerosol depth and the water vapour are estimated, while the ozone content is retrieved from http://jwocky.gsfc.nasa.gov. The information in these places was taken at the time the satellite pass, although remain a punctual information. Despite that the measurements are level 2.0 verified the distance from the study area to the closes sunphotometer in the aeronet network (120 km) indicates that the information derived from there is only indicative.

After completing the atmospheric correction with the available information, the meteorological information is needed in SEBS. All meteorological information should be instantaneous collected at the time that the satellite passed. These meteorological data are:

- Z: Reference height in (m). Where measurements are made.
- Q: Specific humidity in ($kg.kg^{-1}$)
- U: Wind speed in ($m.s^{-1}$)
- Ta: Air temperature at reference height in (°C)
- Pa: Air pressure at reference height in (Pa)
- Ps: Air pressure at land surface land in (Pa)
- PBL height: Estimated. Height of the Planetary Boundary Layer (PBL) in (m). Most of the times is used the value by default 1000 m (Brutsaert 1999).
- R_{swd}: Incoming Solar radiation or global radiation in ($watt.m^{-2}$)

Finally maps related to the land use and surface parameters (LAI, canopy height, displacement height and surface roughness) are optional because is possible the inclusion or calculation of them. This automation needs to be handled with care as the results of SEBS can be highly distorted by wrong evaluation of roughness and air temperature. This is perhaps the main disadvantages of using SEBS at local scale.

3.2.2.2. Data processing

Here a summary of the solution round in SEBS is explained, for more detail information we refer to the author pages. The SEBS model solves the surface energy balance equation (Equation 1). Where the net radiation (R_n) is given by the next equation:

$$R_n = (1-\alpha)R_{swd} + \varepsilon R_{lwd} - \varepsilon\sigma T_o^4$$ **Equation 12**

Where 'α' is the albedo (-), 'R_{swd}' is the downward solar radiation ($watt.m^{-2}$), 'R_{lwd}' is the downward long wave radiation ($watt.m^{-2}$), 'ε' is the emissivity of the surface (-), 'σ' is the Stefan-Bolzmann constant ($watt.m^{-2}.K^{-4}$) and T_o is the surface temperature (K).

The downward solar radiation calculated by using:

$$Rswd = I_{sc} e_0 \cos\theta_z \exp(-m\tau)$$ **Equation 13**

Where 'I_{sc}' is the solar constant equal to 1367 ($watt.m^{-2}$), 'e_o' the eccentricity factor, 'θ_z' the solar zenith angle, 'm' the air mass and 'τ' is the optical thickness. The downward solar radiation is normally measured directly with solarimeters.

The downward long wave radiation is calculated from:

$$R_{lwd} = \varepsilon_a \sigma T_a^4$$ **Equation 14**

Where ‘εa’ is the apparent emissivity of the atmosphere and ‘Ta’ is the air temperature at the reference height. The apparent emissivity of the atmosphere is calculated as:

$$\varepsilon_a = 9.2 \times 10^{-6} (T_a + 273.15)^2$$ **Equation 15**

The soil heat flux (G_o) is small or negligible comparing with the other energy. However for calculations in hourly time steps or instantaneous time is important to take into account. This flux is related with the net radiation and the type of land cover. In SEBS it is given as:

$$Go = R_n (\Gamma_c + (1 - P_v)(\Gamma_s - \Gamma_c))$$ **Equation 16**

Where ‘Γ_c’ and ‘Γ_s’ are the ratio of soil heat flux to net radiation (for full vegetation canopy Γ_c is equal to 0.05 and for bare soil Γ_s is equal to 0.315) and ‘P_v’ is the fractional vegetation coverage.

The Normalized Difference Vegetation Index (NDVI) is calculated from the atmospherically corrected reflectance red and near infrared bands (in MODIS band 1 and band 2):

$$NDVI = \frac{b2 - b1}{b1 + b2}$$ **Equation 17**

The fractional vegetation coverage can be obtained from (Carlson and Ripley 1997):

$$Pv = \left(\frac{NDVI - NDVI_{\min}}{NDVI_{\max} - NDVI_{\min}} \right)^2$$ **Equation 18**

Where $NDVI_{max}$=0.5 and NVI_{min}=0.2 and for pixels with NDVI values less than 0.2 P_v is 0 and for values greater than 0.5 the pixel is assumed to be fully vegetated therefore P_v is 1

The land surface emissivity is calculated for four different types of surface based on the NDVI (Sobrino and Raissouni 2000):

- Bare soils, NDVI<0.2 and the emissivity (e) and the emissivity difference (Δe) are

$$e = 0.9825 - 0.051 \times band1$$
$$\Delta e = -0.0001 - 0.0041 \times band1$$

- Mixed pixels 0.2 ≤NDVI≤0.5 and the emissivity and the emissivity difference are

$$e = 0.971 + 0.018 \times P_v$$
$$\Delta e = 0.006 \times (1 - P_v)$$

- Vegetated pixels NDVI>0.5

$$e = 0.990$$
$$\Delta e = 0$$

- Water bodies and surface albedo< 0.035

$$e = 0.995$$

The leaf area index can be obtained by using the NDVI values (Su 2002):

$$LAI = \left(\frac{NDVI(1 + NDVI)}{1 - NDVI + 10^{-6}} \right)^{1/2}$$ **Equation 19**

To compute the Land Surface Temperature (LST) the thermal bands of MODIS (bands 31 and 32), and the water vapour 'W' are used (Sobrino and Raissouni 2000):

$$\begin{aligned} LST &= btm31 + (1.97 + 0.2W)(btm31 - btm32) - \\ &(0.026 - 0.08W)\sqrt{btm31 - btm32} + (0.02 - 0.067W) + \\ &(64.5 - 7.35W)(1 - e) - ((119 - 20.4W)\Delta e \end{aligned}$$ **Equation 20**

Where 'btm31' and 'btm32' are the brightness temperatures from band 31 and 32 respectively. If there is no information about water vapour it can be obtained using the following equation (Li, Jia et al. 2001):

$$w = 13.73 - 13.662 \frac{T_{31}}{T_{32}}$$ **Equation 21**

Where 'T_{31}' and 'T_{32}' are the transmittances of band 31 and 32 respectively. The transmittances ratio could be calculated from the covariance between the two bands.

The sensible heat flux (H) is estimated by using two models the Monin-Obukov Similarity model (MOS) and the Bulk Atmospheric Similarity model (BAS). The criterion for using the MOS or BAS model is evaluated automatically by SEBS. This criterion consists if the reference height is below than the top of the atmospheric surface layer then MOS model is used, otherwise BAS model is used.

The roughness length for heat transfer (Z_{oh}) is obtained from the following equation:

$$Z_{oh} = \frac{Z_{om}}{\exp(kB^{-1})}$$ **Equation 22**

The estimation of kB^{-1} is done by (Su, Schmugge et al. 2001):

$$kB^{-1} = \frac{kC_d}{4C_t \frac{u_*}{u(h)}\left(1-e^{-n_{ec}/2}\right)} P_v^2 + 2P_v\left(1-P_v\right)\frac{k\frac{u*}{u(h)}\frac{Z_{om}}{h}}{C_t^*} + kB_s^{-1}\left(1-P_v\right)^2 \qquad \textbf{Equation 23}$$

Where 'P_v' is the fractional canopy coverage, 'C_t' is the heat transfer coefficient of the leaf, 'C_t^*' is the heat transfer coefficient of the soil, 'u_*' is the friction velocity, 'C_d' is the drag coefficient of the foliage elements, 'u(h)' is the horizontal wind speed at the canopy height, 'n_{ec}' is formulated as a function of the cumulative leaf area drag at the canopy top and 'Z_{om}' is the roughness for momentum. And extensive and detailed description and calculation of these variables are explained in (Su, Schmugge et al. 2001).

The height of measurements is 2 m and a PBL is estimated as 1000 m, therefore Z_{om} is 0.96 and h_{st} is 120 which is greater than the 2 m of Z_{ref}. Then MOS model is applied. This model applies basically 3 main equations in an iterative manner:

$$u = \frac{u_*}{k}\left[\ln\left(\frac{z-d_o}{Z_{om}}\right) - \Psi_m\left(\frac{z-d_o}{L}\right) + \Psi_m\left(\frac{Z_{om}}{L}\right)\right] \qquad \textbf{Equation 24}$$

$$\theta_0 - \theta_a - = \frac{H}{ku_*\rho C_p}\left[\ln\left(\frac{z-d_o}{Z_{oh}}\right) - \Psi_h\left(\frac{z-d_o}{L}\right) + \Psi_h\left(\frac{Z_{oh}}{L}\right)\right] \qquad \textbf{Equation 25}$$

$$L = \frac{\rho C_p u_*^3 \theta_v}{kgH} \qquad \textbf{Equation 26}$$

Where 'θ_0' is the potential surface temperature, 'θ_a' is the potential air temperature and 'θ_v' is the mean virtual potential temperature. 'Ψ_m' and 'Ψ_h' are the stability corrections functions for stable atmosphere.

The sensible heat flux, the Obukhov stability length and friction velocity are obtained from Equation 24, Equation 25 and Equation 26. The Broyden method is used to solve this non-linear system. The process of solution stars assuming neutral conditions where 'Ψ_m' and 'Ψ_h' are set to zero. From Equation 24 'u*' is derived and replaced in Equation 25 for the first estimate of 'H'. After that the first estimation of 'L' from Equation 26 and 'Ψ_m' and 'Ψ_h' (see below) are possible. After that the iteration is reinitiated using Equation 24 where now 'Ψ_m' and 'Ψ_h' are not zero. The iteration stops after that two consecutives differences between the values of H are less or equal than a fixed threshold.

'Ψ_m' and 'Ψ_h' are defined by:

$$\left\{\begin{array}{l}\Psi_m(y)=\ln(a+y)-3by^{1/3}+\dfrac{ba^{1/3}}{2}\ln\left(\dfrac{x^2+2x+1}{x^2-x+1}\right)+\ldots\\ \ldots+3^{1/2}ba^{1/3}\tan^{-1}\left(\dfrac{2x-1}{3^{1/2}}\right)+\Psi_0,\ for\ y\le b^{-3}\\ \Psi_m(y)=\Psi_m\left(b^{-3}\right),\ for\ y>b^{-3}\end{array}\right\}$$ **Equation 27**

$$\Psi_h(y)=\left[\frac{(1-d_o)}{n}\right]\ln\left[\frac{c+y^n}{c}\right]$$ **Equation 28**

$$y=\frac{d-z}{L}$$ **Equation 29**

$$x=\left(\frac{y}{a}\right)^{1/3}$$ **Equation 30**

$$\Psi_0=\left(-\ln a+3^{1/2}ba^{1/3}\pi/6\right)$$ **Equation 31**

Where ‘a’ is 0.33, ‘b’ is 0.41, ‘m’ is 1.0, ‘c’ is 0.33, ‘d’ is 0.057 and ‘n’ is 0.78. If the atmosphere is unstable the prior equations are replaced by:

$$\Psi_m=-\left[a_sy_s+b_s\left(y_s-\frac{c_s}{d_s}\right)\exp\left(-d_sy_s\right)+b_s\frac{c_s}{d_s}\right]$$ **Equation 32**

$$\Psi_h=-\left[\left(1+\frac{2a_s}{3}y_s\right)+b_s\left(y_s-\frac{c_s}{d_s}\right)\exp\left(-d_sy_s\right)+\left(\frac{b_sc_s}{d_s}-1\right)\right]$$ **Equation 33**

Where y_s= (z-d)/L, ‘a_s’ is 1, ‘b_s’ is 2/3, ‘c_s’ is 5 and ‘d_s’ is 1. The height above the surface is ‘z’ (normally coincides with z_{ref}), $u_*=(\tau_0/\rho)^{0.5}$ is the friction velocity, ‘τ_0’ is the surface shear stress, ‘ρ’ is the density of air, ‘k’ is the von Karman constant (0.41) and ‘L’ is the Obukhov length. Due this research is working only with the MOS model a description of the BAS model is not given in this document, however a detailed description of this model is in Brutsaert (1999).

The determination of the relative evaporative fraction is made assuming two limiting or extreme conditions. In the dry limit the latent heat stops and becomes 0 due to the limitation of SM and the sensible heat flux is at its maximum value.

$$H_{dry}=R_n-G_0$$ **Equation 34**

At the wet limit the evaporation takes place at potential rate, the sensible heat flux takes its minimum value.

$$H_{wet} = R_n - G_0 - \lambda E_{wet}$$ **Equation 35**

At the wet limit λE_{wet} reaches the maximum and H_{dry} the minimum, but no zero. At the same time λE_{wet} is equal to the PET, therefore it can be written using Penman-Monteith equation (see Equation 2).

$$\lambda E = \frac{\Delta r_e (Rn - G_0) + \rho C_p (e_{sat} - e)}{r_e(\gamma + \Delta) + \gamma r_i}$$ **Equation 36**

At the wet limit it is assumed that the internal resistance r_i is 0, then H_{wet} is:

$$H_{wet} = \frac{(R_n - G_0) - \frac{\rho C_p}{r_{ew}} \frac{e_s - e}{\gamma}}{1 + \frac{\Delta}{\gamma}}$$ **Equation 37**

Since the external resistance r_e depends on 'L', the external resistance at wet limit is expressed as:

$$r_{ew} = \frac{1}{ku_*}\left[\ln\left(\frac{z - d_0}{z_{0h}}\right) - \Psi_h\left(\frac{z - d_0}{L_w}\right) + \Psi_h\left(\frac{z_{0h}}{L_w}\right)\right]$$ **Equation 38**

$$L_w = -\frac{\rho u_*^3}{kg \cdot 0.61 \cdot (R_n - G_0)/\lambda}$$ **Equation 39**

Where L_w can be calculated as:

The relative evaporation is evaluated after the limiting cases:

$$\Lambda_r = \frac{\lambda E}{\lambda E_{wet}} = 1 - \frac{\lambda E_{wet} - \lambda E}{\lambda E_{wet}} = 1 - \frac{H - H_{wet}}{H_{dry} - H_{wet}}$$ **Equation 40**

Then the evaporative fraction is given as:

$$\Lambda = \frac{\lambda E}{H + \lambda E} = \frac{\lambda E}{R_n - G} = \frac{\Lambda_r \cdot \lambda E_{wet}}{R_n - G}$$ **Equation 41**

If the daily net radiation R_n^{day}, soil heat flux is near 0 and the evaporative fraction are known and assuming that the evaporative fraction is conservative, the E_{daily} is finally estimated as:

$$E_{daily} = 8.64\times10^{7}\,\Lambda_{0}^{24}\frac{\overline{R}_n - \overline{G}_o}{\lambda\rho_w} = 8.64\times10^{7}\,\Lambda\frac{\overline{R}_n}{\lambda\rho_w}$$ **Equation 42**

$$\overline{R}_n = (1-\alpha)k_{24}^{\downarrow} + \varepsilon L_{24}$$ **Equation 43**

Where '$K^{\downarrow}_{24}$' is the daily incoming global radiation and 'L_{24}' is the daily net long wave radiation, 'λ' is the latent heat of vaporization ($J.Kg^{-1}$), 'ρ_w' is the density of water ($Kg.m^{-3}$). The daily average albedo 'α' and the emissivity 'ε' can be approximated by using the previous values in the energy balance equation.

3.2.3. Images acquisition

The images used for this research are from the Moderate resolution Imaging Spectroradiometer (MODIS). These MODIS images are arranged in 36 spectral bands that cover the visible and infrared spectrum. Free cloudy images were collected in order to obtain more accurate results by using the SEBS tools in ILWIS. These images are in appendix D.

The following table indicates the characteristics of the images, like date and time of the overpass, and the instantaneous measurements at the ground stations at the time the satellite passes.

Table 10 Instantaneous atmospheric parameters at satellite over pass time

Overpass date and time UTC	Julian day number	Reference height (m)	Pressure at reference height (pa)	Pressure at surface map (pa)	Instantaneous downward solar radiation (watts/m^2)	Instantaneous specific humidity (kg/kg)	Instantaneous wind speed (m/s)	Instantaneous air temperature (°C)
4/22/2009 10:40	112	2	93553.3	93573.3	946	0.003936	3.4	16
5/19/2009 12:00	139	2	93553.3	93573.3	889	0.00404	1.7	22.1
4/17/2008 11:05	106	2	93553.3	93573.3	431	0.00521	6.75	11.1
5/20/2008 11:35	141	2	93553.3	93573.3	796	0.00657	2.65	15.5
4/22/2007 11:00	112	2	93553.3	93573.3	904	0.00505	2.95	22.2
5/10/2007 10:45	130	2	93553.3	93573.3	881	0.00643	5.83	24.2
4/19/2006 11:00	109	2	93553.3	93573.3	733	0.00613	1.84	15.97
5/31/2006 11:35	151	2	93553.3	93573.3	936	0.00315	5.4	19.3

These instantaneous values were obtained from the meteorological stations near to the study area (Figure 1-1 REMENDHUS area). During the years 2009 and 2008 availability of data were in all the stations near the area (stations Villamor, Ema Granja, Ema Cañizal and Va_02) therefore each instantaneous parameter is assumed as the average from all the instantaneous of these stations. On the other hand during the years 2006 and 2007 only is available data from the station Va_02 thus the parameters are obtained just from this station. On the 17th of April 2008 the instantaneous downward solar radiation is much lower than the other images this is because of partial cloudiness at the station (see images in appendix D).

3.2.4. Pre-processing

The pre-processing consists in 6 main steps:

- Raw data into radiances/reflectance (MODIS)

The MODIS Level 1b data are given in SI (simplified number); therefore those images has to be converted to reflectance and radiance. Bands 1 to 7 are converted to reflectance, and bands 31 and 32 are converted to radiance. For these conversion coefficients of the scale and offset are needed (HDF header file is used to access to these information). Solar and satellite zenith and azimuth angles need to be corrected by multiplying the scale factor 0.01.

- Brightness temperature computation

This computation consists in converting the bands 31 and 32 from radiances to blackbody temperatures by applying the Planck equation.

- SMAC (atmospheric correction)

As it was discussed before the SMAC method (Rahman and Dedieu 1994) requires input data of aerosol optical thickness (550 µm), average in the air pressure (hPa) and water vapour content (g.cm^{-3}).

- Land Surface Albedo Computation

The computation of the albedo is done by using the bands 1 to 7 except 6. The equation is obtained from Liang (2001):

$$albedo = 0.16 band_1 + 0.291 band_2 + 0.243 band_3 + 0.116 band_4 + 0.112 band_5 + 0.018 band_7 - 0.0015$$

- Land Surface Emissivity Computation

The calculation of the emissivity is explained in the section 3.2.2.2. In the same way the equation for computing the NDVI values is explained in the Equation 17.

- Land Surface Temperature Computation

The LST calculation is done by using the Equation 20 and Equation 21 from the section 3.2.2.2.

3.2.5. Processing and results

In order to extrapolate to daily values from instantaneous SEBS requires the mean daily air temperature (°C) and the number of sunshine per day. These values are summarized in the following table

Table 11 Daily parameters

Mean daily air temperature (°C)	Sunshine hours per day
11.81	12.7
15.9	13.5
8.05	10.3
13.09	13.5
14.66	11.9
16.77	12.4
10.46	12.1
11.97	13.7

In addition to these atmospheric and meteorological parameters, the maps resulting of the pre-processing are used (Land surface temperature, Emissivity, Land surface Albedo, NDVI, Vegetation proportion, Leaf Area Index, Sun zenith angle and DEM).

The results of daily actual ET shows high values (Figure 3-23 and Figure 3-24) and even some of these values are over the PET, therefore those results are not took into account. On the other hand other results like May 2006 and April 2009 are significantly lower than the PET so probably are reasonably near to the real values. Table 12 and Table 13 summarize the values of AET by SEBS in the locations of the SM stations and the values of the PET.

Table 12 Daily AET and PET by SEBS and FAO Penman-Monteith respectively on April for the years 2006 to 2009

Model	Station	Date			
		19-04-06	22-04-07	17-04-08	22-04-09
AET by SEBS	Q08	4.34	6.06	4.06	2.33
	J14	3.56	5.58	4.96	4.16
	K10	4.24	5.31	4.75	3.71
PET by FAO 56 (mm/day)	--	4.30	5.29	3.06	5.40

Table 13 Daily AET and PET by SEBS and FAO Penman-Monteith respectively on May for the years 2006 to 2009

Model	Station	Date			
		31-05-06	20-05-07	10-05-08	19-05-09
AET by SEBS (mm/day)	Q08	1.11	6.51	3.95	5.97
	J14	1.70	8.71	3.89	6.96
	K10	2.01	6.32	6.03	6.83
PET by FAO 56 (mm/day)	--	7.37	7.40	4.95	6.33

Figure 3-23 Actual ET from SEBS on April for years 2006 to 2009

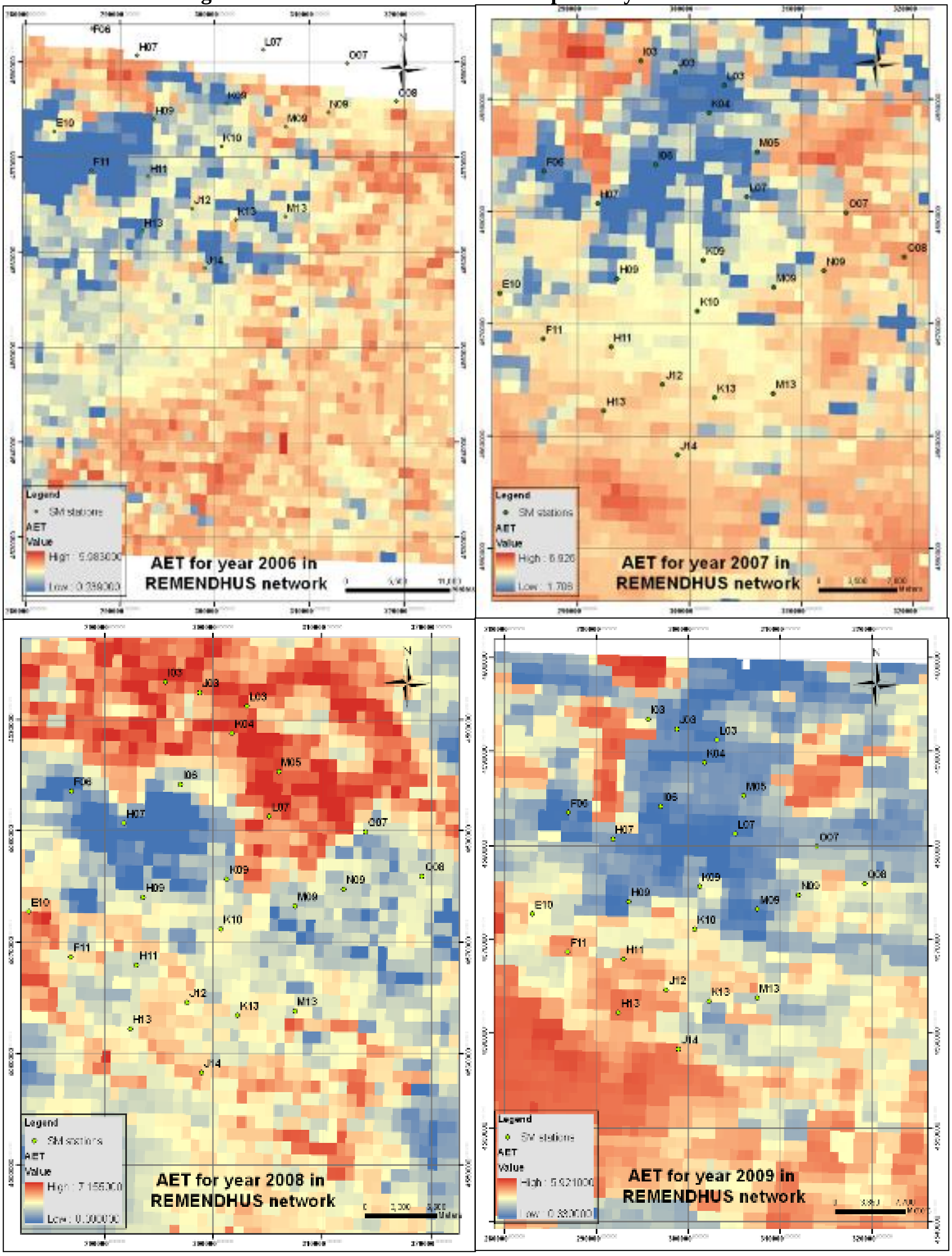

The years 2006 and 2008 yields values to high of AET. The overestimation of the evapotranspiration is normally caused by a misleading low temperature at pixel level. Normally this is caused by cloud contaminated pixels that normally affect images in coarse resolution (see images in appendix D).

Figure 3-24 Actual ET from SEBS on May for years 2006 to 2009

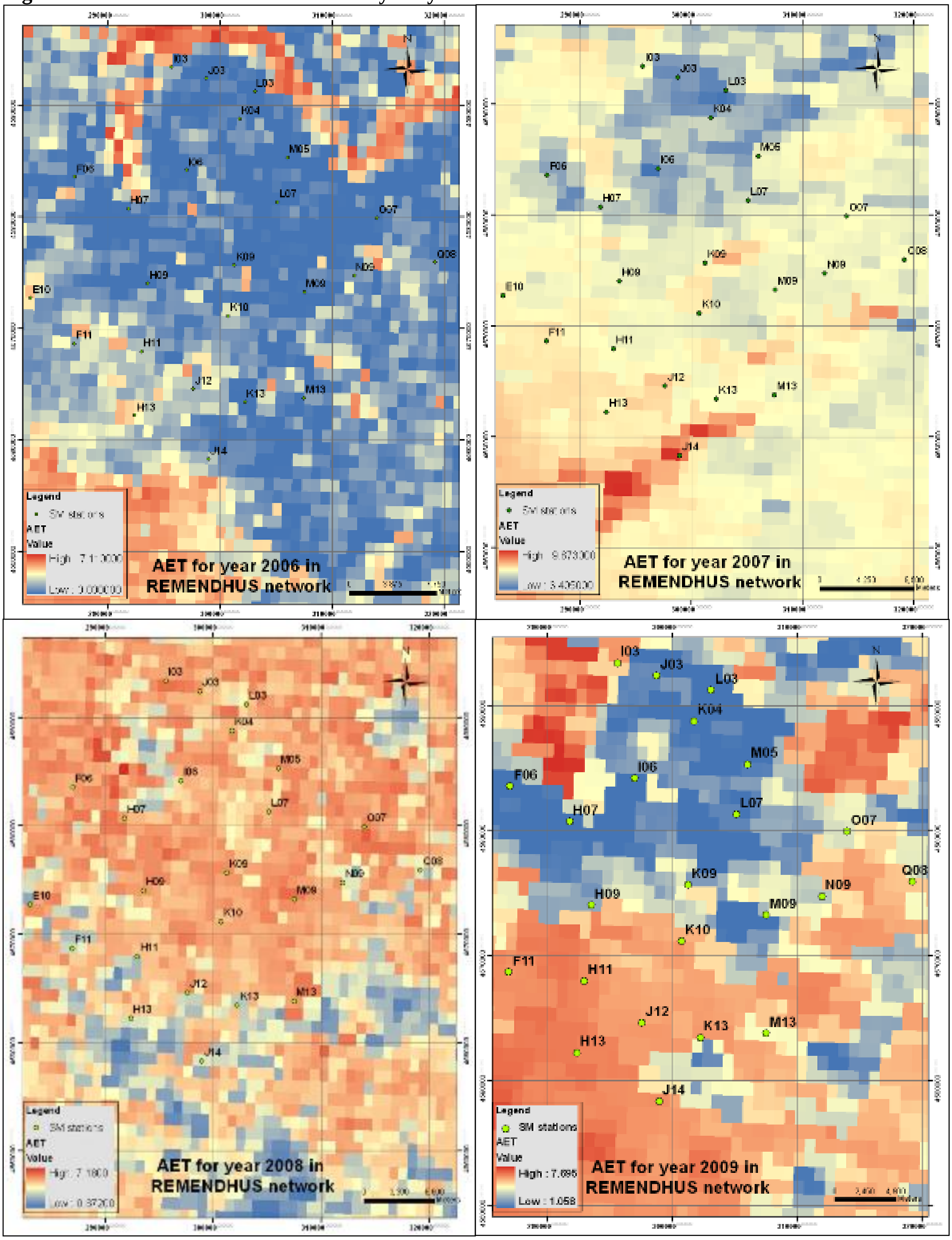

In the same way the years 2007 and 2009 shows high values of AET (see images in appendix D).

The reviewing of SEBS process was done, finding a possible explanation of the high values obtained for the daily actual evapotranspiration. From Equation 22 is possible to express KB^{-1} as the ratio of the roughness length for momentum transfer and the roughness length associated with the vertical flux:

$$kB^{-1} = \ln\left(\frac{Z_{om}}{Z_{oh}}\right)$$ **Equation 44**

The calculation for the KB^{-1} values is done for each SEBS process, yielding high values. In the literature some authors have suggested values are around 2.5 ±0.5 (Verma 1989; Brutsaert 1984) for vegetated areas having more porous and fibrous nature and densely spaced, however the values obtained from SEBS are around 3.99 to 13.75 which has been recommended for bluff-rough surfaces. The Table 14 summarizes the KB^{-1} values for each SEBS modeling.

Table 14 KB^{-1} values from SEBS

Date	Range	Mean	Median	Std. Dev
22-Apr-09	4.43 - 13.75	10.16	11.05	2.95
17-Apr-08	3.99 - 13.75	6.83	4.52	3.37
22-Apr-07	6.31 - 13.75	10.99	11.36	1.93
19-Apr-06	6.28 - 13.75	8.01	6.82	2.27
19-May-09	5.72 - 13.73	8.71	7.9	2.71
20-May-08	6.59 - 13.75	9.96	8.45	2.61
10-May-07	4.88 - 13.75	10.39	11.01	2.56
31-May-06	4.49 - 13.75	7.77	5.78	3.39

Burke and Stewart (1997) suggests using KB^{-1} values around 7 for the estimation of surface fluxes from satellite measurements, because the estimation of the sensible heat flux from thermal infrared temperature requires an estimate of the excess resistance to be added to the aerodynamic resistance to the transfer of heat from the surface, this excess resistance can be expressed in terms of KB^{-1}.

Verhoef, De Bruin et al. (1997) concludes that the concept of kB^{-1} is questionable and complex as it is based upon extrapolating a theoretical profile through a region where this profile does not hold, toward a “surface temperature” that is difficult to define and to measure. Consequently should be avoided in meteorological models, unfortunately, in remote sensing, the bulk transfer equations are up to now the only option, which requires the use of kB^{-1}.

Anne Verhoef indicated that the KB^{-1} should not be higher than 2 to 4 on croplands in a personal communication (email to C. vd Tol, 5/feb/2010). All these opinions are encircled by the common feeling born from all these top researchers that the solution of KB^{-1} is far from ideal, and from my position I cannot do more but open a question mark in the achievements I got on this value in this research.

The uncertainty on the adequate value of KB^{-1} can have severe implications in the results of the SEBS model. The internal structure of SEBS algorithm is very rigid as compared with other SEB models like SEBAL which fixes the KB^{-1} value and establishes a sensible heat solution following the Monin-Obukhov theory between two user selected conditions (dry and wet pixels). This rigidity is seen as a strong point in SEBS as it is not attached to subjective user decisions, but in turn it requires high accuracy in the inputs and it relies on models sensitive parameters (in general under research) that in a sense, they restrict the accuracy of the methodology.

The following table expresses a simple sensitivity analysis of sensible heat flux 'H' for a range of roughness that corresponds to grass and maize when KB^{-1} varies between 2 to 6. For the calculation wind speed was taken as 2 $m.s^{-1}$, Ts= 305 K, Ta= 300K.

Table 15 Values of H calculated by SEBS for a range of KB-1 values

KB^{-1}	Sensible Heat 'H'	
	Grass Z_{0m} = 0.034 and d_0=0.1	Maize Z_{0m}= 0.13 and d_0=1.2
2	101	307
3	83	238
4	71	194
5	61	164
6	55	142
7	49	125

This is not a complete sensitive analysis as the evaluation of KB^{-1} is complex because includes Z_{0m}, wind speed, temperature and the structure of the vegetations (LAI, vegetation coverage), the Table 15 shows that any miscalculation of KB^{-1} for any error in the input parameters will have tremendous influence in the final results.

3.3. Estimation of K_c

By inverting Equation 3 is possible to express K_c as the ratio of ET_o and ET_{adj}:

$$K_c = \frac{ET_{cadj}}{ET_o \times K_s}$$ **Equation 45**

K_s is represented in Equation 5 as function of the TAW and D_r. FAO 56 paper indicates that K_s is equal to 0 when D_r<TAW. For this research, the calculation of D_r is not possible due the lack of parameters (net irrigation, capillary rise from ground water or depth percolation) for its determination. However it is possible to obtain the K_s values using the Figure 2-1, Hydrus-1D provides daily information of the soil water content and it is available the values of the SM at the wilting point and field capacity therefore is possible to obtain the estimate of K_s values.

Table 16 summarizes the necessary input information to build up the K_s curve. With this K_s curve is possible to obtain the value at one specific moment and use this value in Equation 45 to calculate K_c.

Table 16 Input parameters for the determination of K_s curve

Station	Crop	Zr	p	θ_{FC}	θ_{WP}	TAW	RAW
J14	Sunflower	1.2	0.45	0.163	0.041	146.4	65.88
	Onion	0.5	0.3	0.194	0.036	79	23.7
Q08	Sugar beet	1	0.55	0.194	0.036	158	86.9
	Wheat	1.5	0.55	0.194	0.036	237	130.35
K10	Wheat	1.5	0.55	0.07	0.022	72	39.6

With Figure 2-1, the soil moisture obtained from Hydrus-1D and with the values of TAW and RAW, is possible to obtain the value of K_s. These values are plotted in Figure 3-25, Figure 3-26 and Figure 3-27.

Figure 3-25 Ks values for station J14 at 2007 and 2009

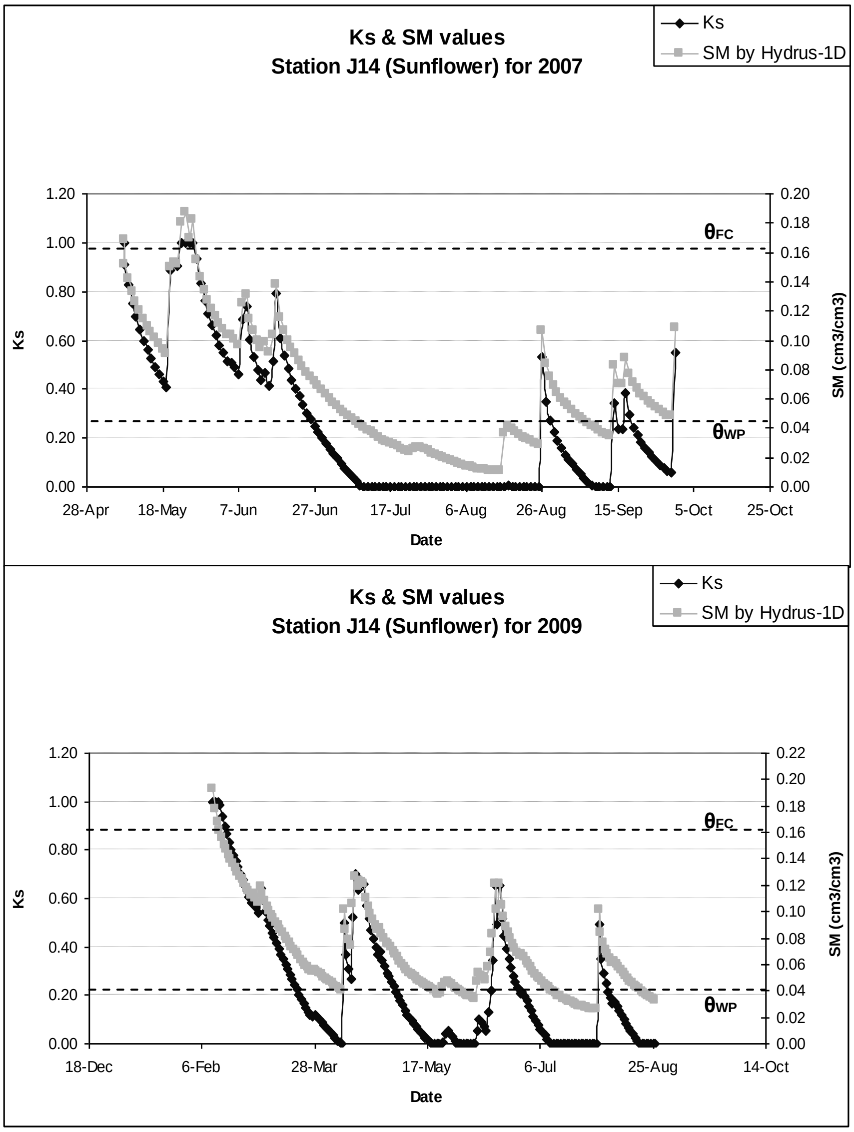

Figure 3-25, Figure 3-26 and Figure 3-27 shows the values of K_s obtained from using the SM of Hydrus-1D. When the SM is greater or equal to the field capacity K_s is 1, but when it is lower than the wilting point K_s is 0 and transpiration stops.

The high values of Ks for sunflower (station J14 and Figure 3-25) are only during the initial stage when the sunflower is under irrigation, and for summer, K_s approaches 0 as water supply is quite low (only precipitation) therefore the crop is under stress.

Figure 3-26 Ks values for station Q08 at 2008 and 2009

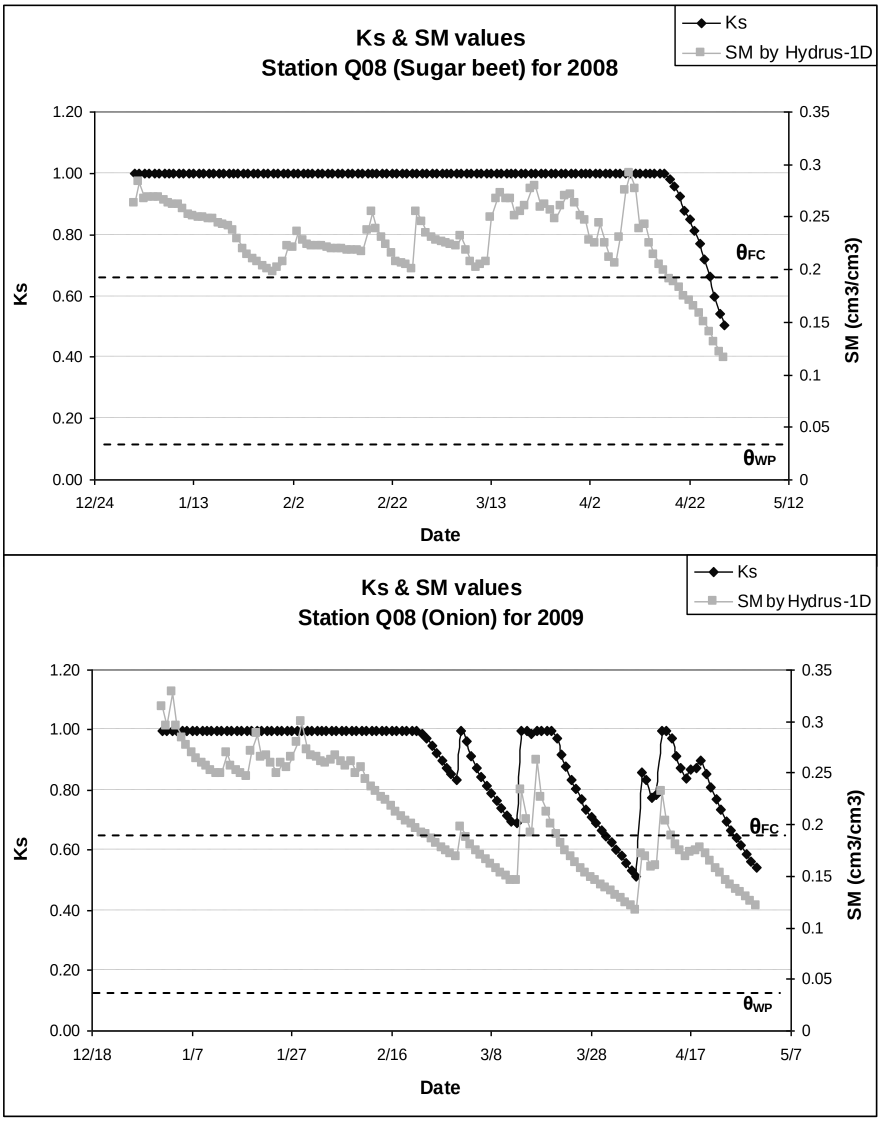

Figure 3-26 shows the values of K_s for sugar beet (year 2008) and onion (year 2009). The first one (sugar beet) is not under stress because K_s is 1 almost during all the vegetative cycle but decreases when it is near to the summer season. On the other hand the onion follows a similar trend, having high values of K_s in the first stage of the vegetative cycle.

Figure 3-27 Ks values for station K10 at 2006 to 2009

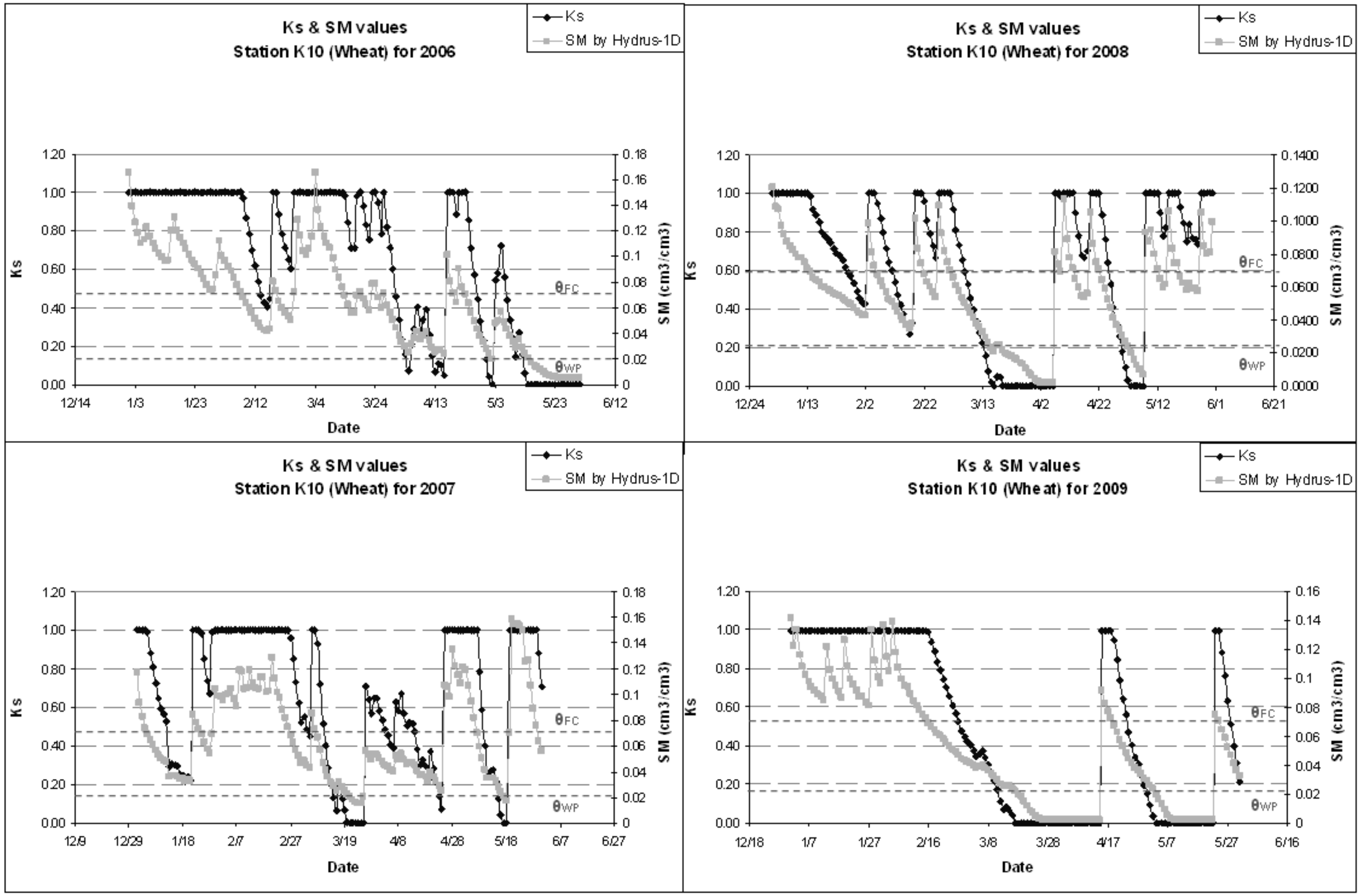

Figure 3-27 explains the values of K_s for wheat, in all the years are present peaks where K_s are 1 o near to it; this is because events of precipitation, especially when the summer season is close and no irrigation is supplied.

This information of K_s is very useful; as from these values is possible to observe when the soil water stress occurs and consequently define the periods when is possible to estimate K_c by using only ET_o and AET (Ks=1), which is the aim of this research.

The determination of K_c is done by using the AET by Hydrus-1D and the ET_o calculated by FAO Penman-Monteith (if the calculation is realized over a date where K_s is different than 1, the values of this factor can be obtained from the previous analysis). The values of these K_c factors for the different dates are summarized in the following tables.

Table 17 K_c factor on April for the years 2006 to 2009

	K_c			
Station	**19-04-06**	**22-04-07**	**17-04-08**	**22-04-09**
Q08	0.40	--	0.40	0.28
J14	--	0.33	0.24	0.53
K10	0.38	0.84	0.45	0.24

Table 18 K_c factor on May for the years 2006 to 2009

	K_c			
Station	**31-05-06**	**20-05-07**	**10-05-08**	**19-05-09**
Q08	--	--	--	--
J14	--	--	0.30	NA
K10	NA	0.18	0.27	NA

The comparison between these K_c calculated (Table 17 and Table 18) and the values from literature are explained in next section, also these values are plotted in Figure 4-2 and Figure 4-3.

4. Analysis of results and discussion

The outputs of Hydrus-1D yield quite accurate results as the model closely matches the measurements of field soil moisture (see Table 5, Table 6 and Table 7). However, this research has detected the need to measure the precipitation data at the same site where SM stations are, and additionally the records of the amount of water supplied by irrigation would complete the adequate, clean and simple data set required for crop water requirements.

The soil data properties predicted (Table 3) by Hydrus-1D using some soil data available (Table 2) is fairly good comparing with Sanchez Martin (2009). In addition the approach presented here is adequate when soils properties do not vary significantly spatially (i.e. sandy texture that is in the Guareña basin) under these circumstances, a comparison between point modelling (Hydrus-1D) and spatial modelling (SEBS) is possible.

The SEBS result shows a good trend, as for areas with crops under irrigation the AET are higher than areas with no irrigation. However this trend not necessary explains the real situations in the area due the model uses many parameters and variables therefore the uncertainty increases on a 1 km pixel resolution (that is the final trade-off of MODIS when SEBS applies). For instance some pixels presents higher values that the PET by Penman-Monteith which is not realistic. On the other hand some pixels present values feasible and even are quite similar to Hydrus-1D outputs.

There are several possible reasons that explain the lack of quantitative match between SEBS and the outcome of the model. They might not be isolated as they may contribute in different ways to errors, but the identification of the most sensible information leading to errors is difficult when the scale of the remote sensing image does not match the ground field information.

The instantaneous to daily approach relies on a preservation of the evaporative fraction during the day which is not normally the case as the meteorological conditions may vary significantly, the land cover and roughness selected for a MODIS pixel (1x1 kilometres) is by all means affecting the results.

It has been detected that SEBS produces high values of KB^{-1} when compared with values found in the literature. If KB^{-1} is high then the roughness for heat becomes very small and as a consequence the aerodynamic resistance for heat transport is very high, leading to very small sensible heat flux (H), therefore the AET by SEBS routinely becomes high.

Figure 4-1 Influence of KB^{-1} over daily AET on SEBS process

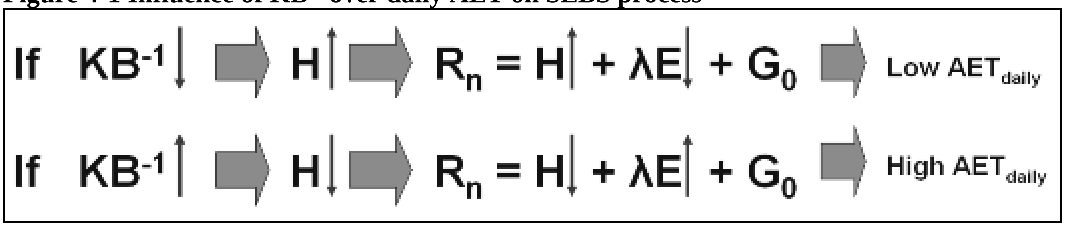

The validation of the actual evapotranspiration is done in relation to the limiting values and matches of the actual humidity. The estimated values should not be higher than the PET (by FAO Penman-Monteith). Then field measurements are needed to compare the real values with the modelling results, in this case SM by Hydrus-1D are compared with the SM measured in field, thus if the SM predicted by Hydrus-1D is close to the value in field the rest of the outputs (AET) are assumed to agreed in this balance.

Therefore the AET by Hydrus-1D is accepted as very promising to estimate the K_c factors for specifics crops in the Guareña basin, and proved to be a simple and useful tool in this research. A K_c curves were built using the values from (Allen, Pereira et al. 1998). These curves (Figure 4-2 and Figure 4-3) are used to compare the values from the literature and the values from the modelling. The green dots are the calculated K_c of this research.

Figure 4-2 Kc curves for Sunflower and Sugar Beet crops

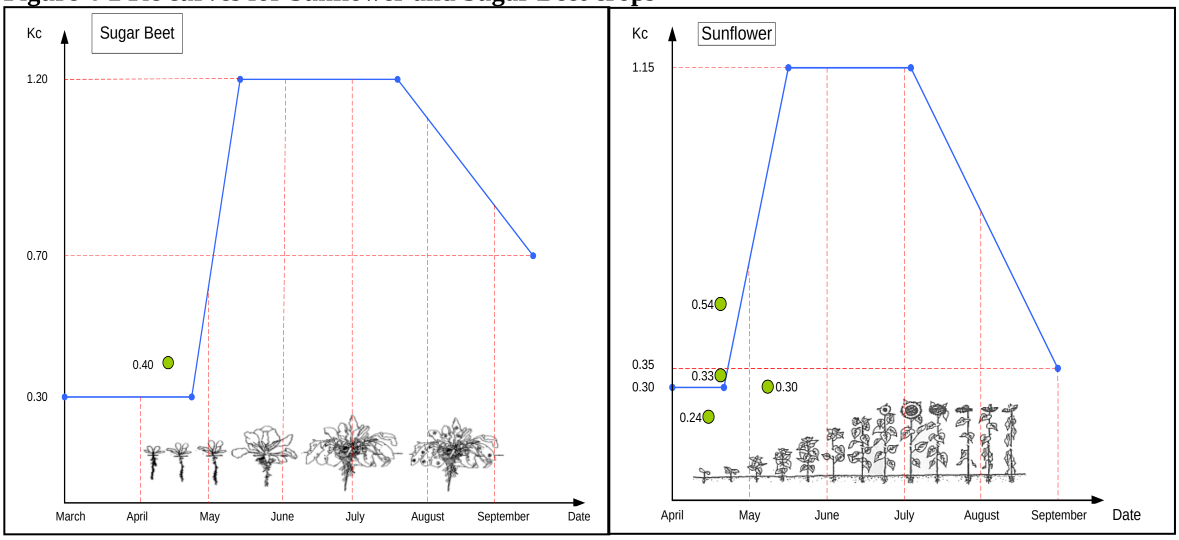

From Figure 4-2 and Table 17 are possible to summarize that most of the values of K_c calculated are quite near to the literature. The K_c for the sunflower (station J14 from 2007 to 2009) is fairly explained for the 22nd April on 2007 where the value is 0.33, and the value from FAO is around 0.30 for this date. The 17th and 22nd April on 2008 and 2009 the K_c values calculated are 0.24 and 0.53, these coefficients are inside the range of FAO, because from the end of April to the middle of May K_c can vary between 0.3 and 1.15.

On the 20th May of 2008 the predicted K_c is 0.3 and according to the K_c curve from the literature the value should be higher (around 1.0), this is possible caused because the vegetative cycle (planting) started late.

For Sugar Beet (station Q08 in year 2008) is quite complex to obtain a general output because only is available one year of modeling. However during this modeling (on 17th April) the K_c obtained (0.40) is quite near to the K_c from the literature (around 0.30).

Figure 4-3 Kc curves for Onion and Wheat crops

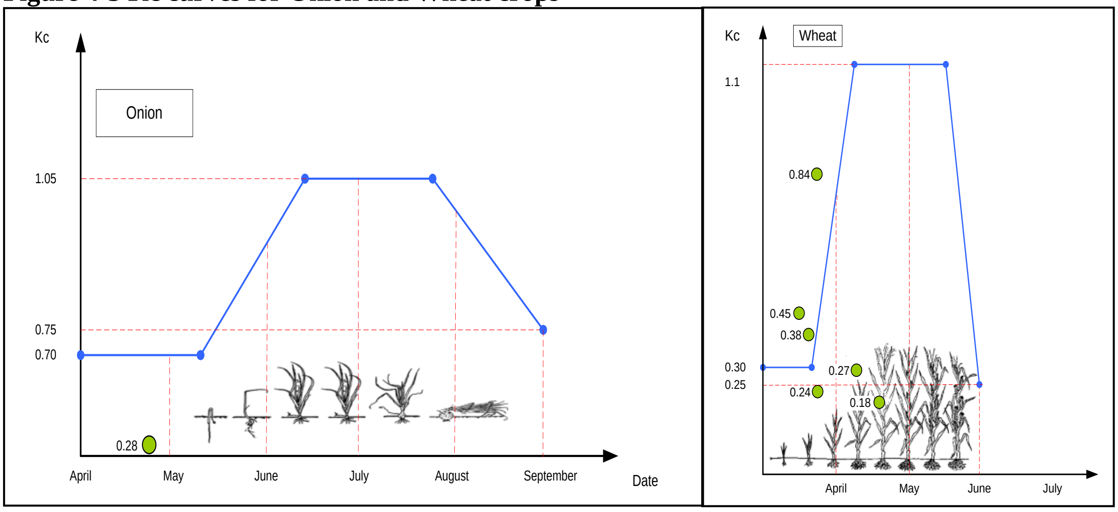

For the onion Crop (station Q08 year 2009) is hard to build up a conclusion because is available just one year of modelling and the records about what crop is in the area are contradictory (some of the records says that the crop in this area is Onion and others says is Sugar Beet). In addition to this the K_c calculated is equal to 0.28 on 19th April which is far away from the value of the literature (0.70) however is close to the value of Sugar Beet crop (0.30).

Finally for wheat crop (station K10 from 2006 to 2009 and Q08 for 2006 and 2007) the predicted values of K_c shows a good trend, at the beginning and at the end of the vegetative cycle the K_c values are lower than the maximum. On 17th at 2008 April the predicted K_c is 0.45, on 19th April at 2006 the K_c values is 0.38 and for the 24th April at 2009 the predicted K_c is 0.24, all these value are close to the values from the literature which indicates for the middle and end of April K_c is around 0.3 and 1.1.

The same behaviour is for the end of the vegetative cycle where on 10th and 20st May the values of K_c predicted are lower (0.18 and 0.27 respectively), however these values are lower to the values from the literature (around 0.35).

Is possible to build up a K_c curve for a specific crop in the area, however is important and necessary to have an accurate vegetative cycle and more modelling dates. Also is important highlight that the literature K_c values are for a specific area under specific conditions, therefore it will never explains precisely the crop coefficients for other areas.

5. Conclusions and recommendations

At present there are already many techniques to quantify the actual evapotranspiration. This research attempted to use a 1D model (Hydrus-1D) and validated its results by using a remote sensing model (SEBS).

The calibration and validation of Hydrus-1D is done by using field measurements of soil moisture, atmospheric and physiological variables and soil characteristics. With these initial variables as constraints, Hydrus-1D optimization routines iterate until the SM predicted is matches to the SM measured in field (final values).

A total of 9 modelling were done between the years 2006 to 2009 showing a quite good prediction of the SM. The minimum percentage of prediction is 72% and the maximum is 92%, however only one is below the threshold of 80%. The number of trials to match the measurements is also an advantage of the procedure as not many are required to obtain a running model.

The AET predicted by Hydrus-1D (values between 0.02 and 4.18 mm/day) presents a realistic performance since during all the modelling present high values during and after precipitations events and present very low values during the summer season where the radiation and temperature are very high. These low values of AET mean that there is a deficit of irrigation due the PET is much higher than the AET (in some cases the difference is higher than 5 mm/day implying that the soil is almost dry). Deficit of irrigation happens most of the time during the growing season at the sites in REMENDHUS area. This thesis showed that K_s is less than 1 more than 64% of the time; which is a usable indicator for irrigation efficiency and could rise some concern at the irrigation community to adequate the water quota.

SEBS is used for the estimation of the daily AET. This thesis was restricted by time to the use of 8 MODIS images (1 km final resolution). Additional input data were required like meteorological variables. The selection of the days were done basically with the criterion of finding days with free cloudy.

The AET by SEBS presents a good trend because where crops under irrigation the AET are is higher and over crops with no irrigation the AET is lower. However the values of actual ET by SEBS are quite high (values between 1.11 and 8.71 mm/day) so at this point SEBS is overestimating the daily AET.

The validation of the actual evapotranspiration is based in the comparison among the modelling and the real values. In this case only Hydrus-1D is able to make this comparison because the predicted SM can be compared with the field SM measurement. Due the good trend and high percent of prediction by the model is assumed that the AET by Hydrus-1D is adequate to carry on the calculation of the crop coefficients.

The determination of the adapted crop coefficients (K_c) is done using the reference ET by FAO 56 and the actual ET by Hydrus-1D. Additionally the K_s factor is obtained in a continuous time step during each period of each modelling. From these graphs of Ks is possible to decide when the best period for the calculation of K_c because it is possible to observe when Ks is equal to 1, and if it has this value the K_c is just the ration of actual ET and reference ET.

The K_c values obtained in this research follow the trend dictated in the literature, as during the initial and final stages the K_c values are low, but during the middle season K_c is higher. The crop coefficient for sunflower and wheat show an agreement with the values offered by FAO at least for the days with Ks=1 or near to it (4 and 6 days respectively). On the other hand there is just 1 day available for onion and sugar beet so is more complex to come up with a general conclusion.

For wheat the K_c values are between 0.18 and 0.84, and the literature indicates that the range of values is between 0.25 and 1.1 which is a proves that at least for the Mediterranean area of Guareña, the official FAO K_c are overestimated.. However in the case of sunflower and sugar beet is not easy to make this comparison with just one value.

In order to obtain more accurate results it is recommended the following:

- The modelling of Hydrus-1D can be improved by incorporating the information of the irrigation schedule: amount and frequency of water supplied to the crop. Also is suggested to have information of the meteorological variables as close as possible to the point of modelling. This complete dataset ensures a faster achievement of modelling agreements.

- The moisture measurements although accurate were not designed for this kind of agricultural application. As such the good agreement of Hydrus-1D was expected a better setting for this methodology would be a profile of moisture at different depths on daily basis. That scheme is possible at local (private) farms but in too costly for the research objectives of REMEDHUS.

- SEBS is overestimating the values of evaporative fraction and actual evapotranspiration and it is advisable to go through a sensitivity analysis of SEBS routines in software other than SEBS4ILWIS. MATLAB seems flexible enough to detect all the submodel implications. A preliminary study was done in this research proving that the KB^{-1} factor is sensible variable in SEBS process therefore its calculation should be study and perhaps improved.

- The irrigation quantity and schedule is not the adequate in REMENDHUS area, at least for the plots under study. The K_s dropped below 1 most of the time, and water irrigation was less frequent than normal or sometimes neglected. The lack of irrigation schedule and quantity could be rebuilt after the wetting of the moisture sensors, which proves accurate enough to conclude on the deficit situation.

- This research has detected distinctive values of K_c for some main crops in the area other than the standards in FAO literature. The results are promising however it is important to have more days for calculating K_c factor in order to build a more representative K_c curve for the crops in the REMENDHUS area. The actual scheme of data collection requires little adaptations to match the needs of K_c estimates, so it makes sense to encourage the continuation of this line of research in that area.

References

Allen, R. G., L. S. Pereira, et al. (1998). FAO Irrigation and Drainage Paper No. 56. FAO. Rome, Italy.

Brutsaert, W. (1999). "Aspects of bulk atmospheric boundary layer similarity under free-convective conditions." Reviews of Geophysics 37(4): 439-451.

Burke, E. J. and J. B. Stewart (1997). Test of a sensible heat flux : Radiometric surface temperature relationship for HAPEX-Sahel. Dordrecht, PAYS-BAS, Springer.

Carabias-Martínez, R., E. Rodríguez-Gonzalo, et al. (2003). "Evolution over time of the agricultural pollution of waters in an area of Salamanca and Zamora (Spain)." Water Research 37(4): 928-938.

Carlson, T. N. and D. A. Ripley (1997). On the relation between NDVI, fractional vegetation cover, and leaf area index. New York, NY, ETATS-UNIS, Elsevier.

CIMIS (2008). "Crop Coefficients." Retrieved 7/8, 2009, from http://wwwcimis.water.ca.gov/cimis/infoEtoCropCo.jsp.

Hauser, V. L. (2008). Evapotranspiration Covers for Landfills and Waste Sites.

Irmak, S. and D. Haman Z. (2003). "Evapotranspiration: Potential or Reference?". Retrieved November, 2009, from http://edis.ifas.ufl.edu/ae256.

Jensen, M. E. (1968). "WATER CONSUMPTION BY AGRICULTURAL PLANTS." Agricultural research service, USDA, Kimberly, Idaho. Chapter 1.

Kwast, J. and S. M. Jong (2004) Modelling evapotranspiration using the surface energy balance systems (SEBS) and Landsat tm data (Rabat region, Morocco).

Li, Z. L., L. Jia, et al. (2001). "Envisat. Land Surface Process: Estimation of vegetation and soil component temperatures from ATSR-2 data." USP-2B: 43-54.

Liang, S. L. (2001). "Narrowband to broadband conversions of land surface albedo I Algorithms." Remote Sensing of Environment 76(2): 213-238.

Martínez-Fernández, J. and A. Ceballos (2005). "Mean soil moisture estimation using temporal stability analysis." Journal of Hydrology 312(1-4): 28-38.

Rahman, H. and G. Dedieu (1994). "SMAC: a simplified method for the atmospheric correction of satellite measurements in the solar spectrum." International Journal of Remote Sensing 15(1): 123 - 143.

Rana, G. and N. Katerji (2000). "Measurement and estimation of actual evapotranspiration in the field under Mediterranean climate: a review." European Journal of Agronomy 13(2-3): 125-153.

Ritter, M. E. (2006). "The Physical Environment: an Introduction to Physical Geography." Retrieved November, 2009, from http://www.uwsp.edu/geo/faculty/ritter/geog101/textbook/energy/energy_balance.html.

Sánchez Martín, N. (2009). TELEDETECCIÓN ÓPTICA APLICADA A UN MODELO DISTRIBUIDO DE BALANCE HÍDRICO (HIDROMORE) PARA EL CÁLCULO DE EVAPOTRANSPIRACIÓN Y HUMEDAD DE SUELO. Departamento & ingenieria Cartografica y del Terreno. Salamanca, Universidad de Salamanca. PhD: 410.

Schaap, M. G., F. J. Leij, et al. (2001). ": a computer program for estimating soil hydraulic parameters with hierarchical pedotransfer functions." Journal of Hydrology 251(3-4): 163-176.

Seaman, J., J. Singer, et al. (2009). EVALUATING THE RELATIVE IMPORTANCE OF THE VAN GENUCHTEN/MUALEM PARAMETERS. Proceedings of the 2009 Georgia Water Resources Conference. U. o. Georgia. University of Georgia.

Simunek, J., R. Kodesova, et al. (1999) Estimating hysteresis in the soil water retention function from cone permeameter experiments. 35, 1329-1345

Simunek, J., M. Van Genuchten, et al. (2005). THE HYDRUS-1D SOFTWARE PACKAGE FOR SIMULATING THE ONE-DIMENSIONAL MOVEMENT OF WATER, HEAT, AND MULTIPLE SOLUTES IN VARIABLY-SATURATED MEDIA University of California-Riverside Research Reports

Sobrino, J. A. and N. Raissouni (2000). "Toward remote sensing methods for land cover dynamic monitoring: application to Morocco." International Journal of Remote Sensing 21(2): 353-366.

Su, Z. (2002). "The Surface Energy Balance System (SEBS) for estimation of turbulent heat fluxes." Hydrology and Earth System Sciences 6(1): 85-99.

Su, Z., T. Schmugge, et al. (2001). "An evaluation of two models for estimation of the roughness height for heat transfer between the land surface and the atmosphere." Journal of Applied Meteorology 40(11): 1933-1951.

van der Kwast, J., W. Timmermans, et al. (2009). "Evaluation of the Surface Energy Balance System (SEBS) applied to ASTER imagery with flux-measurements at the SPARC 2004 site (Barrax, Spain)." Hydrol. Earth Syst. Sci. Discuss. 6(1): 1165-1196.

Verhoef, A., H. A. R. De Bruin, et al. (1997). "Some Practical Notes on the Parameter kB-1 for Sparse Vegetation." Journal of Applied Meteorology 36(5): 560-572.

Appendix A

Soil textures collected by USAL

Sample code	Easting	Northing	Sand %	Silt %	Clay %	Texture class	Dry bulk density (g/cc)	Wilting point (% vol)	Field capacity (% vol)	Porosity (%)
B10	274500	4571500	76	17	7	sandy loam	1.30	4.8	11.8	41.7
C10	277500	4568500	73	17	10	sandy loam	1.47	6.6	14.1	41.2
C11	277500	4574500	83	14	3	loamy sand	1.57	2.3	8.2	43.1
C9	277500	4571500	87	11	2	sand	1.35	1.6	6.8	43.7
D10	280500	4565500	67	28	6	sandy loam	1.61	4.4	13.3	41.6
D11	280500	4577500	66	19	15	sandy loam	1.35	9.7	18.3	40.7
D12	280500	4574500	82	14	4	loamy sand	1.62	2.9	8.9	42.7
D8	280500	4571500	44	24	32	clay loam	1.47	19.7	31.6	43.0
D9	280500	4568500	66	13	22	sandy clay loam	1.48	13.8	22.3	40.3
E10	283500	4580500	57	23	20	sandy loam	1.64	12.7	22.9	40.9
E11	283500	4577500	69	18	13	sandy loam	1.36	8.5	16.6	40.8
E12	283500	4574500	69	13	18	sandy loam	1.63	11.4	19.4	40.4
E7	283500	4571500	83	11	6	loamy sand	1.14	4.1	9.7	42.3
E8	283500	4568500	49	18	33	sandy clay loam	1.45	20.3	31.5	42.5
E9	283500	4565500	79	15	5	loamy sand	1.21	3.5	10.1	42.3
F10	286500	4583500	82	10	9	loamy sand	1.25	5.9	11.6	41.6
F11	286500	4580500	59	17	24	sandy clay loam	1.06	14.4	24.2	40.8
F12	286500	4577500	62	18	20	sandy loam	1.44	12.7	21.9	40.6
F13	286500	4574500	66	22	12	sandy loam	1.31	7.9	16.7	40.9
F6	286500	4571500	41	38	21	loam	1.44	13.4	26.6	42.1
F7	286500	4568500	54	29	17	sandy loam	1.08	11.0	21.9	41.1
F8	286500	4565500	50	19	31	sandy clay loam	1.22	19.1	30.2	42.2
F9	286500	4562500	25	34	41	clay	1.39	24.6	38.3	47.2
G10	289500	4586500	48	34	19	loam	1.46	12.2	24.2	41.5
G11	289500	4583500	81	14	5	loamy sand	1.52	3.5	9.7	42.4
G12	289500	4580500	74	19	7	sandy loam	1.29	4.8	12.2	41.7
G13	289500	4577500	76	14	10	sandy loam	1.48	6.6	13.4	41.2
G14	289500	4574500	84	11	6	loamy sand	1.59	4.1	9.5	42.4
G5	289500	4571500	79	10	12	sandy loam	1.25	7.8	13.9	40.9
G6	289500	4568500	67	19	15	sandy loam	1.37	9.7	18.1	40.7
G7	289500	4565500	68	15	17	sandy loam	1.55	10.9	19.0	40.5
G8	289500	4562500	80	15	5	loamy sand	1.38	3.5	9.9	42.4
G9	289500	4559500	54	24	22	sandy clay loam	1.42	13.9	24.6	41.2
H10	292500	4589500	89	11	0	sand	1.37	1.5	6.4	43.9
H11	292500	4586500	46	34	21	loam	1.28	13.3	25.6	41.7
H12	292500	4583500	82	11	8	loamy sand	1.48	5.3	11.0	41.8
H13	292500	4580500	79	10	11	sandy loam	1.57	7.2	13.3	41.1
H14	292500	4577500	71	10	19	sandy loam	1.09	12.0	19.6	40.2
H15	292500	4574500	66	14	20	sandy loam	1.13	12.6	21.1	40.4
H4	292500	4571500	61	16	23	sandy clay loam	1.44	14.4	23.8	40.7
H5	292500	4568500	73	9	18	sandy loam	1.18	11.4	18.6	40.2
H6	292500	4565500	71	11	18	sandy loam	1.41	11.4	19.0	40.3
H7	292500	4562500	65	23	12	sandy loam	1.37	7.9	16.9	40.9
H8	292500	4559500	47	19	34	sandy clay loam	1.26	20.8	32.3	42.8
H9	292500	4556500	65	26	9	sandy loam	1.37	6.2	15.3	41.2
I10	295500	4592500	52	28	20	sandy loam	1.51	12.7	23.9	41.3
I11	295500	4589500	67	16	18	sandy loam	1.28	11.5	19.8	40.5
I12	295500	4586500	74	9	17	sandy loam	1.36	10.8	17.8	40.3
I13	295500	4583500	67	15	19	sandy loam	1.38	12.0	20.4	40.4
I14	295500	4580500	86	11	3	loamy sand	1.26	2.2	7.5	43.3
I15	295500	4577500	70	10	20	sandy loam	1.15	12.6	20.4	40.2
I16	295500	4574500	69	16	15	sandy loam	1.52	9.7	17.7	40.6
I3	295500	4571500	84	10	5	loamy sand	1.56	3.5	9.0	42.6
I4	295500	4568500	77	10	12	sandy loam	1.39	7.8	14.3	40.9
I5	295500	4565500	44	27	29	clay loam	1.37	17.9	30.1	42.6
I6	295500	4562500	67	22	11	sandy loam	1.19	7.3	15.9	41.0
I7	295500	4559500	64	11	24	sandy clay loam	1.38	15.0	23.9	40.5
I8	295500	4556500	44	23	34	clay loam	1.23	20.8	32.7	43.2
I9	295500	4553500	63	11	26	sandy clay loam	1.61	16.2	25.2	40.5
J10	298500	4592500	89	8	3	sand	1.32	2.2	6.9	43.6
J11	298500	4589500	77	13	10	sandy loam	1.33	7.2	13.8	41.1
J12	298500	4586500	84	9	7	loamy sand	1.40	4.7	10.1	42.1
J13	298500	4583500	62	26	13	sandy loam	1.19	8.6	18.1	40.9

Sample code	Easting	Northing	Sand %	Silt %	Clay %	Texture class	Dry bulk density (g/cc)	Wilting point (% vol)	Field capacity (% vol)	Porosity (%)
J14	298500	4580500	74	13	13	sandy loam	1.56	8.4	15.5	40.8
J15	298500	4577500	72	15	13	sandy loam	1.51	8.4	15.9	40.8
J16	298500	4574500	86	10	5	loamy sand	1.21	3.4	8.6	42.7
J2	298500	4571500	72	11	17	sandy loam	1.53	10.8	18.2	40.3
J3	298500	4568500	75	8	17	sandy loam	1.43	10.8	17.6	40.2
J4	298500	4565500	70	15	14	sandy loam	1.49	9.1	16.9	40.7
J5	298500	4562500	49	21	29	sandy clay loam	1.33	17.9	29.3	42.1
J6	298500	4559500	67	14	19	sandy loam	1.18	12.0	20.4	40.4
J7	298500	4556500	62	17	22	sandy clay loam	1.46	13.8	23.1	40.6
J8	298500	4553500	54	13	33	sandy clay loam	1.26	20.3	30.8	41.8
J9	298500	4595500	87	11	2	sand	1.33	1.6	6.8	43.7
K10	301500	4592500	81	9	10	loamy sand	1.36	6.5	12.4	41.3
K11	301500	4589500	44	28	28	clay loam	1.39	17.4	29.5	42.5
K12	301500	4586500	51	25	24	sandy clay loam	1.38	15.0	26.2	41.5
K13	301500	4583500	70	15	14	sandy loam	1.39	9.1	16.9	40.7
K14	301500	4580500	82	9	9	loamy sand	1.31	5.9	11.6	41.6
K15	301500	4577500	77	12	11	sandy loam	1.26	7.2	13.8	41.1
K16	301500	4574500	84	11	5	loamy sand	1.60	3.5	9.0	42.6
K2	301500	4571500	62	20	17	sandy loam	1.58	10.9	20.2	40.7
K3	301500	4568500	76	14	10	sandy loam	1.61	6.6	13.4	41.2
K4	301500	4565500	72	12	17	sandy loam	1.24	10.8	18.2	40.3
K5	301500	4562500	62	18	20	sandy loam	1.41	12.7	21.9	40.6
K6	301500	4559500	83	6	11	loamy sand	1.43	7.1	12.5	41.1
K7	301500	4556500	62	16	22	sandy clay loam	1.49	13.8	23.1	40.6
K8	301484	4553500	83	8	9	loamy sand	1.34	5.9	11.4	41.6
K9	301500	4595500	84	13	3	loamy sand	1.31	2.2	8.0	43.2
L10	304500	4589500	69	18	13	sandy loam	1.39	8.5	16.6	40.8
L11	304500	4586500	77	15	8	sandy loam	1.40	5.4	12.1	41.6
L12	304500	4583500	79	14	7	loamy sand	1.19	4.7	11.1	41.9
L13	304500	4580500	56	18	26	sandy clay loam	1.45	16.2	26.4	41.2
L14	304500	4577500	71	12	17	sandy loam	1.48	10.8	18.4	40.4
L15	304500	4574500	70	17	14	sandy loam	1.27	9.1	16.9	40.7
L2	304500	4571500	71	14	15	sandy loam	1.35	9.6	17.3	40.6
L3	304500	4568500	83	11	5	loamy sand	1.51	4.1	9.7	42.3
L4	304500	4565500	67	13	20	sandy loam	1.29	12.6	21.0	40.4
L5	304500	4562500	81	10	9	loamy sand	1.41	5.9	11.8	41.5
L6	304500	4559500	70	15	15	sandy loam	1.33	9.1	16.9	40.7
L7	304500	4556500	74	13	13	sandy loam	1.09	8.4	15.5	40.8
L8	304500	4595500	70	18	12	sandy loam	1.32	7.9	15.8	40.9
L9	304500	4592500	69	21	9	sandy loam	1.30	6.1	14.4	41.2
M10	307500	4586500	87	9	3	sand	1.25	2.2	7.3	43.4
M11	307500	4583500	86	10	4	loamy sand	1.32	2.8	8.0	43.0
M12	307500	4580500	86	10	4	loamy sand	1.32	2.8	8.0	43.0
M13	307500	4577500	62	17	21	sandy clay loam	1.36	13.3	22.5	40.6
M14	307500	4574500	67	17	16	sandy loam	1.30	10.3	18.7	40.6
M3	307500	4571500	52	20	28	sandy clay loam	1.62	17.4	28.2	41.7
M4	307500	4568500	63	16	21	sandy clay loam	1.51	13.2	22.3	40.6
M5	307500	4565500	74	13	14	sandy loam	1.42	9.0	16.1	40.6
M6	307500	4562500	84	8	8	loamy sand	1.51	5.3	10.6	41.9
M7	307500	4559500	82	9	9	loamy sand	1.58	5.9	11.6	41.6
M8	307500	4592500	86	8	6	loamy sand	1.33	4.0	9.1	42.5
M9	307500	4589500	86	10	4	loamy sand	1.35	2.8	8.0	43.0
N10	310500	4583500	62	21	17	sandy loam	1.52	10.9	20.2	40.7
N11	310500	4580500	79	15	6	loamy sand	1.07	4.1	10.6	42.1
N12	310500	4577500	74	15	11	sandy loam	1.47	7.2	14.4	41.0
N13	310500	4574500	80	12	9	loamy sand	1.45	5.9	12.0	41.5
N4	310500	4571500	93	6	1	sand	1.52	1.5	5.6	44.3
N5	310500	4568500	42	28	31	clay loam	1.37	19.1	31.4	43.1
N6	310500	4565500	77	15	8	sandy loam	1.23	5.4	12.1	41.6
N7	310500	4562500	68	11	21	sandy clay loam	1.60	13.2	21.4	40.3
N8	310500	4589500	98	2	0	sand	1.32	1.4	4.9	44.6
N9	310500	4586500	77	14	10	sandy loam	1.59	6.0	12.7	41.4
O10	313500	4580500	58	12	30	sandy clay loam	1.37	18.5	28.4	41.2
O11	313500	4577500	74	12	14	sandy loam	1.33	9.0	16.1	40.6
O12	313500	4574500	64	10	25	sandy clay loam	1.24	15.6	24.5	40.5
O5	313500	4571500	80	14	6	loamy sand	1.14	4.1	10.4	42.1
O6	313500	4568500	56	10	34	sandy clay loam	1.33	20.9	31.1	41.7
O7	313500	4565500	76	13	11	sandy loam	1.15	7.2	14.0	41.1
O8	313500	4586500	77	14	9	sandy loam	1.40	6.0	12.7	41.4

Sample code	Easting	Northing	Sand %	Silt %	Clay %	Texture class	Dry bulk density (g/cc)	Wilting point (% vol)	Field capacity (% vol)	Porosity (%)
O9	313500	4583500	76	13	11	sandy loam	1.29	7.2	14.0	41.1
P10	316500	4577500	63	10	26	sandy clay loam	1.41	16.2	25.2	40.5
P11	316500	4574500	69	10	21	sandy clay loam	0.96	13.2	21.2	40.2
P6	316500	4571500	79	13	8	loamy sand	1.27	5.4	11.7	41.7
P7	316500	4568500	24	47	29	clay loam	1.31	17.9	33.4	44.9
P8	316500	4583500	60	25	15	sandy loam	1.25	9.7	19.6	40.9
P9	316500	4580500	57	12	31	sandy clay loam	1.40	19.1	29.2	41.3
Q10	319500	4574500	65	12	23	sandy clay loam	1.51	14.4	23.1	40.4
Q7	319500	4571500	81	14	5	loamy sand	1.32	4.1	10.2	42.2
Q8	319500	4580500	68	13	19	sandy loam	1.46	12.0	20.2	40.4
Q9	319500	4577500	89	7	4	sand	1.21	2.8	7.4	43.3
R7	322429	4580500	70	17	13	sandy loam	1.34	8.5	16.4	40.8
R8	322500	4577500	68	10	22	sandy clay loam	1.42	13.8	21.9	40.2
R9	322500	4574500	67	20	13	sandy loam	1.35	8.5	17.0	40.8
S8	325500	4577500	63	13	23	sandy clay loam	1.57	14.4	23.5	40.5

Appendix B

Soil moisture observed in field

Station K10								Station Q08							
x	y 2006	y 2007	y 2008	y 2009	type	position	weight	x	y 2006	y 2007	y 2008	y 2009	type	position	weight
1	0.108	0.055	0.073	0.097	2	1	1	1	0.229	0.219	0.264	0.252	2	1	1
2	0.100	0.051	0.087	0.097	2	1	1	2	0.221	0.214	0.289	0.254	2	1	1
3	0.092	0.050	0.107	0.138	2	1	1	3	0.216	0.210	0.277	0.285	2	1	1
4	0.089	0.049	0.094	0.119	2	1	1	4	0.214	0.207	0.273	0.281	2	1	1
5	0.089	0.050	0.088	0.107	2	1	1	5	0.212	0.210	0.273	0.271	2	1	1
6	0.109	0.051	0.085	0.102	2	1	1	6	0.240	0.211	0.270	0.266	2	1	1
7	0.126	0.048	0.081	0.097	2	1	1	7	0.260	0.207	0.268	0.261	2	1	1
8	0.124	0.046	0.079	0.092	2	1	1	8	0.252	0.208	0.267	0.256	2	1	1
9	0.118	0.044	0.076	0.089	2	1	1	9	0.245	0.208	0.264	0.253	2	1	1
10	0.111	0.042	0.073	0.092	2	1	1	10	0.240	0.203	0.264	0.251	2	1	1
11	0.108	0.040	0.073	0.093	2	1	1	11	0.236	0.198	0.264	0.249	2	1	1
12	0.108	0.038	0.072	0.090	2	1	1	12	0.235	0.194	0.260	0.248	2	1	1
13	0.107	0.039	0.069	0.118	2	1	1	13	0.234	0.193	0.259	0.252	2	1	1
14	0.108	0.038	0.071	0.119	2	1	1	14	0.234	0.192	0.258	0.263	2	1	1
15	0.124	0.039	0.071	0.109	2	1	1	15	0.267	0.193	0.258	0.260	2	1	1
16	0.149	0.040	0.071	0.104	2	1	1	16	0.275	0.195	0.255	0.260	2	1	1
17	0.138	0.039	0.068	0.102	2	1	1	17	0.261	0.194	0.255	0.259	2	1	1
18	0.135	0.037	0.068	0.099	2	1	1	18	0.259	0.193	0.252	0.258	2	1	1
19	0.131	0.036	0.065	0.112	2	1	1	19	0.255	0.192	0.251	0.271	2	1	1
20	0.128	0.035	0.063	0.116	2	1	1	20	0.252	0.190	0.249	0.279	2	1	1
21	0.125	0.035	0.063	0.106	2	1	1	21	0.251	0.188	0.249	0.268	2	1	1
22	0.120	0.076	0.063	0.103	2	1	1	22	0.248	0.223	0.246	0.267	2	1	1
23	0.112	0.095	0.061	0.106	2	1	1	23	0.242	0.254	0.240	0.271	2	1	1
24	0.110	0.086	0.059	0.103	2	1	1	24	0.241	0.242	0.223	0.268	2	1	1
25	0.106	0.080	0.058	0.105	2	1	1	25	0.237	0.236	0.223	0.266	2	1	1
26	0.094	0.073	0.057	0.105	2	1	1	26	0.233	0.229	0.221	0.264	2	1	1
27	0.083	0.052	0.055	0.099	2	1	1	27	0.227	0.221	0.220	0.262	2	1	1
28	0.068	0.045	0.052	0.106	2	1	1	28	0.222	0.206	0.219	0.267	2	1	1
29	0.112	0.061	0.050	0.136	2	1	1	29	0.222	0.214	0.218	0.293	2	1	1
30	0.116	0.113	0.047	0.118	2	1	1	30	0.222	0.269	0.217	0.280	2	1	1
31	0.123	0.103	0.045	0.111	2	1	1	31	0.221	0.256	0.217	0.274	2	1	1
32	0.114	0.097	0.043	0.132	2	1	1	32	0.220	0.250	0.228	0.269	2	1	1
33	0.118	0.092	0.069	0.126	2	1	1	33	0.231	0.245	0.229	0.270	2	1	1
34	0.115	0.105	0.072	0.118	2	1	1	34	0.249	0.247	0.241	0.271	2	1	1
35	0.099	0.107	0.099	0.133	2	1	1	35	0.243	0.251	0.234	0.270	2	1	1
36	0.084	0.112	0.087	0.137	2	1	1	36	0.239	0.267	0.233	0.269	2	1	1
37	0.082	0.104	0.083	0.130	2	1	1	37	0.236	0.259	0.230	0.272	2	1	1
38	0.080	0.098	0.076	0.119	2	1	1	38	0.231	0.254	0.228	0.272	2	1	1
39	0.076	0.117	0.072	0.112	2	1	1	39	0.227	0.281	0.226	0.268	2	1	1
40	0.075	0.125	0.067	0.109	2	1	1	40	0.223	0.295	0.224	0.268	2	1	1
41	0.082	0.107	0.060	0.103	2	1	1	41	0.221	0.277	0.222	0.270	2	1	1
42	0.076	0.102	0.053	0.097	2	1	1	42	0.220	0.272	0.220	0.267	2	1	1
43	0.068	0.127	0.048	0.091	2	1	1	43	0.214	0.294	0.219	0.263	2	1	1
44	0.063	0.113	0.043	0.086	2	1	1	44	0.209	0.284	0.217	0.259	2	1	1
45	0.059	0.115	0.039	0.080	2	1	1	45	0.203	0.287	0.217	0.254	2	1	1
46	0.057	0.104	0.037	0.076	2	1	1	46	0.198	0.275	0.216	0.250	2	1	1

Station K10								Station Q08							
x	**y 2006**	**y 2007**	**y 2008**	**y 2009**	**type**	**position**	**weight**	**x**	**y 2006**	**y 2007**	**y 2008**	**y 2009**	**type**	**position**	**weight**
46	0.057	0.104	0.037	0.076	2	1	1	46	0.198	0.275	0.216	0.250	2	1	1
47	0.056	0.120	0.034	0.071	2	1	1	47	0.196	0.282	0.214	0.246	2	1	1
48	0.053	0.132	0.032	0.066	2	1	1	48	0.189	0.295	0.230	0.240	2	1	1
49	0.051	0.118	0.058	0.061	2	1	1	49	0.187	0.281	0.247	0.235	2	1	1
50	0.067	0.110	0.087	0.057	2	1	1	50	0.262	0.275	0.245	0.229	2	1	1
51	0.077	0.140	0.098	0.053	2	1	1	51	0.249	0.307	0.238	0.224	2	1	1
52	0.074	0.126	0.091	0.049	2	1	1	52	0.238	0.296	0.234	0.222	2	1	1
53	0.069	0.117	0.084	0.044	2	1	1	53	0.232	0.286	0.230	0.218	2	1	1
54	0.058	0.116	0.075	0.040	2	1	1	54	0.226	0.288	0.228	0.208	2	1	1
55	0.054	0.113	0.071	0.037	2	1	1	55	0.221	0.289	0.227	0.198	2	1	1
56	0.080	0.109	0.066	0.033	2	1	1	56	0.238	0.282	0.225	0.189	2	1	1
57	0.130	0.102	0.058	0.030	2	1	1	57	0.268	0.274	0.225	0.181	2	1	1
58	0.140	0.097	0.060	0.028	2	1	1	58	0.269	0.267	0.249	0.172	2	1	1
59	0.139	0.091	0.114	0.026	2	1	1	59	0.263	0.258	0.249	0.173	2	1	1
60	0.123	0.083	0.102	0.026	2	1	1	60	0.259	0.250	0.244	0.160	2	1	1
61	0.129	0.076	0.095	0.025	2	1	1	61	0.260	0.243	0.240	0.200	2	1	1
62	0.125	0.070	0.087	0.024	2	1	1	62	0.262	0.234	0.238	0.160	2	1	1
63	0.148	0.063	0.077	0.021	2	1	1	63	0.286	0.223	0.237	0.147	2	1	1
64	0.151	0.066	0.063	0.020	2	1	1	64	0.278	0.216	0.233	0.144	2	1	1
65	0.135	0.064	0.047	0.021	2	1	1	65	0.263	0.214	0.231	0.145	2	1	1
66	0.129	0.080	0.036	0.022	2	1	1	66	0.258	0.254	0.229	0.147	2	1	1
67	0.121	0.077	0.031	0.021	2	1	1	67	0.254	0.267	0.228	0.143	2	1	1
68	0.108	0.068	0.028	0.020	2	1	1	68	0.249	0.254	0.231	0.140	2	1	1
69	0.095	0.061	0.025	0.018	2	1	1	69	0.242	0.244	0.231	0.136	2	1	1
70	0.084	0.050	0.023	0.017	2	1	1	70	0.237	0.230	0.229	0.133	2	1	1
71	0.074	0.044	0.023	0.016	2	1	1	71	0.226	0.217	0.232	0.131	2	1	1
72	0.067	0.041	0.023	0.015	2	1	1	72	0.215	0.206	0.243	0.174	2	1	1
73	0.062	0.038	0.021	0.014	2	1	1	73	0.203	0.193	0.259	0.228	2	1	1
74	0.056	0.041	0.020	0.013	2	1	1	74	0.189	0.181	0.267	0.205	2	1	1
75	0.053	0.040	0.019	0.012	2	1	1	75	0.173	0.169	0.266	0.192	2	1	1
76	0.049	0.037	0.017	0.011	2	1	1	76	0.160	0.161	0.269	0.264	2	1	1
77	0.053	0.034	0.015	0.009	2	1	1	77	0.159	0.154	0.267	0.234	2	1	1
78	0.074	0.030	0.023	0.007	2	1	1	78	0.252	0.147	0.262	0.216	2	1	1
79	0.079	0.026	0.024	0.005	2	1	1	79	0.246	0.140	0.256	0.208	2	1	1
80	0.074	0.025	0.021	0.004	2	1	1	80	0.245	0.136	0.258	0.194	2	1	1
81	0.068	0.026	0.019	0.003	2	1	1	81	0.237	0.136	0.271	0.174	2	1	1
82	0.064	0.026	0.015	0.002	2	1	1	82	0.244	0.135	0.272	0.159	2	1	1
83	0.072	0.026	0.013	0.002	2	1	1	83	0.263	0.133	0.262	0.150	2	1	1
84	0.069	0.026	0.016	0.001	2	1	1	84	0.243	0.130	0.256	0.143	2	1	1
85	0.054	0.027	0.016	0.001	2	1	1	85	0.226	0.127	0.254	0.142	2	1	1
86	0.042	0.055	0.013	0.001	2	1	1	86	0.209	0.131	0.249	0.143	2	1	1
87	0.034	0.062	0.012	0.000	2	1	1	87	0.191	0.130	0.258	0.140	2	1	1
88	0.030	0.056	0.012	0.000	2	1	1	88	0.175	0.135	0.270	0.134	2	1	1
89	0.029	0.047	0.012	0.000	2	1	1	89	0.163	0.135	0.279	0.131	2	1	1
90	0.026	0.045	0.009	0.000	2	1	1	90	0.146	0.140	0.264	0.129	2	1	1
91	0.023	0.041	0.008	0.000	2	1	1	91	0.135	0.178	0.260	0.128	2	1	1
92	0.020	0.038	0.008	0.000	2	1	1	92	0.127	0.187	0.260	0.128	2	1	1
93	0.019	0.036	0.008	0.001	2	1	1	93	0.121	0.188	0.245	0.127	2	1	1
94	0.017	0.033	0.006	0.001	2	1	1	94	0.117	0.187	0.230	0.127	2	1	1
95	0.013	0.032	0.004	0.001	2	1	1	95	0.111	0.183	0.238	0.126	2	1	1

Station K10								Station Q08							
x	y 2006	y 2007	y 2008	y 2009	type	position	weight	x	y 2006	y 2007	y 2008	y 2009	type	position	weight
96	0.014	0.033	0.003	0.000	2	1	1	96	0.111	0.213	0.227	0.123	2	1	1
97	0.019	0.031	0.002	0.000	2	1	1	97	0.195	0.220	0.213	0.163	2	1	1
98	0.023	0.034	0.000	0.000	2	1	1	98	0.231	0.222	0.207	0.170	2	1	1
99	0.019	0.033	0.041	0.000	2	1	1	99	0.199	0.220	0.203	0.159	2	1	1
100	0.014	0.046	0.082	0.000	2	1	1	100	0.166	0.218	0.281	0.169	2	1	1
101	0.020	0.046	0.110	0.020	2	1	1	101	0.144	0.213	0.311	0.220	2	1	1
102	0.015	0.041	0.109	0.033	2	1	1	102	0.129	0.221	0.286	0.208	2	1	1
103	0.016	0.042	0.098	0.035	2	1	1	103	0.119	0.259	0.269	0.189	2	1	1
104	0.016	0.042	0.090	0.034	2	1	1	104	0.112	0.239	0.252	0.175	2	1	1
105	0.100	0.038	0.087	0.044	2	1	1	105	0.131	0.221	0.226	0.171	2	1	1
106	0.090	0.036	0.074	0.080	2	1	1	106	0.261	0.204	0.203	0.174	2	1	1
107	0.110	0.032	0.056	0.094	2	1	1	107	0.270	0.189	0.190	0.176	2	1	1
108	0.090	0.031	0.045	0.090	2	1	1	108	0.254	0.175	0.186	0.179	2	1	1
109	0.080	0.027	0.092	0.087	2	1	1	109	0.234	0.162	0.187	0.180	2	1	1
110	0.070	0.023	0.105	0.083	2	1	1	110	0.212	0.199	0.189	0.178	2	1	1
111	0.080	0.027	0.111	0.074	2	1	1	111	0.231	0.276	0.186	0.170	2	1	1
112	0.070	0.028	0.105	0.066	2	1	1	112	0.231	0.263	0.181	0.157	2	1	1
113	0.080	0.024	0.095	0.059	2	1	1	113	0.205	0.249	0.177	0.146	2	1	1
114	0.050	0.020	0.092	0.053	2	1	1	114	0.175	0.227	0.168	0.139	2	1	1
115	0.030	0.054	0.080	0.045	2	1	1	115	0.143	0.236	0.160	0.134	2	1	1
116	0.009	0.125	0.060	0.039	2	1	1	116	0.125	0.277	0.154	0.130	2	1	1
117	0.005	0.129	0.043	0.036	2	1	1	117	0.118	0.277	0.150	0.127	2	1	1
118	0.003	0.134	0.034	0.035	2	1	1	118	0.111	0.281	0.148	0.127	2	1	1
119	0.002	0.133	0.028	0.033	2	1	1	119	0.106	0.281	0.141	0.126	2	1	1
120	0.001	0.118	0.020	0.031	2	1	1	120	0.102	0.268	0.138	0.125	2	1	1
121	0.001	0.102	0.019	0.029	2	1	1	121	0.196	0.256	0.137	0.123	2	1	1
122	0.001	0.104	0.018	0.028	2	1	1	122	0.192	0.252	0.137	0.135	2	1	1
123	0.001	0.139	0.016	0.025	2	1	1	123	0.140	0.273	0.137	0.217	2	1	1
124	0.019	0.119	0.015	0.021	2	1	1	124	0.123	0.262	0.137	0.165	2	1	1
125	0.035	0.102	0.013	0.017	2	1	1	125	0.117	0.246	0.138	0.216	2	1	1
126	0.033	0.086	0.010	0.015	2	1	1	126	0.114	0.229	0.136	0.185	2	1	1
127	0.023	0.068	0.009	0.012	2	1	1	127	0.292	0.210	0.136	0.152	2	1	1
128	0.017	0.052	0.006	0.009	2	1	1	128	0.275	0.191	0.134	0.140	2	1	1
129	0.013	0.040	0.021	0.006	2	1	1	129	0.262	0.176	0.136	0.221	2	1	1
130	0.006	0.032	0.066	0.005	2	1	1	130	0.310	0.164	0.140	0.180	2	1	1
131	0.002	0.025	0.100	0.004	2	1	1	131	0.297	0.156	0.137	0.148	2	1	1
132	0.004	0.020	0.095	0.004	2	1	1	132	0.277	0.164	0.138	0.139	2	1	1
133	0.002	0.015	0.089	0.005	2	1	1	133	0.261	0.157	0.141	0.132	2	1	1
134	0.001	0.012	0.078	0.003	2	1	1	134	0.238	0.151	0.141	0.129	2	1	1
135	0.001	0.013	0.067	0.003	2	1	1	135	0.200	0.150	0.139	0.225	2	1	1
136	0.001	0.013	0.064	0.003	2	1	1	136	0.163	0.148	0.138	0.168	2	1	1
137	0.000	0.011	0.103	0.003	2	1	1	137	0.138	0.146	0.138	0.224	2	1	1
138	0.000	0.011	0.088	0.003	2	1	1	138	0.127	0.146	0.140	0.228	2	1	1
139	0.001	0.008	0.074	0.003	2	1	1	139	0.118	0.144	0.137	0.278	2	1	1
140	0.001	0.072	0.069	0.002	2	1	1	140	0.111	0.203	0.128	0.252	2	1	1
141	0.000	0.155	0.057	0.002	2	1	1	141	0.108	0.300	0.112	0.198	2	1	1
142	0.000	0.133	0.041	0.003	2	1	1	142	0.100	0.390	0.136	0.245	2	1	1
143	0.000	0.158	0.032	0.035	2	1	1	143	0.098	0.430	0.139	0.214	2	1	1
144	0.000	0.164	0.029	0.066	2	1	1	144	0.096	0.371	0.138	0.206	2	1	1
145	0.001	0.157	0.036	0.064	2	1	1	145	0.095	0.327	0.138	0.216	2	1	1

Station K10								Station Q08							
x	**y 2006**	**y 2007**	**y 2008**	**y 2009**	**type**	**position**	**weight**	**x**	**y 2006**	**y 2007**	**y 2008**	**y 2009**	**type**	**position**	**weight**
146	0.001	0.158	0.064	0.059	2	1	1	146	0.158	0.305	0.137	0.232	2	1	1
147	0.001	0.132	0.077	0.052	2	1	1	147	0.265	0.291	0.135	0.219	2	1	1
147	0.001	0.132	0.077	0.052	2	1	1	147	0.265	0.291	0.135	0.219	2	1	1
148	0.001	0.111	0.071	0.046	2	1	1	148	0.240	0.280	0.131	0.193	2	1	1
149	0.001	0.091	0.095	0.043	2	1	1	149	0.213	0.266	0.123	0.240	2	1	1
150	0.001	0.075	0.093	0.039	2	1	1	150	0.182	0.249	0.127	0.216	2	1	1
151	0.001	0.059	0.082	0.033	2	1	1	151	0.161	0.232	0.136	0.207	2	1	1

Where ‘x’ is the number of the day, ‘y’ is the soil moisture observed in field, ‘type’ is the kind of variable chosen (water content, pressure head, concentration of nutrients, etc), ‘position’ is the depth of the observation node in the soil profile and ‘weight’ is the coefficient associate at any point.

Appendix C

Input data for ETo calculation by Penman-Monteith

Date	Incom. solar radiation	Latitude	Max. daily Temperature	Min. daily Temperature	Max. daily relative air moisture	Min. daily relative air moisture	Elevation	Wind speed at 2 m height
	(MJ/day/m^2)	(decimal degree)	(°C)	(°C)	(°C)	(°C)	(m)	m/s
19-05-09	27.57	41.21	20.24	2.06	88.1	17.16	780	1.83
20-05-09	15.51	41.21	11.72	5.23	93.2	57.03	780	5.49
10-05-07	28.05	41.21	24.61	8.94	85.1	22.4		3.43
31-05-06	23.83	41.21	17.59	2.45	97.6	38.9	780	1.87
17-04-09	29.78	41.21	24.68	5.09	85.3	18.56	780	1.74
22-04-08	25.66	41.21	20.39	4.71	96.3	30.69	780	1.23
22-04-07	25.26	41.21	24.21	4.77	93.6	24.92	780	1.24
19-04-06	31.58	41.21	20.7	2.71	83.4	18.03	780	4.16

ETo calculated by FAO Penman-Monteith

Date	Net radiation at the crop surface	Soil heat flux density	Mean saturation vapor pressure	Actual vapor pressure	Saturation vapor pressure deficit	Slope vapor pressure	Psychometric constant	Reference ET
	Rn	G	es	ea	es - ea	Δ	γ	ETo
	(MJ $m^{-2}day^{-1}$)	(MJ $m^{-2}day^{-1}$)	(Kpa)	(Kpa)	(Kpa)	(Kpa $°C^{-1}$)	(Kpa $°C^{-1}$)	(mm day^{-1})
19-05-09	15.45	0	1.99	0.66	1.33	0.11	0.0615	5.277
20-05-09	14.17	0	1.63	0.78	0.85	0.10	0.0615	4.126
10-05-07	14.70	0	2.12	0.83	1.29	0.12	0.0615	6.170
31-05-06	16.46	0	1.59	0.53	1.06	0.09	0.0615	6.140
17-04-09	13.35	0	1.54	0.52	1.03	0.09	0.0615	4.499
22-04-08	9.22	0	1.14	0.81	0.33	0.08	0.0615	2.551
22-04-07	13.27	0	1.94	0.78	1.16	0.11	0.0615	4.405
19-04-06	12.49	0	1.40	0.76	0.64	0.08	0.0615	3.579

Appendix D

Images collected from MODIS on April

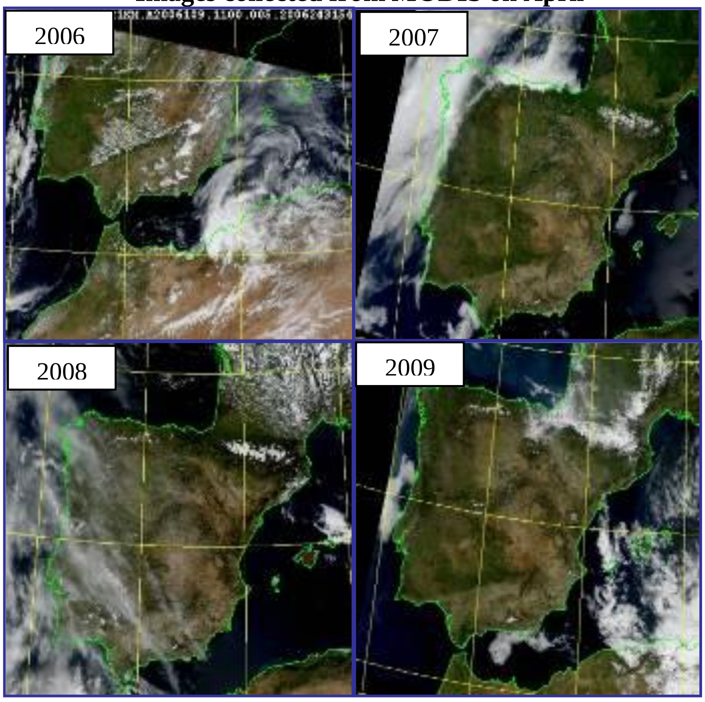

Images collected from MODIS on May